THE ROLE OF LINKER HISTONE VARIANT H1.X IN DOUBLE STRAND BREAK REPAIR

BY

DARREN DAVID ARBON

A thesis submitted to
The University of Birmingham
for the degree of
DOCTOR OF PHILOSOPHY

College of Medicine & Dentistry
The University of Birmingham
August 2010

Abstract

Eukaryotic DNA is packaged into chromatin, providing a physical and structural barrier for regulatory and effector proteins to access the DNA. It has been shown that linker histone variants inhibit the double strand break (DSB) repair pathway known as non-homologous end joining (NHEJ). NHEJ, *in vivo*, requires the KU complex, the DNA dependent protein kinase (DNA-PK) and the DNA ligase IV/XRCC4 (LX) complex. *In vitro* analysis has shown that H1.1, H1.3 and H1.X are all phosphorylated by DNA-PK. Importantly, H1.X contains and is phosphorylated at the DNA-PK consensus sequence. Depletion of H1.X protein levels by short interfering RNA renders cells radiosensitive and increases the levels of un-repaired DSBs following exposure to ionising radiation. H1.X interacts with both DNA ligase IV and XRCC4 *in vivo*, along with DNA-PK, the KU complex and nucleolin. Interestingly, the interaction with nucleolin only occurs in the presence of DNA damage following exposure to ionising radiation. *In vitro* analysis has shown that H1.X is able to form stable complexes in the presence of DNA and the LX complex, and very efficiently stimulates LX-mediated ligation of double stranded DNA. These findings establish a role for the linker histone variant H1.X in the NHEJ pathway.

Acknowledgments

I would like to thank all members of the Medical & Molecular Genetics Group at the University of Birmingham for their help and support throughout my time there. You're a great bunch of people who always manage to make me laugh! Special thanks go to Chris Bruce, aka Yoda, for his general help with anything and everything. Special thanks also to both Ashraf Dallol and Luke Hesson for their help with protein purification and to Luke for taking the time to look over my thesis all the way down under. I would also like to thank Boris Kysela for allowing me to work in his lab and for his help and guidance supervising this project. The image of your little dance the day I told you H1.X was phosphorylated will bring a smile to my face for the rest of my life! Thanks also to Grant Stewart for his help with the *in vivo* work.

Huge thanks to all my friends for their continued support. However, now I am in the real world of work, none of you can call me the "eternal student" anymore!

None of this would have been possible if it was not for the support from my parents. To you both I am forever indebted. I know you have always been extremely proud of me and what I do, and for that I am grateful. It is a shame that it is all coming to end as I think you both finally understand what it is I do!!

Last, but by no means least, Amy. I will be forever thankful for your love and support over these past 5 years, without you, I don't think I would have got through it. Hopefully now the dreaded thesis is finished we can start and enjoy life again, which I am sure will inevitably mean me beating you at Wii Tennis!!

Table Of Contents

List of Figures

List of Tables

List of Abbreviations

APS – Ammonium PerSulphate

ATM – Ataxia Telangiectasia Mutated

ATP – Adenosine TriPhosphate

ATR – Ataxia Telangiectasia mutated and Rad-3 related

Backup Non-Homologous End Joining – B-NHEJ

BrdU – BRomoDeoxyUridine

BRCA1 – BReast and ovarian Cancer type 1 susceptibility protein

BRCT – BReast and ovarian cancer type 1 susceptibility protein Carboxyl Terminus motif

BSA – Bovine Serum Albumin

CDK – Cyclin Dependent Kinase

CTD – Carboxyl Terminal Domain

DAPI - 4',6-DiAmidino-2-PhenylIndole

DMEM – Dulbecco's Modified Eagles Medium

DNA-PK – DNA dependent Protein Kinase

DNA-PK$_{CS}$ – DNA dependent Protein Kinase Catalytic Subunit

DSB – Double Strand Break

dsDNA – Double Stranded DNA

DTT – DiThioThreitol

EDTA – EthyleneDiamineTetraAcetic Acid

EGTA – EthyleneGlycolTetraAcetic acid

EMSA – Electrophoresis Mobility Shift Assay

FBS – Foetal Bovine Serum

FHA – Fork Head Associated

FRAP - Flourescence Recovery After Photobleaching

GFP – Green Fluorescent Protein

HP1 – Heterchromatin Protein 1

HR – Homologous Recombination

IPTG – IsoPropyl ThioGalactoside

IR – Ionising Radiation

LUC – Luciferase gene

LX – DNA Ligase IV / XRCC4 complex

MDC1 – Mediator of the DNA damage Checkpoint 1

MMS – Methyl MethaneSulfonate

MRN – Mre11/Rad50/Nbs1

NHEJ – Non-Homologous End Joining

NTD – Amino Terminal Domain

PBS – Phosphate Buffered Saline

PCR – Polymerase Chain Reaction

PIKK – Phosphatidyl Inositol-3-Kinase related Kinases

PMSF – PhenylMethylSulfonylFluoride

PTM – Post Translational Modification

PVDF – PolyVinyliDene Fluoride

RPA – Replication Protein A

SDS – Sodium Dodecyl Sulfate

SDS-PAGE - Sodium Dodecyl Sulfate PolyAcrylamide Gel Electrophoresis

siRNA – Short Interfering RNA

SMC – Structural maintenance of chromosomes

ssDNA – Single Stranded DNA

TEMED – TEtraMethylEthyleneDiamine

UV – Ultra Violet

γH2A.X – phosphorylated H2A.X

CHAPTER ONE: INTRODUCTION

1.1 DNA Damage and Repair

DNA damage arises from environmental factors, along with metabolic processes within the cell. It is estimated that there are between 1,000 and 1,000,000 lesions induced per cell genome per day (Lodish et al., 2007). Whilst this may seem alarmingly high, it is only a very small fraction of the 6 billion DNA bases in each cell. However, mutations in genes involved with DNA repair itself (P. C. Chen et al., 2005c, Miki et al., 1994, Prolla et al., 1998), cell cycle regulation (DeLeo et al., 1979) and apoptosis (Irvin et al., 2003) can ultimately lead to tumour formation.

DNA damage affects the primary structure of the DNA. The normally regular structure of the double-helix is altered by the addition or removal of chemical bonds, the introduction of bulky lesions, or by single and double strand breaks (DSB).

Damage can arise from endogenous and exogenous sources. Endogenous sources include replication errors where the incorrect base is inserted, resulting in a mis-match and a stalled replication fork, and base modifications such as oxidation, alkylation and the hydrolysis of bases. Oxidation arises from reactive oxygen species produced in the mitochondrial electron transport chain. An estimated 10^5 oxidative hits per day occur in every cell in the human body (Valko et al., 2004).

Exogenous sources include: ultra-violet (UV) irradiation from the sun resulting in lesions such as cyclobutane pyrimidine dimers and pyrimidine (6-4) pyrimidone photoproducts, resulting

in the bonding of two adjacent bases; ionizing radiation (IR), including X-rays and gamma rays from cosmic radiation and radioactive decay which result in DSB formation; and many mutagenic chemicals such as ethidium bromide which intercalates between the DNA base pairs.

DNA DSBs are the most lethal form of DNA damage and are generated when complimentary strands of the DNA double helix are broken simultaneously. These breaks are produced by exogenous damaging agents such as IR, or radiomimetic molecules such as bleomycin, neocarzinostatin and etoposide. DSBs can also occur endogenously as a consequence of oxidative metabolism, and in lymphocytes during gene rearrangement, a process known as V(D)J recombination (Bassing et al., 2002). It has been estimated that a typical mammalian cell will incur at least 10 spontaneous DSBs per day (Pastwa and Blasiak, 2003). If left unrepaired, DSBs can lead to a wide array of problems including chromosome translocation, cancer predisposition and the induction of cell death.

There are evolutionary conserved pathways to deal with DNA damages. DNA base modifications, including deamination, base loss, oxygen free radical attack and methylation are predominantly repaired by the base excision repair pathway (for review, Robertson et al., 2009). Those base modifications which are unable to be repaired by this pathway, along with UV induced (6-4) photoproducts and cyclobutane pyrimidine dimers are repaired by the nucleotide excision repair pathway (for review, Fousteri and Mullenders, 2008, Shuck et al., 2008). Mis-incorporated bases are removed by the mismatch repair pathway (G. M. Li, 2008), and for the removal of DSBs there are two evolutionary conserved pathways,

homologous recombination (HR; Section 1.1.3.1) and the non-homologous end joining (NHEJ; Section 1.1.3.2) pathway.

1.1.1 DNA Damage Responses in Mammalian Cells

Upon sensing DNA damage or a stalled replication fork, it is essential that the cell responds to halt the cell cycle so that potential deleterious mutations are not passed on to daughter cells. Along with the activation of cell cycle checkpoints, DNA repair pathways are initiated, and if the damage is too severe, apoptosis is initiated (B. B. Zhou and Elledge, 2000). Cell cycle checkpoints exist to ensure that each phase of the cell cycle has been executed properly. The three checkpoints exist in the G1 and S phases of the cell cycle, and the G2 to M transition (Figure 1.1).

The key regulators of the cell cycle checkpoints in mammalian cells are the ataxia telangiectasia mutated (ATM) and ATM and RAD3 -related (ATR) protein kinases (Kastan et al., 1992, Paulovich and Hartwell, 1995). These proteins belong to a family of proteins, the phosphatidylinositol-3-kinase related kinases (PIKKs), characterised by a phosphatidylinositol 3-kinase domain in their carboxyl terminal domain (CTD). Although ATM and ATR are able to phosphorylate the same targets, it depends on the type of damage incurred as to which kinase is activated. ATM is primarily involved in DSB repair in response to IR, whereas ATR acts as a backup for ATM in response to IR, and also deals with UV irradiation and stalled replication forks.
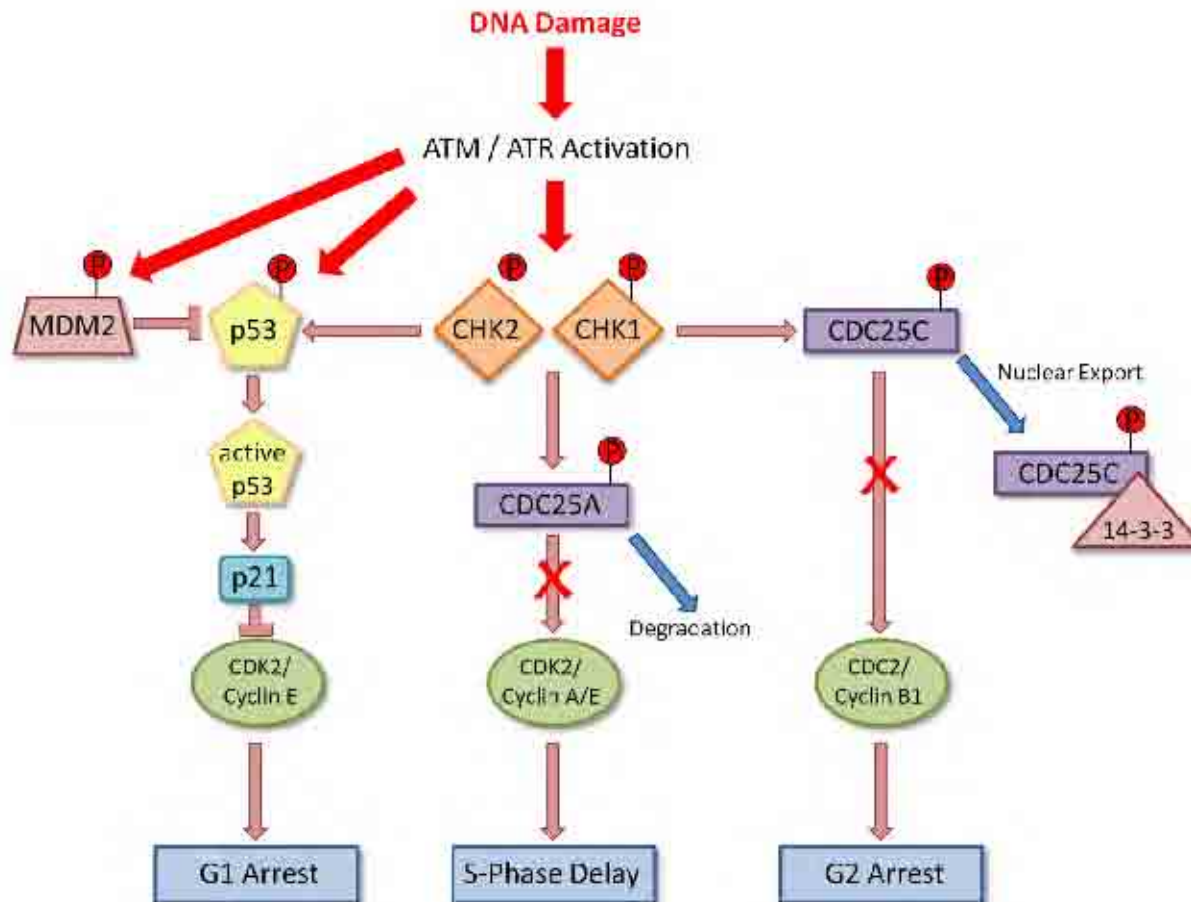
Figure 1.1 - Cell Cycle Arrest Following DNA Damage
Upon DNA damage the ATM and ATR kinases are activated. During G1, phosphorylation by ATM/ATR and CHK2 activates p53 leading to the transcription of p21. p21 suppresses CDK2/Cyclin E activity resulting in G1 arrest. During S phase, CHK1 and CHK2 will phosphorylate CDC25A targeting it for proteosomal degradation, therefore the CDK2/Cyclin A/E complexes remain inactive, preventing DNA synthesis. During G2, CDC25C is phosphorylated by CHK1/CHK2, allowing the binding of 14-3-3 proteins. This subsequently targets CDC25C for nuclear export, therefore the CDC2/Cyclin B1 complex remains inactive, resulting in G2 arrest.

1.1.1.1 G1 Phase Checkpoint

The G1 checkpoint is currently the most understood checkpoint in mammalian cells and prevents damaged DNA from being replicated. Central to this checkpoint is the accumulation of the tumour suppressor protein, p53 (Kastan et al., 1991). Under normal conditions, p53 is bound by MDM2 which targets p53 for nuclear export and ultimately proteosomal degradation (Inoue et al., 2001, Y. Zhang and Xiong, 2001). Following IR, ATM activates CHK2 by phosphorylation (threonine 68; Matsuoka et al., 2000). CHK2 then phosphorylates p53 (serine 20), blocking the p53-MDM2 interaction, allowing p53 to accumulate in the nucleus (Chehab et al., 2000, Unger et al., 1999). ATM can also directly phosphorylate MDM2 (serine 395) which, although allowing the p53-MDM2 interaction to occur, does not allow p53 to be targeted for nuclear export (Maya et al., 2001). ATM and/or ATR are also able to phosphorylate p53 directly (serine 15) in response to IR (ATM and ATR), UV (ATR) and stalled replication forks (ATR), resulting in the activation of p53 (Banin et al., 1998, Canman et al., 1998, Zhao et al., 2008). The nuclear accumulation and activation of p53 allows it to up-regulate a number of genes including p21 (Waldman et al., 1995). p21 is a cyclin dependent kinase (CDK) inhibitor and suppresses the CDK2/cyclin E activity resulting in G1 arrest (el-Deiry et al., 1993, Gu et al., 1993, Harper et al., 1993; Figure 1.1)

1.1.1.2 S Phase Checkpoint

The S phase checkpoint monitors DNA synthesis during cell cycle progression and will slow the rate of DNA synthesis following DNA damage. There are two branches which will activate

the S phase checkpoint (Figure 1.1). The first branch is initiated by the phosphorylation of CHK2 (threonine 68) by ATM (Matsuoka et al., 2000). CHK2, once activated by phosphorylation, is able to phosphorylate CDC25A (serine 123) which will target it for ubiquitin-dependant degradation (Matsuoka et al., 1998). CDC25A is therefore no longer able to remove the inhibitory phosphate groups from CDK2 (threonine 14 and tyrosine 15), therefore the CDK2/cyclin E and CDK2/cyclin A complexes remain inactive, preventing DNA synthesis (Falck et al., 2001, Gu et al., 1992).

The second branch of the S phase checkpoint, involves the direct phosphorylation of NBS1 (serine 343), breast and ovarian cancer type 1 susceptibility protein (BRCA1, serine 1387) and structural maintenance of chromosomes 1 (SMC1; serine 957 and serine 966) by ATM. All of these proteins are needed for the activation of the S phase checkpoint, however, the exact function of these proteins in the checkpoint remains to be elucidated (S. T. Kim et al., 2002, Lim et al., 2000, Xu et al., 2001, Xu et al., 2002).

1.1.1.3 G2 to M Phase Checkpoint

The G2 to M phase checkpoint is extremely important as it regulates cell cycle progression prior to chromosome segregation. The G2/M checkpoint is initiated by the phosphorylation of CHK1 and CHK2 by ATR and ATM respectively, thus activating them (Q. Liu et al., 2000, Matsuoka et al., 2000, Zhao and Piwnica-Worms, 2001). Once activated CHK1 and CHK2 can phosphorylate CDC25C (serine 216), enabling the binding of 14-3-3 proteins (Ogg et al., 1994, Peng et al., 1997, Sanchez et al., 1997). CDC25C/14-3-3 complexes are then

sequestered to the cytoplasm, stopping CDC25C from removing the inhibitory phosphate groups from CDC2 (Dalal et al., 1999). The CDC2/cyclin B1 complex therefore remains inactive, halting the progression into mitosis (Figure 1.1).

1.1.1.4 Apoptosis

If DNA repair is unsuccessful and the damage persists, the cell has to be removed from the population by death in a process known as apoptosis. DNA damage activates the ATM and ATR kinases which stabilise p53 (Section 1.1.1.1; Banin et al., 1998, Canman et al., 1998, Zhao et al., 2008). p53 is then able to up-regulate the expression of several genes involved in apoptosis, specifically members of the BCL-2 family (Miyashita et al., 1994, Miyashita and Reed, 1995). This family consists of both pro- and anti-apoptotic proteins which regulate the permeability of the mitochondrial membrane (Chipuk et al., 2010). Pro-apoptotic members of the BCL-2 family, including BAX and BID, function to permeabilise the mitochondrial membrane resulting in the release of cytochrome c from the mitochondria to the cytoplasm (Kluck et al., 1997, J. Yang et al., 1997). Once in the cytoplasm, cytochrome c is able to activate caspase 9 (Hakem et al., 1998, Kuida et al., 1998). Caspases are aspartate specific proteases which are responsible for the disassembly of the cell in a controlled manner. Caspase 9 then activates other caspases causing a caspase cascade, ultimately resulting in the controlled destruction of the cell (T. J. Fan et al., 2005).

There are also reports of p53-independent apoptosis pathways including the activation of the JNK pathway (McNamee and Brodsky, 2009), the interaction between p19^{ARF} and BAX

(Suzuki et al., 2003) and by the transcriptional up-regulation of PUMA by p73 (Melino et al., 2004). PUMA binds to BCL-2 and BCL-X$_L$, translocates to the mitochondria, resulting in cytochrome c release and the caspase cascade (Nakano and Vousden, 2001, Yu et al., 2003a, Yu et al., 2001).

1.1.2 DNA Double Strand Break Recognition

Currently, the primary sensor of a DSB is unknown. One branch of evidence suggests the MRE11 (Section 1.1.2.1)/RAD50 (Section 1.1.2.2)/NBS1 (Section 1.1.2.3) (MRN) complex recognises the damage (Uziel et al., 2003). Whereas another branch of evidence suggests localised perturbations of the chromatin structure following IR cause the activation of ATM (Bakkenist and Kastan, 2003, Y. C. Kim et al., 2009).

MRN is able to tether damaged DNA which increases the local concentration of DSBs promoting the recruitment, monomerisation and activation of ATM, which exists in unstressed cells as inactive dimers (Dupre et al., 2006). Along with tethering the damaged DNA, NBS1 as part of the MRN complex, is also capable of unwinding DNA at the ends of the breaks which also promotes ATM monomerisation and activation (J. H. Lee and Paull, 2005, Paull and Gellert, 1999).

1.1.2.1 MRE11

MRE11 is known to exist as a dimer which is essential for cellular survival against DSBs (Hopfner et al., 2001, R. S. Williams et al., 2008). Dimerisation occurs via two N-terminal dimerisation motifs which overlap the NBS1 interacting domain (Figure 1.2). *In vitro*, MRE11 has been shown to exhibit single stranded DNA (ssDNA) endonuclease, 3'->5' ssDNA exonuclease, double stranded DNA (dsDNA) exonuclease and hairpin opening activities. These are enhanced when MRE11 is in a heterotetrameric structure with RAD50 and in the presence of adenosine triphosphate (ATP; Figure 1.2; Furuse et al., 1998, Paull and Gellert, 1998, Trujillo and Sung, 2001, Trujillo et al., 1998). Mutations in MRE11 give rise to the human disorder ataxia-telangiectasia-like disorder (ATLD). Patients with ATLD have radiosensitivity along with other chromosomal abnormalities (Stewart et al., 1999). Patients with ATLD have mutations which occur within the NBS1 interacting domain (Figure 1.2) which disrupts, although not totally abolishing, the MRE11-NBS1 interaction (Stewart et al., 1999).
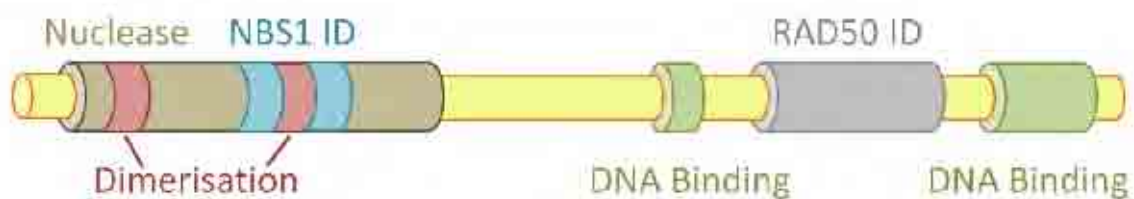
Figure 1.2 - Domain structure of MRE11
The amino terminus of MRE11 contains the nuclease domain, capable of endonuclease and exonuclease activity. Contained within the nuclease domain are two dimerisation domains and two NBS1 interacting domains (ID). MRE11 is capable of binding DNA by its two DNA binding domains, one central, one at the carboxyl terminus. In between the two DNA binding domains there is a RAD50 interacting domain. Adapted from Rupnik et al., 2010.

1.1.2.2 RAD50

RAD50 is a member of the SMC family of proteins which are involved in sister-chromatid cohesion and chromosome condensation in eukaryotes (Sharples and Leach, 1995). RAD50 contains two Walker domains which are required for its ATPase activity (Figure 1.3; J. E. Walker et al., 1982). Mutations in the Walker A domain confer the same radiosensitivity as RAD50 deletion mutants. Defects are seen in both HR and NHEJ, suggesting the Walker domains are crucial for RAD50's role in DSB repair. Defects are also seen in RAD50's ATPase activity, ATP-dependent DNA unwinding and ATP-stimulated endonuclease activity, however, DNA end-bridging does still occur (L. Chen et al., 2005b, de Jager et al., 2002). Scanning force microscopy revealed that RAD50 consists of two highly flexible intramolecular coiled coils protruding from a central globular DNA binding domain. The ends of the coils contain a zinc hook which allows the protein to fold back upon itself. The zinc hook also allows dimerisation and facilitates the end bridging of broken DNA ends (Figure 1.3; de Jager et al., 2001, Hopfner et al., 2002).

Figure 1.3 - Domain structure of RAD50
At the carboxyl and amino termini are Walker domains which are essential for ATPase activity. RAD50 interacts with MRE11 by two MRE11 interacting domains (ID) which are located at the carboxyl and amino termini of the protein. In the centre of the protein there is a "hinged" zinc hook which allows the protein to fold back upon itself and also allow RAD50 dimerisation. Adapted from Rupnik et al., 2010.

1.1.2.3 NBS1

Although there is no enzymatic activity associated with NBS1, it contains many interacting regions which are crucial for its role in DNA repair (Figure 1.4). The fork head-associated (FHA) domain is a phospho-peptide recognition domain which was originally identified in protein kinases and transcription factors (Durocher et al., 1999, Hofmann and Bucher, 1995). NBS1 also contains tandem BRCA1 carboxyl terminus motifs (BRCT), which are known to have affinity towards phospho-peptides in proteins involved in DNA repair (Yu et al., 2003b). Both the BRCT domains and the FHA domain are needed to allow NBS1 to bind to the sites of DBS's following DNA damage (di Masi et al., 2008, Kobayashi et al., 2002).

NBS1 contains an MRE11 interacting domain at its carboxyl terminus (Figure 1.4). Deletion mutants lacking the MRE11 interacting domain still permitted NBS1 to localise to the nucleus and to form IR-induced foci. However the mutant protein could not complement the radiosensitivity of NBS1 deficient cells suggesting the NBS1-MRE11 interaction is essential to survive IR (Desai-Mehta et al., 2001). An ATM interacting domain contained in the carboxyl terminus is crucial to recruit ATM to DNA *in vitro*, and for ATM recruitment to DSBs following IR *in vivo* (Figure 1.4; Falck et al., 2005).

Mutations in the NBS1 gene give rise to Nijmegen breakage syndrome, a disorder similar to ataxia telangiectasia which results in immunodeficiency and radiosensitivity (Carney et al., 1998, Varon et al., 1998).
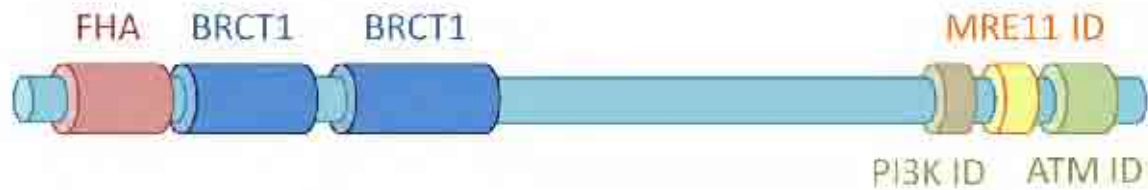
Figure 1.4 - Domain structure of NBS1
At the amino terminus is an FHA domain which mediates NBS1's interaction with phosphopeptides. Also contained at the amino terminus are 2 BRCT motifs which also interact with phosphopeptides, specifically those involved in the DNA damage response. At the carboxyl terminus are three interacting domains (ID) mediating its interaction with the PI3-kinase (PI3K), MRE11 and ATM. Adapted from Rupnik et al., 2010.

1.1.2.4 ATM

ATM, ATR and the DNA-dependent protein kinase catalytic subunit (DNA-PK$_{CS}$; Section 1.1.3.2.1) are all members of the PIKK family due to their phosphatidylinositol 3-kinase domain (Figure 1.5). Mutations in ATM cause the disorder ataxia telangiectasia, causing cerebella degeneration, chromosomal instability, cancer predisposition, immunodeficiency, radiation sensitivity, and cell cycle abnormalities (Savitsky et al., 1995).

Following its activation by DSB induction and MRN foci formation, ATM rapidly phosphorylates the highly conserved serine 139 residue on the histone variant H2A.X (Burma et al., 2001, Rogakou et al., 1998). This phosphorylation signal is propagated to the surrounding H2A.X histones, stretching up to 1 mega base of DNA from the break (Rogakou et al., 1998). This phosphorylation event was originally hypothesised to aid the recruitment of the repair proteins to the site of the break, however, recent evidence suggests that it actually functions to concentrate and stabilise repair proteins in the vicinity of the break (Celeste et al., 2003).

Recent evidence also suggests that phosphorylated H2A.X (γH2A.X) inhibits linker histone binding and therefore the 30nm fiber formation, aiding in relaxing the chromatin structure to allow the repair machinery to access the DNA (A. Li et al., 2010). γH2A.X has also been shown to recruit chromatin remodelling factors including NUA4 (Downs et al., 2004) and INO80 (Morrison et al., 2004, van Attikum et al., 2004) in budding yeast, and TIP60 (Kusch et al., 2004) in *Drosophila melanogaster*.

TIP60 driven chromatin remodelling has also been seen to activate ATM. TIP60 replaces HP1β bound to tri-methylated core histone H3 on lysine 9, activating TIP60s acetyl transferase activity. Once activated, TIP60 will acetylate ATM via its interaction with ATMs FATC domain (Figure 1.5), enhancing ATM's activation (Sun et al., 2005, Sun et al., 2009).

Following the successful repair of the DSB serine 139 is either dephosphorylated or the whole γH2A.X histone is replaced. There are numerous reports of proteins which have been implicated in this dephosphorylation step, including protein phosphatase 2A, protein phosphatase 6 and p53-induced phosphatase 1 (Cha et al., 2010, Chowdhury et al., 2005, Douglas et al., 2010). There is also growing evidence for histone exchange following successful DSB repair. In *D. melanogaster*, TIP60 will acetylate γH2A.X and replace it with normal H2A.X (Kusch et al., 2004).
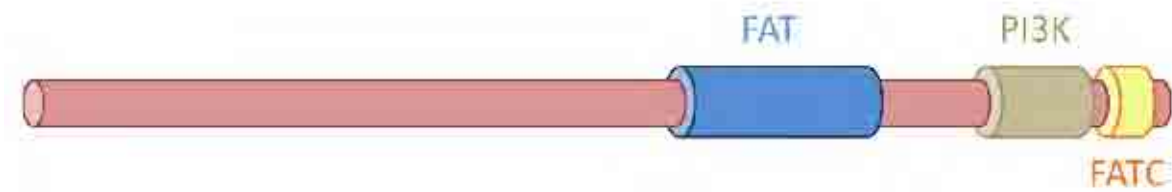
Figure 1.5 - Domain structure of ATM
ATM contains a FAT domain which is a domain found in FRAP (F), ATM (A) and TRRAP (T) proteins. The phosphatidylinositol 3-kinase (PI3K) domain is the catalytic kinase domain which is found in all the PIKKs. The carboxyl terminus contains a FATC domain which is a domain common to all PIKKs. Adapted from Pandita, 2003.

1.1.2.5 MDC1

Mediator of the DNA Damage Checkpoint 1 (MDC1) is an adapter protein which forms a scaffold upon which other repair proteins are supported. MDC1 is initially recruited to the DSB site due to its high affinity for γH2A.X, mediated by its carboxyl terminal tandem BRCT domains (Figure 1.6; M. S. Lee et al., 2005, Shang et al., 2003). Knock-down of MDC1, followed by exposure to IR shows normal formation of γH2A.X foci, however, these foci disappeared much quicker than in the control cells. This suggests that MDC1 creates the initial scaffold at the site of the DSB and spreads out from it, allowing the propagation of the γH2A.X signal (Lou et al., 2006, Stucki et al., 2005). MDC1 has also been shown to recruit and stabilise several other repair proteins including BRCA1, 53BP1, ATM and CHK2 (Goldberg et al., 2003, Stewart et al., 2003). MDC1 has also been shown to interact with the FHA domain of NBS1 in a phosphorylation dependent manner. This occurs via its SDT domain enabling the accumulation of MRN at the sites of DSBs (Figure 1.4 & Figure 1.6; Melander et al., 2008, Spycher et al., 2008).

MDC1 is also phosphorylated by ATM on "TQXF" motifs which promote the recruitment of

RNF8, an E3 ubiquitin ligase, to the site of repair (Figure 1.6; Huen et al., 2007, Kolas et al.,

2007). RNF8, in conjunction with the E2 ubiquitin conjugating enzyme UBC13, catalyses the

ubiquitylation of histones, suspected to make the chromatin more accessible to repair

factors (Huen et al., 2007, Kolas et al., 2007, Mailand et al., 2007, B. Wang and Elledge,

2007). Depletion studies of RNF8 show increased sensitivity to IR suggesting it plays a key

role in chromatin remodelling during DSB repair (Mailand et al., 2007). RNF8 also recruits

both 53BP1 and BRCA1 to the sites of DSBs (Kolas et al., 2007, B. Wang and Elledge, 2007).

RNF168 is also recruited to sites of DSBs and binds to ubiquitylated H2A where it enhances

the ubiquitylation signal, poly-ubiquitylating H2A histones (Stewart et al., 2009).
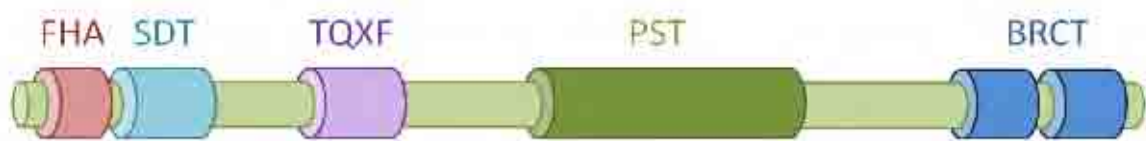
Figure 1.6 - Domain structure of MDC1
At the amino terminus of MDC1 there is an FHA domain promoting its interaction with phosphopeptides, along with 2 BRCT domains at the carboxyl terminus which also promote its interaction with phosphopeptides, specifically those involved in the DNA damage response. The SDT motif consists of a small patch of serine and threonine residues separated by an aspartate residue and are responsible for MDC1's interaction with the MRN complex. The TQXF motif is a cluster of ATM phosphorylation consensus sites, which are phosphorylated by ATM following a DSB, and promote the recruitment of RNF8 to the site of damage. The PST motif is a region which contains proline-serine-threonine repeats, although the function of this motif is unknown. Adapted from Jungmichel and Stucki, 2010.

1.1.2.6 53BP1

The 53BP1 protein was initially isolated as a binding partner of p53 and was shown to be

recruited early to the site of DSBs (Bork et al., 1997, Iwabuchi et al., 1994, Schultz et al.,

2000). Its precise role in the damage response is still uncertain, however it has been

implicated in regulating the activation of the G2 to M phase checkpoint (DiTullio et al., 2002,

B. Wang et al., 2002) and the repair of a subset of DSBs in NHEJ (Difilippantonio et al., 2008).

More recently, 53BP1 has been shown to prevent the resection of DNA ends to produce a

single stranded overhang at one end, the preliminary step required for HR (Section 1.1.3.1),

therefore potentially favouring NHEJ (Section 1.1.3.2; Bunting et al., 2010).

1.1.2.7 BRCA1

BRCA1 was the first cloned breast cancer susceptibility gene and was quickly linked to a role

in DNA repair (Miki et al., 1994, Moynahan et al., 1999, Moynahan et al., 2001, Scully et al.,

1997a). Evidence for its role in DNA repair came from its association with RAD51, a key

protein in HR (Section 1.1.3.1; Scully et al., 1997b). Subsequently, BRCA1 has also been

shown to interact with the MRN complex and co-localise with MRN foci (Wu et al., 2000a,

Zhong et al., 1999). H2A.X deficient mice are unable to recruit BRCA1 to the sites of DSBs

suggesting a physical link between BRCA1 and H2A.X (Celeste et al., 2002).

A complex containing BRCA1, named BRCA1A, has been shown to co-localise to sites of DSB

repair (X. Chen et al., 2006, Feng et al., 2009, H. Kim et al., 2007a, H. Kim et al., 2007b, Z. Liu

et al., 2007, Shao et al., 2009, Sobhian et al., 2007, B. Wang et al., 2007). The recruitment of

the BRCA1A complex to the sites of DSB repair is mediated through the ubiquitylation of

chromatin in the immediate vicinity of the DSB by the aforementioned RNF8/UBC13

partnership and two ubiquitin interacting domains contained within RAP-80, a member of

the BRCA1A complex (H. Kim et al., 2007a, B. Wang and Elledge, 2007). Recruitment is also dependent on ATM mediated phosphorylation of RAP-80 following exposure to IR (J. Yan et al., 2008). BRCA1 also forms a complex with BARD1 which is recruited to the sites of DSB repair where they are able to further ubiquitylate chromatin and activate the G2 to M phase checkpoint (H. Kim et al., 2007a, Polanowska et al., 2006).

1.1.3 DNA Double Strand Break Repair Pathways

1.1.3.1 Homologous Recombination

HR is the primary pathway in repairing DSBs during the late S and G2 phases of the cell cycle. During this period there is an identical genetic copy available to the repair machinery which enables high fidelity repair of DSBs. HR utilises the RAD52 epistasis group of proteins originally identified in *S. cerevisiae*, which includes RAD50, RAD51, RAD52, RAD54, RAD55, RAD57, RAD59, MRE11 and XRS2 (homologue of eukaryotic NBS1; Section 1.1.2.3; Game and Mortimer, 1974).

Following DSB recognition, the initial stage of HR is the resection of DNA to generate 3' ssDNA tails (Figure 1.7c). Resection is achieved through the nuclease activity of MRE11, which is enhanced by CTIP, both of which are crucial for efficient HR (Paull and Gellert, 1998, Sartori et al., 2007, Trujillo et al., 1998). The exposed ssDNA tails are then bound by the replication protein A (RPA), a heterotrimeric protein consisting of three subunits (70 kDa, 32 kDa and 14 kDa; Longhese et al., 1994, Moore et al., 1991). RPA is not unique to HR, having

roles in replication along with nucleotide excision repair and base excision repair (Binz et al., 2004).

RAD52 subsequently targets RAD51 to ssDNA specifically loaded with RPA, exchanging RPA for RAD51 to form the RAD51 nucleoprotein filament (Benson et al., 1998, New et al., 1998, Shinohara and Ogawa, 1998). BRCA2 has also been implicated in loading RAD51 onto ssDNA (Shivji et al., 2006, H. Yang et al., 2002, H. Yang et al., 2005). RAD51 has significant homology with the bacterial recombinase RECA, specifically in those areas that are crucial for recombination, DNA binding and ATP hydrolysis (Aboussekhra et al., 1992, Basile et al., 1992, Shinohara et al., 1992). The RAD51 nucleoprotein filament is then stabilised by RAD54, which also promotes strand invasion and increases the rate of pairing between homologous ssDNA and dsDNA (Clever et al., 1997, Petukhova et al., 1998; Figure 1.7d-e).
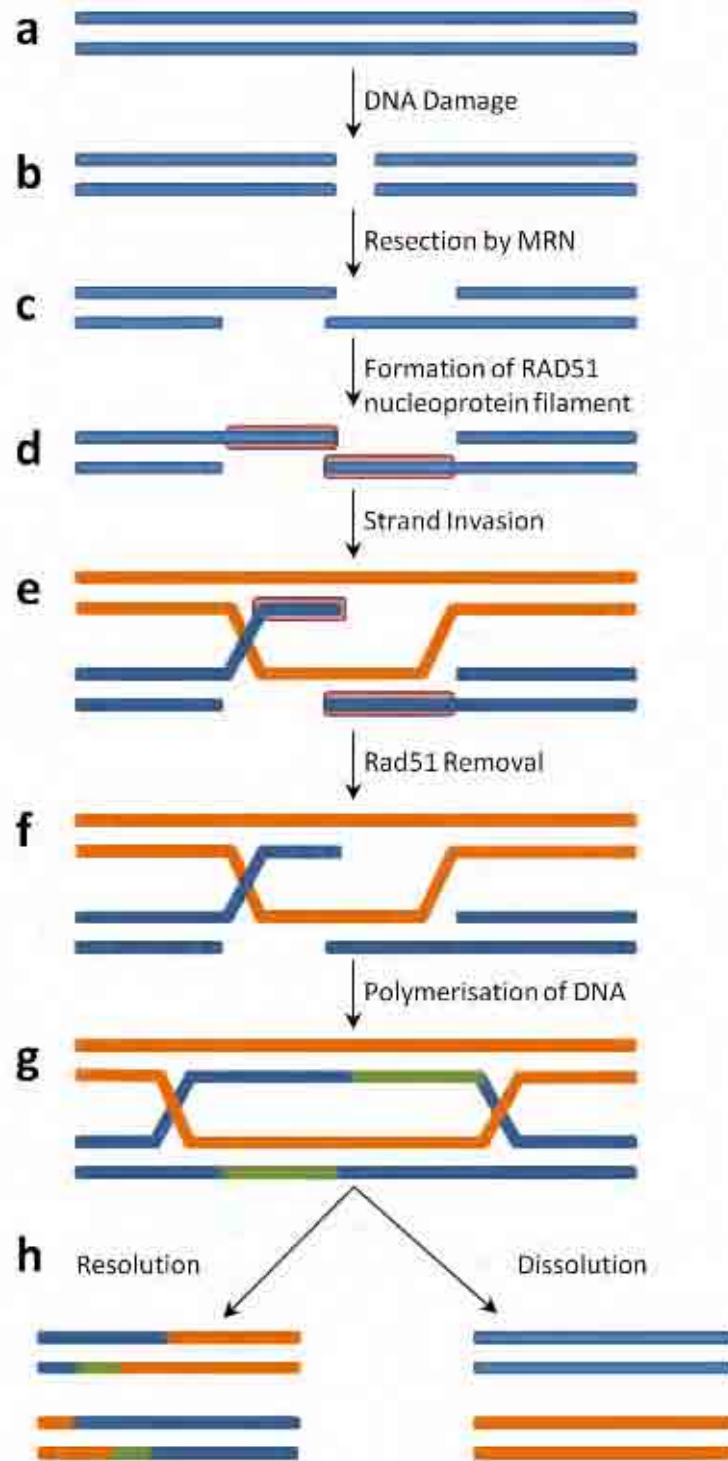
Figure 1.7 - Homologous Recombination
Following a DNA DSB (b), the DNA ends are resected to create 3' ssDNA tails by the MRN complex (c). RAD51 is loaded on to the ssDNA to form the RAD51 nucleoprotein filament (d). The subsequent binding of RAD54 promotes strand invasion and DNA pairing (e). Following pairing, RAD51 is removed from the DNA (f) and new DNA is synthesised (g). Two potential outcomes are resolution whereby there is an exchange of genetic information, and dissolution where there is not (h).

Following pairing, RAD51 and RAD54 need to be removed from the DNA (Figure 1.7f). Recent work in *C. elegans* has shown that the HELQ-1 and RFS-1 proteins are both independently able to remove RAD51 from dsDNA, not ssDNA (Ward et al., 2010). Once the DNA is devoid of RAD51 and RAD54, DNA helicases and DNA polymerases are able to unwind and synthesize new DNA respectively (Figure 1.7g). At this point two DNA crossover structures are created, referred to as Holliday junctions (Holliday, 1964). There are two potential outcomes of the Holliday junctions: dissolution, whereby no exchange of genetic information occurs and resolution where there is an exchange of genetic information (Figure 1.7h). Dissolution is facilitated by BLM, an RECQ helicase, topoisomerase III, and BLAP75 (Raynard et al., 2006, Wu et al., 2006, Wu and Hickson, 2003). Resolution involves the resolvase GEN1 which will symmetrically cleave the DNA at the Holliday junction, which is then ligated by DNA ligase I (Goetz et al., 2005, Ip et al., 2008).

1.1.3.2 Non Homologous End Joining

NHEJ is the predominant pathway for the repair of DSBs and is more active during the G1 phase of the cell cycle. Due to the lack of a sister chromatid, repair by this pathway can be deleterious as nucleotides are often removed or added prior to ligation of the broken ends.

1.1.3.2.1 DNA-Dependent Protein Kinase Complex Formation

The first NHEJ protein to bind the DSB is the KU protein complex, a heterodimer consisting of a 73kDa subunit (KU70) and an 83kDa subunit (KU80, also known as KU86; Lieber, 1999). KU has been implicated in many cellular processes including telomere maintenance (Baumann

and Cech, 2000), apoptosis (Sawada et al., 2003) and transcription (Downs and Jackson, 2004).

The crystal structure of the KU complex associated with DNA shows it forms a doughnut shape with a positively charged central hole which is large enough to accommodate DNA (J. R. Walker et al., 2001). KU is able to bind to DSBs in a non structural manner, i.e. binding occurs to blunt ends, to ends with 5' and 3' overhangs, and to hairpin ends, and is largely independent of DNA sequence (Mimori and Hardin, 1986, Paillard and Strauss, 1991). UV cross-linking experiments have shown that KU70 binds tightly to DNA protecting a 5'-end label from nuclease degradation (W. W. Zhang and Yaneva, 1992). Similar experiments with KU80 suggest it does not offer this protection but is able to protect an internal label, suggesting KU80 may bind distal to the DSB (W. W. Zhang and Yaneva, 1992).

KU is the most abundant non-histone nuclear protein, with an estimated 400,000 molecules per cell compared to a typical housekeeping protein having 10,000 molecules (Lieber, 1999). Due to its abundance and affinity for DNA ends, KU has been shown to be recruited to laser induced DSBs within a few seconds, suggesting it could either sense DNA damage, or prevent the nucleolytic degradation of DNA ends (Mari et al., 2006).

Once bound to the DSB the KU complex is able to move freely, without energy input, inward along DNA and recruit DNA-PK$_{CS}$ (de Vries et al., 1989, Dvir et al., 1992, Dynan and Yoo, 1998, Gottlieb and Jackson, 1993). Inhibition of KU translocation by cisplatin–DNA adducts results in the failure to recruit DNA-PK$_{CS}$ and therefore failure to repair the DSB (Kysela et al.,

2003, Turchi et al., 2000). The recruitment of DNA-PK$_{CS}$ is facilitated by the CTD of the KU80 subunit, specifically the last 12 amino acids (Gell and Jackson, 1999, Singleton et al., 1999). Deletion of this region does not affect the ability of KU80 to bind DSBs, however DNA-PK$_{CS}$ will not be recruited to the site of the DSB (Singleton et al., 1999).

DNA-PK$_{CS}$, a 469kDa protein, has a carboxyl terminal catalytic domain which bears amino acid similarity to the catalytic domain of phosphoinositide-3,4-kinase family of lipid kinases, placing DNA-PK$_{CS}$ in the PIKK family (Hartley et al., 1995, Poltoratsky et al., 1995). Upon recruitment to DNA by the KU complex, DNA-PK$_{CS}$ requires the ends of the DSB as a cofactor to become activated, a characteristic biologically unique to this ligase (Anderson and Carter, 1996). Bound and activated DNA-PK$_{CS}$ along with the KU complex, referred to as DNA-PK, subsequently exhibits serine/threonine protein kinase activity (discussed in more detail in Section 3.1). It is believed that the formation of this complex aids in the spatial coupling of the DNA ends thus allowing DNA end processing (Section 1.1.3.2.2) and finally ligation (Section 1.1.3.2.3; Hefferin and Tomkinson, 2005).

1.1.3.2.2 End Processing

Due to the random nature of the DSBs, DNA overhangs and hairpins may need to be removed to allow the final ligation step. A protein believed to be involved in DNA end processing is Artemis (Moshous et al., 2001, Moshous et al., 2000). Cells deficient in Artemis exhibit radiosensitivity and defective V(D)J recombination, although the sensitivity is not as severe as cells deficient in other components of NHEJ (Rooney et al., 2003, J. Wang et al.,

2005b). Artemis alone has 5'-3' exonuclease activity which is converted to endonuclease activity following phosphorylation by DNA-PK$_{CS}$. Once activated, Artemis is also available to accommodate more substrates including 5' and 3' overhangs and hairpins (Ma et al., 2002). DNA-PK$_{CS}$ is implicated twice in Artemis mediated end processing, it is suggested that conformational changes in DNA-PK$_{CS}$ following IR allow Artemis access to the DSB (Goodarzi et al., 2006). Also, the CTD of Artemis is a target of phosphorylation by DNA-PK$_{CS}$ following IR. It is suggested that Artemis' unmodified CTD stops it binding to DNA substrates as some DNA structures created during replication and transcription mimic Artemis substrates. Phosphorylation of the CTD of Artemis subsequently alleviates this inhibition allowing it to bind DNA substrates involved in DNA repair (Ma et al., 2005). Artemis has also been shown to interact with the MRN complex when phosphorylated having a role in the G2 to M cell cycle checkpoint control (L. Chen et al., 2005a, X. Zhang et al., 2004). Another nuclease has been implicated in NHEJ, knockout of FEN-1 in *S. cerevisiae* leads to a 4.4 fold reduction of end joining which requires the removal of 5' flaps (Wu et al., 1999).

1.1.3.2.3 End Ligation

One DNA ends have been processed, the final step of NHEJ is ligation which is mediated by the protein complex of XRCC4 and DNA Ligase IV (LX; Critchlow et al., 1997, Grawunder et al., 1997, Wilson et al., 1997). Deletion of either of these components leads to embryonic lethality in mice due to neuronal apoptosis (Barnes et al., 1998, Z. Li et al., 1995), and patients with mutations in DNA Ligase IV are radiosensitive and have developmental delay (Girard et al., 2004).

XRCC4 has been shown to interact with DNA, DNA-PK$_{CS}$ and the KU complex suggesting they aid the recruitment of LX to the site of the DSB (Hsu et al., 2002, Modesti et al., 1999, Nick McElhinny et al., 2000). Effective ligation will only occur however, in the presence of both the KU complex and DNA-PK$_{CS}$, however DNA- PK$_{CS}$ mediated phosphorylation of LX seems dispensable for its ligation activity (Calsou et al., 2003). Should the DNA ends not be fully compatible and need the addition of extra bases, DNA polymerase mu has been shown to add nucleotides in a template independent manner (Gu et al., 2007a).

More recently another protein has been identified which interacts and aids the LX complex. It was originally isolated in a patient who exhibited radio-sensitivity symptoms which could not be complemented with any known NHEJ factors (Dai et al., 2003). In 2006, two independent groups published their results on this protein and its role in NHEJ and it was given the name XLF (Ahnesorg et al., 2006, Buck et al., 2006). XLF has weak sequence homology with XRCC4 but is predicted to be structurally similar. Its suggested role in NHEJ is to act as a heteromultimer with XRCC4 to promote and stimulate the ligase activity of DNA Ligase IV (Ahnesorg et al., 2006).

1.1.3.3 DNA Double Strand Break Repair Pathway Choice

As NHEJ is active throughout the cell cycle, both the HR and NHEJ pathways are available for DSB repair during the late S to G2 phases of the cell cycle. Studies in avian cells suggest the protein CTIP, which is present in both pathways, controls the choice between the two pathways. As cells enter S-phase of the cell cycle, phosphorylation of CTIP at serine 327, a

weak CDK consensus site, results in the recruitment of BRCA1 (Yu and Chen, 2004, Yun and Hiom, 2009). Studies with BRCA1 deficient human cancer cells lines show an inability to repair breaks by HR, which can be fully complemented with the addition of wild-type BRCA1 protein (Moynahan et al., 1999, Scully et al., 1999). This evidence suggests that the recruitment of BRCA1 could be the key decider in favouring HR.

53BP1 has been shown to prevent the resection of DNA to form ssDNA tails which is an absolute requirement for HR, demonstrating that 53BP1 favours NHEJ (Bunting et al., 2010). This suggests a model whereby 53BP1 is able to prevent HR and favour NHEJ. However, during the late S and G2 phases of the cell cycle, phosphorylated CTIP is able to recruit BRCA1 to the sites of DSBs. BRCA1 is then able to promote HR, potentially by alleviating 53BP1's inhibitory effect (Figure 1.8; Boulton, 2010). These interactions however, are unconfirmed in mammalian systems.

Incidentally, there are conflicting reports about the involvement of BRCA1 during NHEJ. *In vitro* studies using cellular extracts depleted in BRCA1 by targeted antibodies, show inhibition of DNA end-joining, as do BRCA1-deficient mouse embryonic fibroblast cellular extracts (Zhong et al., 2002). However, *in vivo* studies using pulse field gel electrophoresis show no difference between wild type cells and a human breast cancer cell line expressing a non-functional BRCA1 protein (H. Wang et al., 2001).
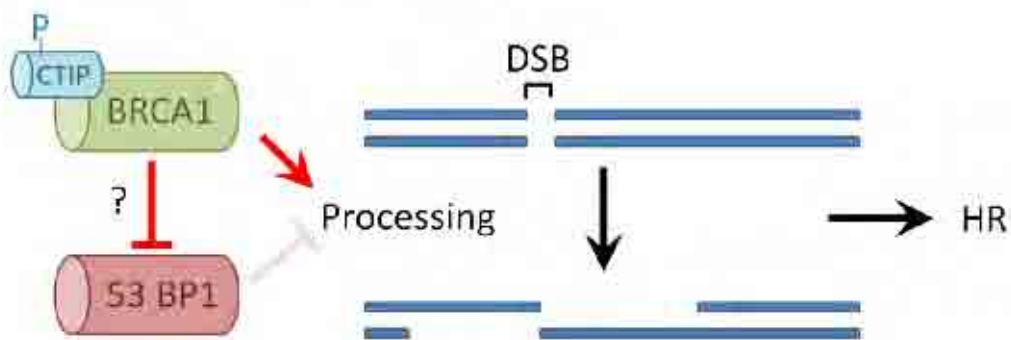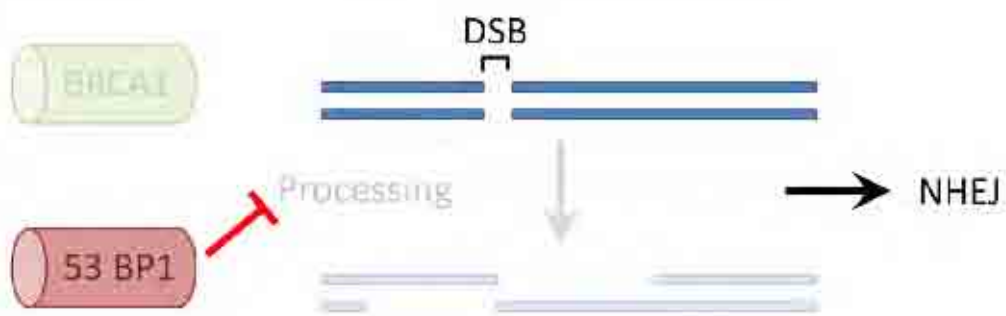
Figure 1.8 – Model for deciding which pathway will repair DSBs.
a. Under normal circumstances, during late S to G2 phases of the cell cycle, BRCA1 is recruited to the sites of DSB by phosphorylated CTIP. BRCA1 is able to then promote repair by HR and potentially inhibit 53BP1's ability to prevent DNA resection.
b. When BRCA1 is not present at the site of a DSB, during any stage of the cell cycle excluding late S to G2, 53BP1 prevents the resection of DNA to produce ssDNA, therefore repair of the DSB is by the NHEJ pathway.
Image modified from Boulton, 2010.

1.2 Chromatin

In eukaryotic genomes, DNA is organised in a nucleoprotein complex known as chromatin. The fundamental repeating unit of eukaryotic chromatin is the nucleosome (Kornberg and Thomas, 1974, Olins and Olins, 1974, Oudet et al., 1975). A nucleosome is the packaging of 145bp – 147bp of DNA wrapped around an octamer of histone proteins, occurring every 200 ± 40bp throughout all eukaryotic genomes (Figure 1.9). The histone octamer consists of 2 copies of the H2A, H2B, H3 and H4 histones. Inter-nucleosomal DNA, termed the linker DNA, is bound by members of the linker histone family, also known as H1. The combination of the nucleosome, the linker DNA and the linker histone forms a structure known as the chromatosome (Simpson, 1978; Figure 1.10). It is believed that a more compact DNA structure, known as the 30nm fibre, is stabilised by the addition of linker histones, although there is currently no data to support this theory (Davey et al., 2002, Syed et al., 2010, Tremethick, 2007).

Core histone proteins, H2A, H2B, H3 and H4, are very small proteins ranging from 10-22kDa in size and are the most naturally occurring basic proteins known (Lindner, 2008). Their structure consists of folded globular domains, known as the histone fold domain. The histone fold domain consists of three alpha helices connected by two loops which interact with DNA and are required for the structural organisation of the nucleosome. The histone fold domains account directly for the organisation of 121bp of DNA, with approximately 27-28bp of DNA per histone fold (Luger et al., 1997). Binding to the DNA occurs via the

phosphodiester backbone, with each helical turn providing two consecutive phosphate groups to hydrogen bond with the histone fold pairs.

Core histones also consist of amino-terminal tails which extend from the nucleosome (Davey et al., 2002, Hacques et al., 1990, Luger et al., 1997). The amino-terminal tails are extremely basic due to their high numbers of lysine and arginine residues, and are subject to post translational modifications (PTM). For example, lysine residues can be acetylated, lysine and arginine residues can be methylated, serine, threonine and tyrosine residues can be phosphorylated and lysine residues can be ubiquitylated. These modifications rarely occur singularly and solely, with different types and multiple modifications typically occurring, making up what is known as the epigenetic code (for review, see Turner, 2007)

The epigenetic code is extremely complex as the number of modifications per nucleosome can be very large. A single chromosome can contain up to as many as 500,000 nucleosomes which can lead to many epigenetic permutations (Luger and Richmond, 1998). The epigenetic code is also not as straightforward as the genetic code, where it is known exactly which DNA triplet codes for which amino acid (Lodish et al., 2007). There are conflicting arguments for the exact purpose of the modifications. Some evidence suggests that the modifications themselves alter the conformation of the nucleosome, allowing proteins to access the otherwise restricted DNA (Ruthenburg et al., 2007). Alternatively it is thought that the DNA is always accessible but proteins have nothing to bind to, and it is these modifications which provide that docking station (Ruthenburg et al., 2007).
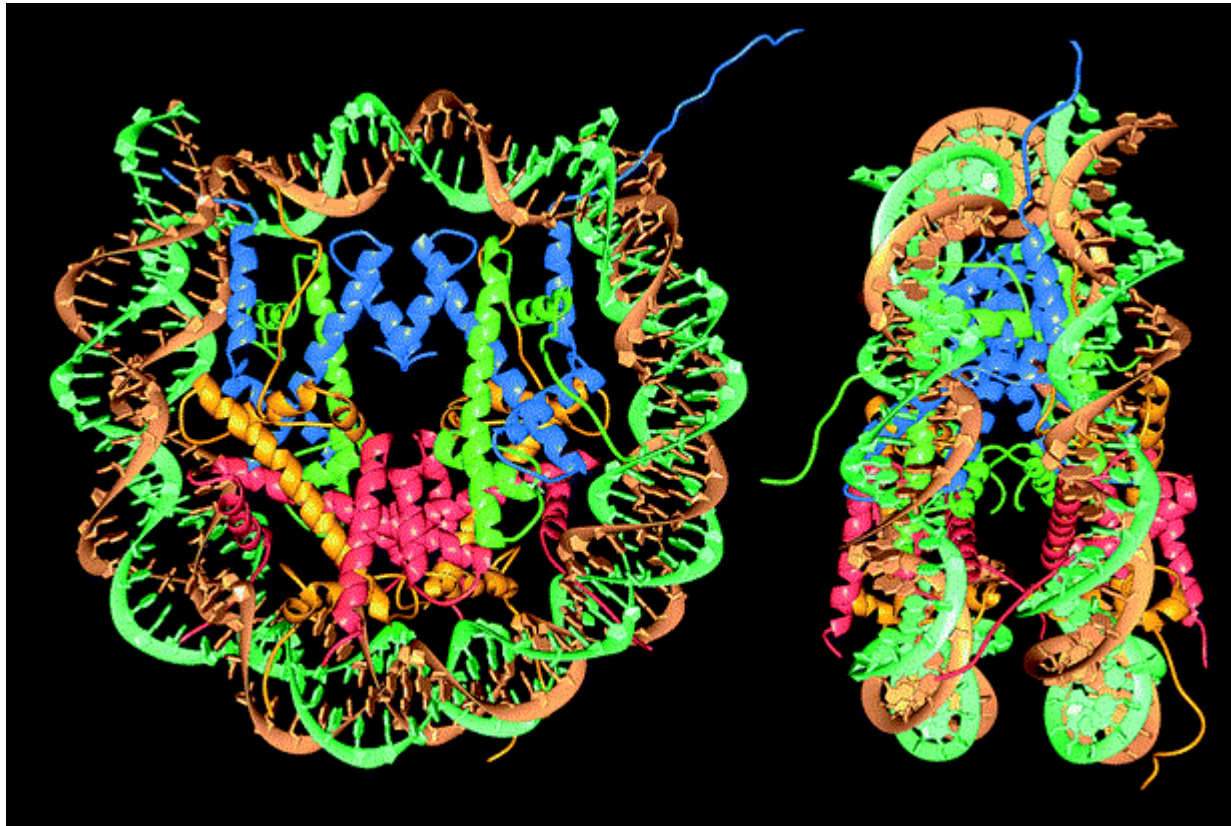
Figure 1.9 - Crystal Structure of the Nucleosome at 2.8Ä
The crystal structure of the nucleosome particle at a resolution of 2.8Ä. The phosphodiester backbones is highlighted in brown and turquoise, core histone H3 coloured blue, H4 coloured green, H2A coloured yellow and H2B coloured red. Image taken from Luger et al., 1997.
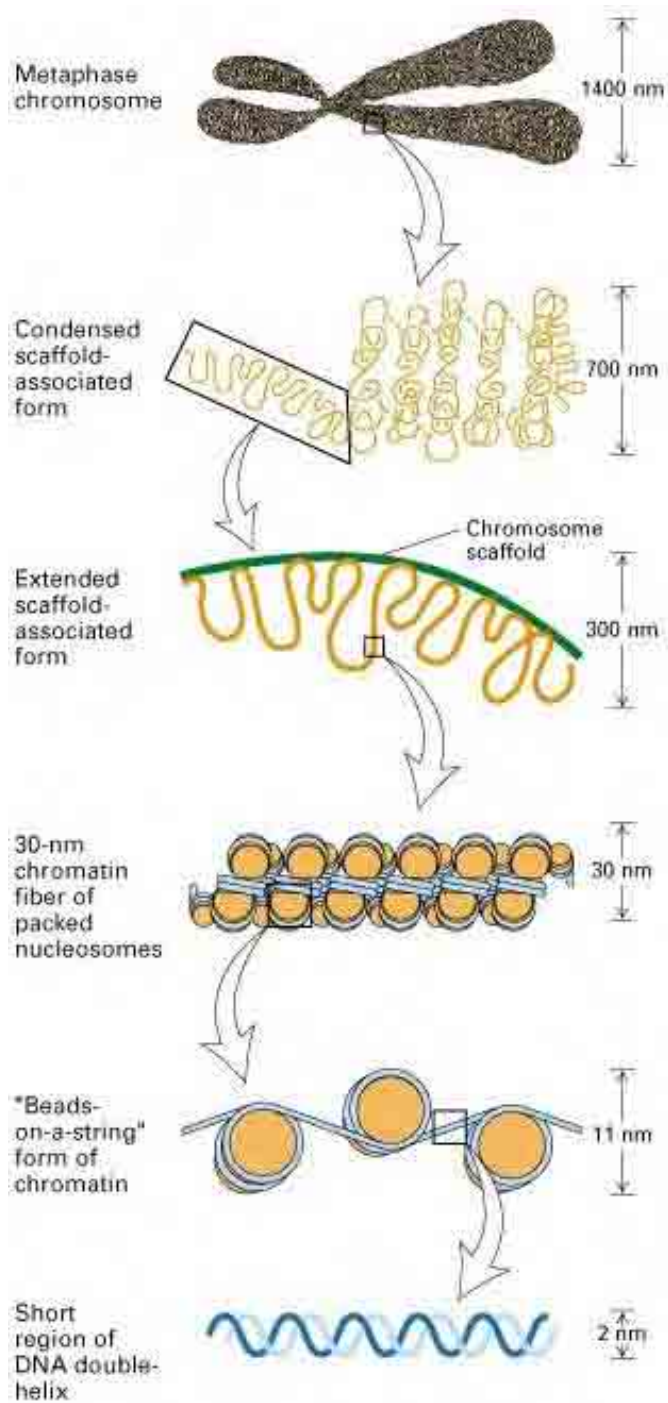
Figure 1.10 - Chromatin - The Nucleosome, Chromatosome, Chromatin and the Chromosome
146bp of DNA is bound by an octamer of core histones, two of the H2A, H2B, H3 and H4 histones, to form the nucleosome of 11 nm. The elusive 30 nm fibre is formed when the linker DNA is bound by the linker histones which are believed to compact the DNA further. Binding of the 30 nm fibre to a chromosomal scaffold aids the further condensation to achieve the metaphase chromosome, the ultimate condensed form of DNA (Taken from Lodish et al., 2007).

Linker histones bind the inter-nucleosomal DNA and are believed to mediate 30nm chromatin fibre formation (Sinha and Shogren-Knaak, 2010). Linker histones have a tripartite structure consisting of an unstructured amino terminal domain (NTD) and CTD of sizes 13-40 amino acids and ~100 amino acids respectively, and a well folded central globular domain of about 80 amino acids (Hartman et al., 1977; Figure 1.11).

The globular domain of the linker histone is expected to interact with DNA as it contains at least 2 separate DNA binding sites: a classical winged helix motif (Figure 1.11, site 1) and a cluster of conserved basic residues (Figure 1.11, site 2; Ramakrishnan et al., 1993). Binding of the globular domain to the DNA occurs at, or near to, the nucleosomal dyad contacting with at least two strands of DNA (Figure 1.12; Duggan and Thomas, 2000, Goytisolo et al., 1996). Site 1 of the globular domain interacts with DNA close to the nucleosomal dyad. Lysine69, lysine71 and arginine74, contained within site 1, are suggested to fit in to the major groove of the DNA, with histidine25, lysine47 and lysine85 positioned to interact with the DNA backbone (Figure 1.11 & Figure 1.12; Brown et al., 2006). Site 2 of the globular domain interacts with one of the entering-and-exiting strands of linker DNA (Figure 1.11 & Figure 1.12; Brown et al., 2006). The globular domain also protects the chromatosome from nuclease digestion, with crucial residues likely to influence the condensation of chromatin (Noll and Kornberg, 1977, Travers, 1999).
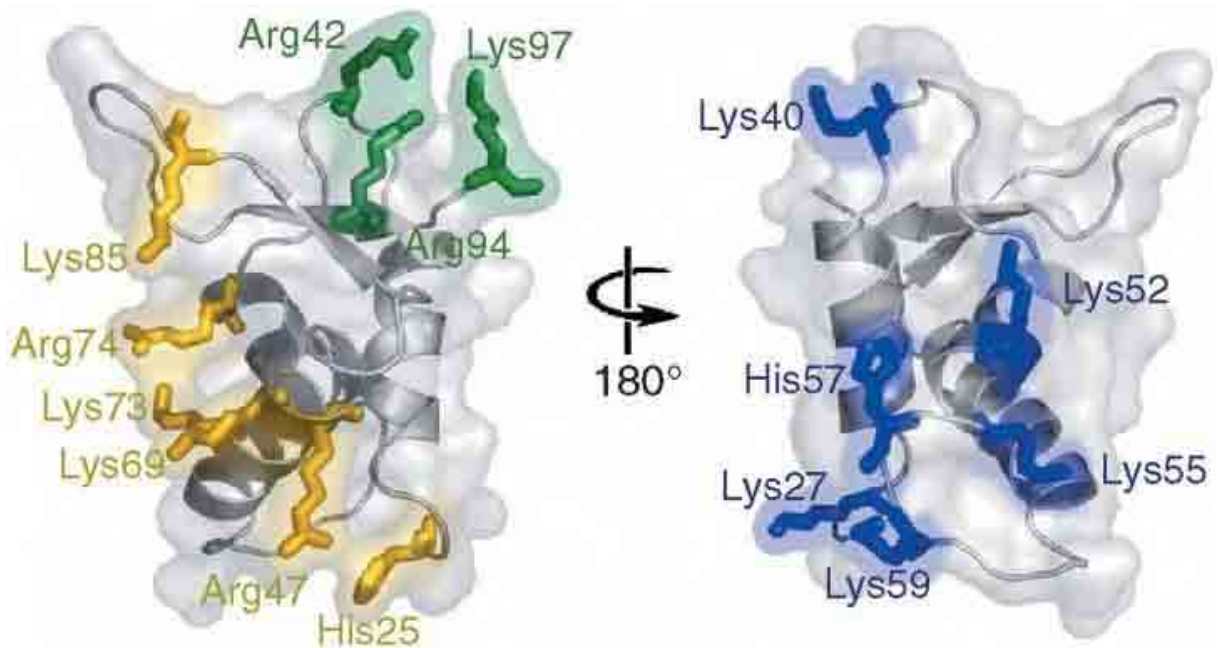
Figure 1.11 – Basic and crystal structure of a linker histone

Top. The basic structure of a linker histone consists of a short amino terminal domain (NTD) of 13-40 amino acids long, a central globular domain of about 80 amino acids long, and a carboxyl terminal domain (CTD) of approximately 100 amino acids long.

Bottom. The crystal structure of the globular domain of histone H5 with crucial residues mapped. The green cluster represents binding residues in site 1, the green cluster represents binding residues in site 2. The blue cluster represents those residues not contributing to binding affinity, and is positioned on the opposite side of the globular domain to sites 1 and 2. Image taken from Brown et al., 2006.
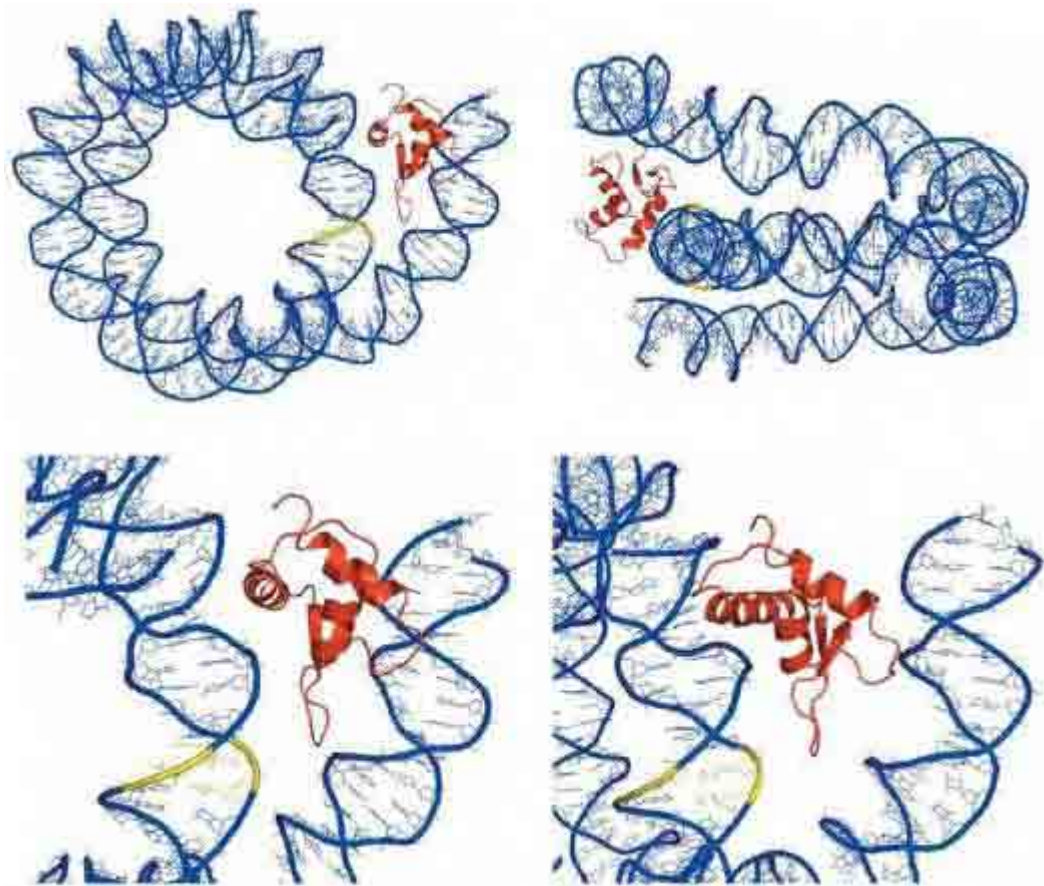
Figure 1.12 - Molecular model of the linker histone within the nucleosome
Molecular model showing the positioning of the linker histone within the nucleosome, along with its contacts with DNA. Nucleosomal DNA shown in blue, nucleosome dyad shown in yellow, globular domain of linker histone shown in red. Image taken from Brown et al., 2006.

Linker histones in chromatin determine the trajectory of the entering-and-exiting DNA, and are also likely to direct the position of successive nucleosomes, along with nucleosome-nucleosome interactions (Sivolob and Prunell, 2003). The structure of the 30nm fibre is hotly debated, with two potential models proposed: the one-start solenoidal helix, where a linear array of nucleosomes are coiled (Finch and Klug, 1976); and the two-start helix, where nucleosomes are assembled in a zig-zag ribbon (S. P. Williams et al., 1986, Woodcock et al., 1984).

Recent crystal structure data of a tetranucleosome has provided evidence of a two-start helix, although the crystals produced in the study were devoid of the linker histones (Schalch et al., 2005). Another study using arrays capable of holding over 50 nucleosomes with varying repeat lengths of 177-207bp and in the presence of one linker histone per nucleosome revealed fibres of diameter 33-34nm, with a nucleosome packaging ratio of ~11 nucleosomes per 11nm (Robinson and Rhodes, 2006). The data presented supports the one-start solenoidal helix, the alternative model to that seen by Richmond and colleagues, although the differences seen by Richmond and colleagues could be due to the absence of the linker histone in their studies (Robinson and Rhodes, 2006, Schalch et al., 2005).

The CTD of the linker histone, which is extremely rich in lysine residues, has also been shown to bind the linker DNA and facilitate the higher order packaging of the 30nm fibre (Allan et al., 1986). There has been no direct function associated with the NTD of the linker histones, however it is hypothesised that the NTD can facilitate protein-protein interactions through PTMs (McBryant et al., 2010). Evidence for this is seen in the NTD of human H1.4 where

lysine 26 can be methylated. Once methylated it can be recognised by HP1, however, this interaction can be blocked by the phosphorylation of the adjacent serine residue (serine 27) creating what the authors call a "phospho switch" model (Daujat et al., 2005).

1.2.1 Core Histones

Although the core histones are often referred to as H2A, H2B, H3 and H4, there are many variants which have very specific roles within the cell (Table 1.1).

Core Histone	Histone Variants
H2A	H2A.1
	H2A.1A-E & H
	H2A.2A-C
	H2A.3
	H2A.J
	H2A.V
	H2A.X
	H2A.Z
	H2A.Bbd
	Macro-H2A.1
	Macro-H2A.2
H2B	H2B1A-D, H, J, K-O
	H2B2E-F
	H2B3B
	H2BFS
H3	H3.1
	H3.2
	H3.3
	H3.1t
H4	

Table 1.1 - Core histones and histone variants
List of core histones and the variants associated with each of the core histones. Adapted from Lindner, 2008 and the NCBI database.

There are 18 H2A variants, with only slight differences seen between them (Table 1.1). H2A.1, H2A.1A-E, H2A.1H, H2A.2A-C, H2A.3, and H2A.J are all very similar with only a few amino acid differences between them (Figure 1.13). H2A.X, although being very similar to the previous mentioned group, has a carboxyl-terminal extension of 10 amino acids containing a conserved serine residue which is rapidly phosphorylated following DSB induction (Figure 1.13, red box; Section 1.1.2.4). H2A.X makes up approximately 10% of the total H2A within chromatin, which suggests that it is present in at least one in every 5 nucleosomes (West and Bonner, 1980). H2A.V and H2A.Z have more differences compared to the previously mentioned H2A variants, however between them they share very similar sequences (Figure 1.13). H2A.Bbd was originally identified due to its exclusion from the inactive X chromosome (known as the Barr body) and is associated with active areas of chromatin. The H2A.Bbd variant is very different from all other H2A variants, and is the shortest of all with 115 amino acids, compared to 128-143 for the other variants (Figure 1.13). There are also two exceptionally large H2A variants, macro-H2A.1 & 2, which are both three times the size of the other H2A variants, however, sequences are conserved around the globular domain (Figure 1.13).

H2A variants have a region which is postulated to interact with the amino terminal tail of histone H4 to promote chromatin condensation and 30nm fibre formation, this region is known as the acidic patch (Sinha and Shogren-Knaak, 2010; Figure 1.13, region highlighted a). H2A.Z has a small but noticeable extension of this acidic patch which results in the tighter compaction of chromatin. This is reflected in the deposition of H2A.Z into areas that are transcriptionally inactive, namely heterochromatin (J. Y. Fan et al., 2004). H2A.Bbd lacks the

acidic patch, resulting in less tightly bound chromatin, and is postulated to inhibit the 30nm fibre formation (J. Zhou et al., 2007). The H2A-H4 interaction can also be abolished by the acetylation of H4 lysine16, leading to fibre unfolding (Shogren-Knaak et al., 2006).

H2A.Bbd is significantly shorter than the other H2A variants, containing a shorter docking domain lacking the residues which interact with H3 (Y. Bao et al., 2004, Chadwick and Willard, 2001). H2A.Bbd also has an NTD differing from the other H2A variants, containing a row of 6 arginine residues and no lysine residues whatsoever (Y. Bao et al., 2004, Gautier et al., 2004). Studies show H2A.Bbd co-localises with regions of H4 acetylation during interphase and metaphase, a mark prominently seen in transcriptionally active euchromatin (Chadwick and Willard, 2001). Further evidence for H2A.Bbd's presence in relaxed chromatin includes GFP tagged H2A.Bbd being exchanged more quickly than GFP tagged H2A in vivo (Gautier et al., 2004) and DNAse I digestion of nucleosomes containing H2A.Bbd exhibiting more frequent random cutting compared to canonical nucleosomes (Okuwaki et al., 2005). Nucleosomes containing H2A.Bbd were also found to bind 130bp DNA, in contrast to the 147bp bound in canonical nucleosomes, allowing a free 10bp of DNA at each end of the nucleosome, further supporting its role in a more relaxed chromatin structure (Doyen et al., 2006).
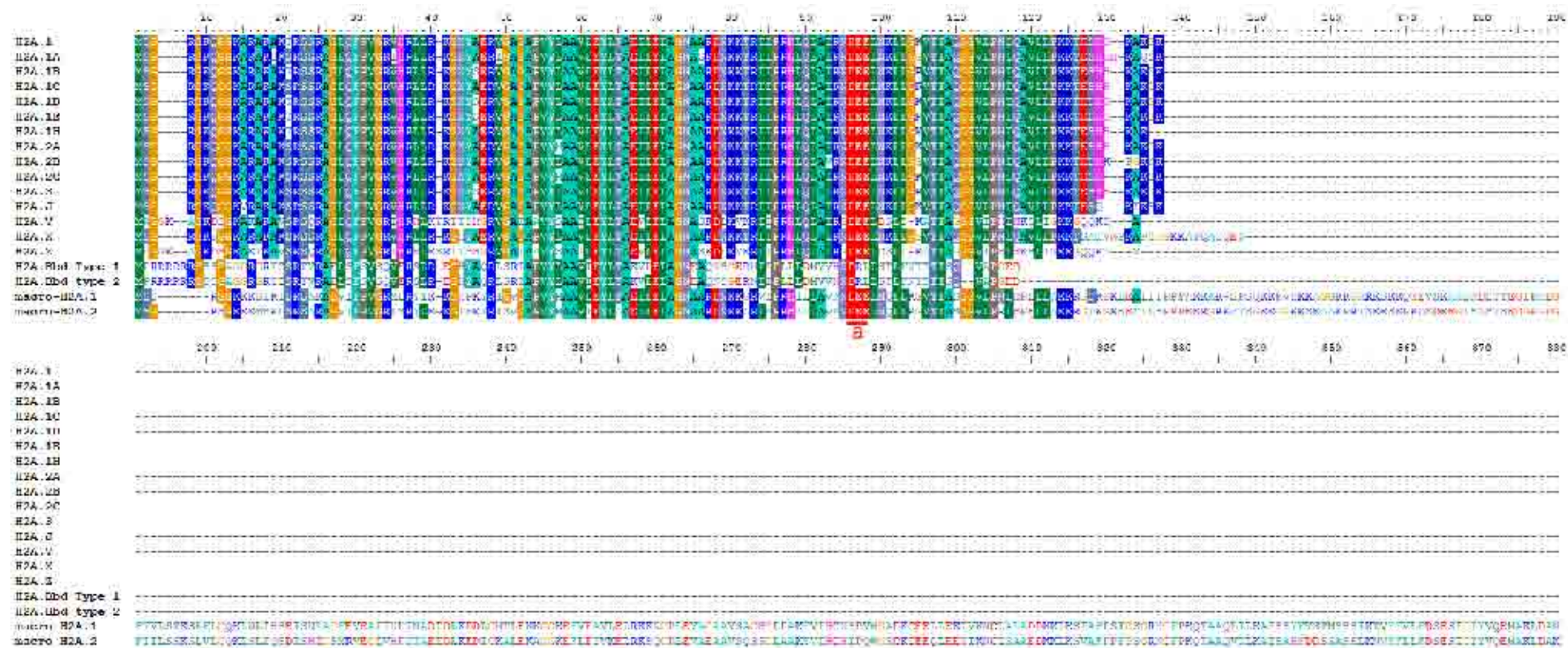
Figure 1.13 - Sequence alignment of H2A variants

H2A variants were aligned to show both similarities and differences. H2A.1 to H2A.J show striking similarities, with only the occasional differences seen. H2A.V and H2A.Z are similar to each other, but less similar to the previous group. H2A.Z shows an extension to the acidic patch (highlighted with red a). H2A.X is very similar to the first group of H2A variants, however has an extension of the CTD which contains a conserved phosphorylation site (boxed in red). Both H2A.Bbd variants are much smaller than the other H2A variants and also display little sequence conservation. Both macro-H2A variants also display low levels of sequence conservation, but are over twice the size of all other H2A variants. Sequences were aligned using ClustalW program (www.ebi.ac.uk). Key - Alanine, Tyrosine and Phenylalanine, Glycine, Proline, Serine and Threonine, Aspartic acid and Glutamine acid, Tryptophan, Histidine, Lysine and Arginine, Isoleucine, Leucine, Methionine and Valine, Asparagine and Glutamine and Cysteine

H2A.Z is a highly evolutionary conserved variant of H2A which is reflected in its requirement for viability in a range of species including the ciliated protozoan *Tetrahymena thermophila* and *Mus musculus* (Faast et al., 2001, X. Liu et al., 1996). H2A.Z is incorporated into heterochromatic nucleosomes and aids the compaction of DNA. However, contrasting reports state that H2A.Z is also deposited into nucleosomes at the sites of transcription, typically euchromatin, where it efficiently promotes RNA polymerase 2 recruitment (Adam et al., 2001). A comprehensive review on the complex roles of H2A.Z is reported in Draker and Cheung, 2009.

1.2.2 Linker Histones

The number of linker histone variants, varies between species, for example, *Saccharomyces cerevisiae* and *T. thermophila* have only one linker histone whereas humans have 11 variants ((Johmann and Gorovsky, 1976, Landsman, 1996 and Section 1.2.3). Knocking out the linker histone in *T. thermophila* shows no effect on viability or growth, just a slightly enlarged nucleus (Shen et al., 1995). *S. cerevisiae* strains with a disruptive mutation in the linker histone gene HHO1 also showed no detectable defects in chromatin structure, transcriptional silencing or growth rates compared to the wild type, however they were shown to have a reduced life span (Downs et al., 2003, Patterton et al., 1998, Ushinsky et al., 1997). Wild type strains did show that the linker histone is inhibitory to HR in *S. cerevisiae*, potentially by occluding binding sites for HR proteins. Inhibition of HR impacts on the recombination-dependent mechanism of telomere maintenance, which could explain the reduced life span (Downs et al., 2003). Genome-wide microarray studies in the HHO1 mutant

yeast showed that expression of only 27 out of 6216 genes tested were affected significantly (Hellauer et al., 2001). Surprisingly all of these genes were down-regulated, contradicting the typical view of histone proteins repressing transcription.

1.2.3 Mammalian Linker Histone Variants

In mammals there are 11 H1 variants (Figure 1.14). One of these variants, H1.Foo, is oocyte specific (Tanaka et al., 2001), and 3 variants are testis-specific, H1.t (Drabent et al., 1993), H1.t2 (Martianov et al., 2005) and HILS1 (W. Yan et al., 2003). Gamete-specific linker histone variants replace the somatic linker histone variants during meiotic prophase and are replaced with transition proteins after meiosis (Pradeepa and Rao, 2007). Knockout studies of H1.Foo suggest they are crucial for oocyte maturation (Furuya et al., 2007), however H1.t null sperm remained viable with H1.1 compensating for its absence (Lin et al., 2004).

The remainder of the linker histone variants, the somatic linker histone variants, can further be subdivided into those which are replication-dependent and those which are replication-independent. The former is made up of H1.1, H1.2, H1.3, H1.4 and H1.5 (Albig et al., 1997) and are expressed in S-phase of the cell cycle, the latter is made up of H1.0 (Panyim and Chalkley, 1969) and H1.X (Happel et al., 2005) which are expressed during the whole cell cycle.

Alignment of the linker histone protein sequences shows that the gamete-specific linker histone variants are very different from one another with the greatest similarity score of

22% between H1.Foo and H1.t (Appendix A). The gamete-specific linker histone variants also share very little similarity to the somatic linker histone variants, with the exception of H1.t which has a slightly higher similarity score represented by its greater conservation of the globular domain compared to the other gamete-specific linker histone variants (Appendix A and Figure 1.14).

Replication dependent linker histone variants are all very similar to each other and have high similarity scores with extremely high conservation in their globular domains. The variation between them however, is seen in the CTD and NTDs (Appendix A and Figure 1.14). Similarities between the replication dependent and replication independent linker histone variants are low due to reduced conservation of the globular domain (Appendix A and Figure 1.14).

Linker histones are often collectively referred to in the literature as H1. However, the variants are structurally very different to one another, and it is these differences which allow specific linker histone variants to play key unique roles within the cell.
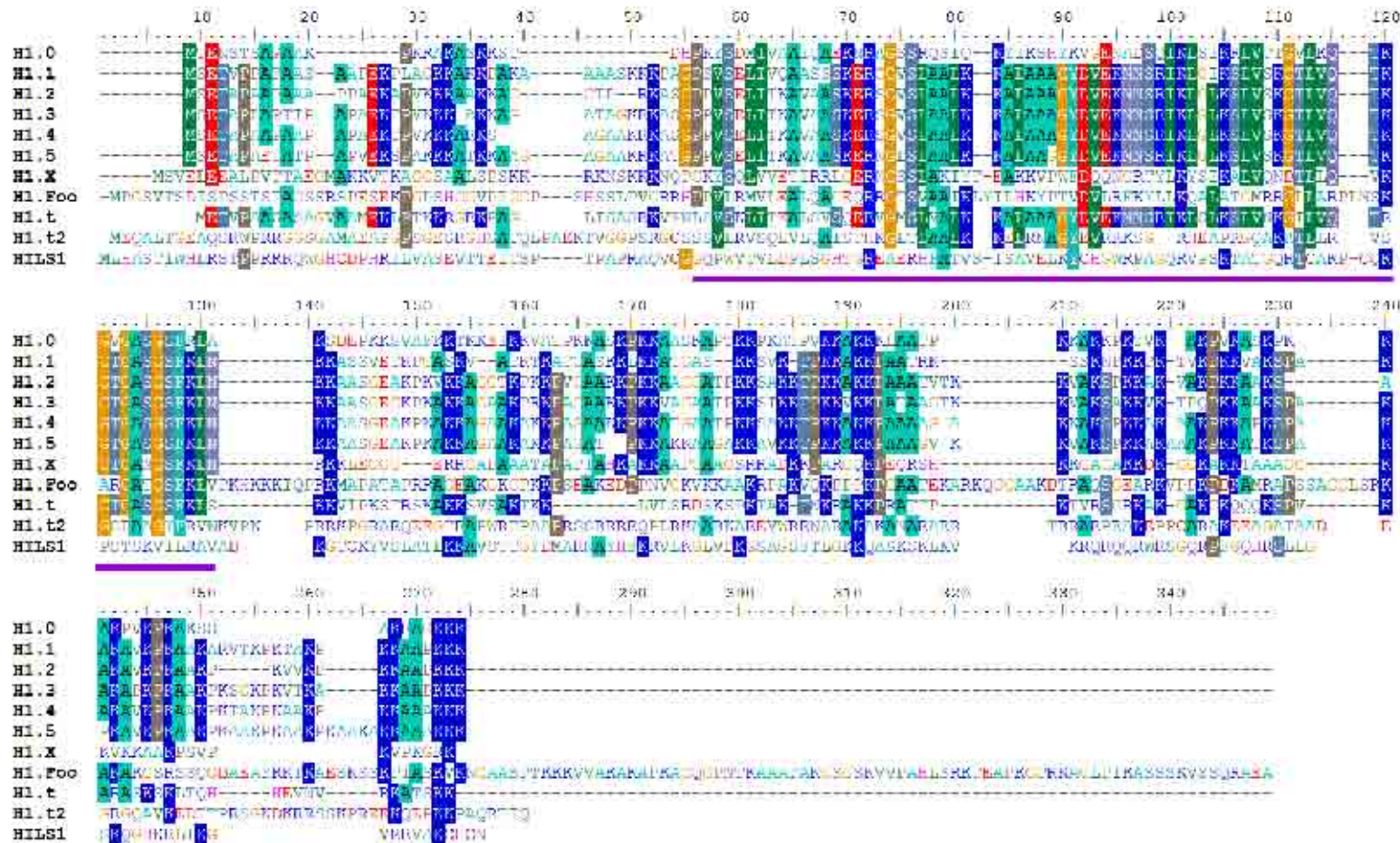
Figure 1.14 – Sequence alignment of all human linker histone variants

Mammalian linker histone variants were aligned to show sequence similarities and differences. H1.1 through to H1.5 are very highly conserved over the globular domain, underlined in purple. There is a low level of sequence conservation amongst this group and the rest of the linker histones, with HILS1 being the least similar. Sequences were aligned using ClustalW program (www.ebi.ac.uk). Accession numbers are in Appendix B. Key - Alanine, Tyrosine and Phenylalanine, Glycine, Proline, Serine and Threonine, Aspartic acid and Glutamine acid, Tryptophan, Histidine, Lysine and Arginine, Isoleucine, Leucine, Methionine and Valine, Asparagine and Glutamine and Cysteine.

Linker histone H1.1 has been shown to be crucial for *Caenorhabditis elegans* germline proliferation and differentiation in the hermaphrodite, whilst depletion of other linker histone variants were shown to have no effect (Jedrusik and Schulze, 2001). In humans, H1.1 also has the most restrictive tissue specificity, only being found in the thymus, spleen, lymphocytes, neuronal cells and the testis (Godde and Ura, 2008). Although being classed as a somatic linker histone, this variant is also predominant in germ cell chromatin during early spermatogenesis, being replaced by the gamete specific linker histone H1.t during meiosis (Franke et al., 1998).

H1.2 has been shown to induce apoptosis following exposure to IR due to the p53-mediated release of H1.2 into the cytoplasm leading to cytochrome c release and mitochondria mediated apoptosis (Section 1.1.1.4). Although all linker histone variants are released into the cytoplasm following IR, it is specifically H1.2 which induces this apoptotic response. It is suggested that this could possibly be to a lack of a KXXKP motif in the CTD (Konishi et al., 2003). However, analysis of the CTD of H1.2 and the other linker histone variants shows that H1.1, H1.2 and H1.5 have 4 KXXKP motifs, H1.3 has 5 and H1.4 has 6, although the penultimate KXXKP motif is absent in H1.2 (Figure 1.14).

Studies in a human breast cancer cell line, T47D, show that H1.2 depletion causes cell cycle arrest at the G1 phase of the cell cycle, along with the reduced expression of selected cell cycle genes including CDC2, CDC23 and AURKB (Sancho et al., 2008). Further studies in the same cells highlight the importance of a single linker histone variant, H1.4, on the survival of the breast cancer cell line. A high level of mortality was seen in these knock-down cells,

however, this was not attributable to apoptosis (Sancho et al., 2008). Interestingly, mouse embryonic stem cells deficient in H1.2, H1.3 and H1.4 (H^{234}) show an increased resistance to IR and the alkylating agent methyl methanesulfonate (MMS; Murga et al., 2007).

Linker histones, like core histones, can harbour a range of PTMs (Wisniewski et al., 2007) resulting in their own linker histone code (reviewed in (Godde and Ura, 2008)). The most studied of the linker histone PTMs is phosphorylation. During mitosis, linker histones are progressively phosphorylated with the peak phosphorylation at the G2/M phase of the cell cycle, however the exact function of these phosphorylation marks remains elusive (Talasz et al., 1996). Phosphorylation of linker histones occurs at (S/T)PXK motifs which are recognised by the cyclin dependent kinases (CDKs; Deterding et al., 2008). A novel phosphorylation site was recently found on H1.5 which undergoes 5 phosphorylation events during mitosis, of which 4 are at known CDK sites (Sarg et al., 2006). The novel site, TPAP, was found to be phosphorylated by glycogen synthase kinase-3 which has been shown to phosphorylate other targets involved in the cell cycle (Happel et al., 2009).

H1.0 was originally identified in terminally differentiated cells (Panyim and Chalkley, 1969). It can however, be detected in mice oocytes and embryos up to the four-cell stage. At this point the levels of H1.0 become undetectable and it is replaced by other somatic linker histone variants (Fu et al., 2003). Knockout studies in mice have also shown that although it is the predominant linker histone in early embryogenesis, it is not essential for embryogenesis with viable offspring having other linker histones compensating for its loss (Y. Fan et al., 2001, Sirotkin et al., 1995). H1.0 shares very little sequence homology with the

other linker histone variants, in fact, it is more homologous to the avian histone H5 ((Zlatanova and Doenecke, 1994, Appendix A and Figure 1.14).

The most recently identified linker histone is H1.X (Happel et al., 2005). This histone shuttles between nuclear compartments during the cell cycle. During the G1 phase of the cell cycle, H1.X resides predominantly in the nucleoli, whereas at the end of the G1 phase, H1.X spreads to the nucleoplasm (Stoldt et al., 2007). Experiments depleting the levels of H1.X have suggested that it is required for correct mitotic progression with defects seen in chromosome alignment, chromosome segregation and spindle morphology (Takata et al., 2007). Interestingly, H1.X has been found to be over-expressed in human neuroendocrine tumours, although the authors do not suggest a reason for these elevated levels (Warneboldt et al., 2008).

Viability studies in mice have shown that individual linker histone variants are dispensable for survival with only subtle changes in gene expression (Y. Fan et al., 2001). Examination of the chromatin in these knock-out mice showed that other linker histone variants compensate for individual loss, maintaining a normal H1 to nucleosome stoichiometry. Double knockout mice showed the same effects as the single knockouts, however after three histone genes were knocked out (H1.2, H1.3 and H1.4) no embryos survived past embryonic day E11.5 (Y. Fan et al., 2003, Y. Fan et al., 2001). Furthermore, embryonic stem cells taken from these embryos exhibit a massive reduction in the total amount of linker histone, ~50% of the normal ratio of linker histones to nucleosomes (Y. Fan et al., 2003).

Chromatin binding studies have shown that H1.2, H1.3 and H1.4 linker histone variants extracted from mouse liver tissue have the highest binding affinities to DNA which could explain their necessity in mice (Talasz et al., 1998). However, studies from different species show differences in the DNA binding affinities. H1.3 and H1.4 have the highest binding, followed by H1.5 and H1.2 with intermediate binding and H1.1 with the lowest binding to nucleosomal arrays of linker histone variants extracted from rat brain tissue (Orrego et al., 2007). Whereas, *in vivo* studies in human cells using GFP tagged linker histone variants and Fluorescence Recovery After Photobleaching (FRAP) show that H1.4 and H1.5 have the highest DNA binding, H1.3 has intermediate DNA binding and H1.1 and H1.2 have the lowest DNA binding (Th'ng et al., 2005).

1.3 Chromatin and the DNA Damage Response

It is widely accepted that DNA recombination, DNA replication, mitotic condensation, transcription and DNA repair all involve the interaction with chromatin, and are ultimately affected by its structure (Cairns, 2009, Mendez-Acuna et al., 2010, Ransom et al., 2010, van Attikum and Gasser, 2005, L. Zhang et al., 2009). All of these processes require the chromatin structure to be temporarily removed, allowing the required proteins access to the DNA.

It is currently unclear as to how the condensed chromatin structure becomes relaxed upon events such as DNA repair. A model proposed by Stewart (2009) suggests that following the poly-ubiquitylation of H2A histones by RNF8 and RNF168, other 'hidden' epigenetic marks on

chromatin become visible (Stewart, 2009). One of these marks, di-methylation of the core histone H4 on lysine 20 is proposed to be inaccessible in condensed chromatin. Following DNA damage by IR and the subsequent chromatin relaxation around the break, these marks are thought to become accessible. One protein, 53BP1 (Section 1.1.2.6), has a very high affinity for di-methylated lysine 20 on histone H4 and plays a part in the stabilisation of 53BP1 at the sites of DSBs (Botuyan et al., 2006).

Three recent studies have highlighted the importance of linker histone variants during DNA repair, specifically DSB repair. A linker histone mix, extracted from calf thymus tissue, was shown to strongly inhibit DNA end joining *in vitro* (Kysela et al., 2005). Following phosphorylation of the linker histone mix, however, DNA end joining is restored, possibly due to the reduced affinity of linker histones for DNA (Dou et al., 2002, Green et al., 1993, Kysela et al., 2005, Roque et al., 2008, Th'ng et al., 1994). Another study showed that a linker histone mix could mildly stimulate DNA end joining when used at lower levels to the previous study. However, when using DNA ligase III, DNA end stimulation was significantly higher. Further work in this study showed that H1.2 was the linker histone responsible for the stimulation (Rosidi et al., 2008). Another study using chicken DT40 cells with individual linker histones knocked out shows a crucial role for H1.R in survival following MMS treatment. Results in the study fail to ascertain exactly how H1.R is involved in DNA repair, however the authors suggest that it may be required for accessibility or efficiency of repair proteins (Hashimoto et al., 2007).

The data presented by Kysela *et. al.* highlights the importance of linker histones during LX-mediated DNA ligation, and specifically as a target of DNA phosphorylation by DNA-PK, both important processes of the NHEJ pathway (Kysela et al., 2005). This highlights the necessity to ascertain the role the linker histone family have during DNA repair, and specifically NHEJ.

CHAPTER TWO: MATERIALS AND METHODS

2.1 Suppliers

Unless otherwise stated, all chemicals were purchased from Sigma-Aldrich. Restriction endonucleases were purchased from New England Biolabs or Fermentas. Tissue culture plastics were ordered from Corning. Tissue culture reagents were ordered from PAA Labs. Radionucleotides were ordered from Perkin Elmer, oligodeoxyribonucleotides were ordered from Invitrogen and oligoribonucleotides were ordered from Eurofins-MWG. Antibodies were purchased from Abcam, Invitrogen, Sigma or Santa Cruz.

2.2 Cells and Cell Culture

2.2.1 MRC5VA Cells

MRC5VA cells were used throughout this thesis, they are an embryonic lung fibroblastic cell line immortalised by SV40 transformation.

2.2.2 Cell Maintenance

All solutions and equipment used in cell maintenance were either obtained sterile or autoclaved, where appropriate, prior to use. All cell culture work was undertaken in sterile conditions in a class 2 tissue culture hood (Holten LaminAir).

Cells were maintained in a humidified chamber (37°C, 5% CO_2, 95%; MCO-15AC, Sanyo) in $75cm^2$ cell culture flasks containing 10mL Dulbecco's Modified Eagle's Medium (DMEM;

containing 1000mg/L glucose) supplemented with 10% (v/v) foetal bovine serum (FBS), 2mM

L-glutamine, 1mM sodium pyruvate and 1% non-essential amino acids (Sigma-Aldrich)

(supplemented DMEM), and where applicable with an additional 600μg/mL G418 (G418

DMEM). Cells were seeded at a density of 1x10^6 cells/flask and routinely passaged on day 3.

2.2.3 Trypsinisation of Confluent Cells

Upon confluency of the cells, media was aspirated from the flask using a sterile pipette. Cells

were washed with 10mL of phosphate buffered saline (PBS; 2.7mM KCl, 137mM NaCl, 10mM

phosphate buffer, pH 7.4). PBS was aspirated and replaced with 3mL of trypsin-

ethylenediaminetetraacetic acid (EDTA; 0.25%:0.02%, 37°C). Flasks were placed in a

humidified chamber until the cells detached from the bottom (~3 minutes), sometimes

requiring gentle agitation. Following detachment, 7mL of supplemented DMEM was added

and the cell suspension gently mixed using a sterile pipette. The suspension was

subsequently transferred into a 15mL centrifuge tube (Falcon, Becton Dickinson Labware)

and centrifuged at 1,200 rpm for 5 minutes at 20°C. The supernatant was carefully aspirated

without disturbing the pellet, the subsequent pellet was either reseeded (Section 2.2.4),

frozen (Section 2.2.5), transfected (Sections 2.2.6 and 2.2.7), or used for protein

quantification (Section 2.3).

2.2.4 Cell Reseeding

For routine cell maintenance, trypsinised cell pellets were resuspended in 10mL of supplemented DMEM and $1x10^6$ cells were transferred to a $75cm^2$ cell culture flask containing 10mL of supplemented DMEM, or G418 DMEM where necessary. The flask was gently agitated to ensure an even distribution of the cells, and then placed in a humidified chamber and allowed to grow to confluency (~3 days).

2.2.5 Cell Cryopreservation

Trypsinised cell pellets were resuspended in 1mL FBS containing 10% (v/v) dimethyl sulphoxide as a cryoprotectant. The cell suspension was transferred into a 2mL cryovial (Nunc) and placed in a cryogenic freezing vessel (Mr. Frostie, Nalgene). The container was stored at $-80^{o}C$ overnight, after which the cryovials were removed and placed into liquid nitrogen for long-term storage.

2.2.6 Short Interfering RNA Transfection

Trypsinised cell pellets were resuspended in 10mL of supplemented DMEM, cells were counted and seeded according to manufacturer's instructions (Table 2.1). Twenty four hours later cells were transfected according to the manufacturer's instructions (Summarised in Table 2.1). Briefly, serum free DMEM was added to a sterile, RNAse free, labelled 1.5mL microcentrifuge tube. Short interfering RNA (siRNA) oligonucleotides (Table 2.2) were added to the serum free DMEM to a final concentration of $10\mu M$ and the tube was vortexed gently.

INTERFERin (Polyplus transfection; Table 2.1) was added to the siRNA duplex solution and vortexed immediately for 10 seconds. The microcentrifuge tube was left at room temperature for 10 minutes before being added to the cells with replenished supplemented DMEM. Alongside targeted knockdowns, a negative control targeted towards the *Photinus pyralis* Luciferase (LUC) gene and an un-transfected negative control were also used.

Vessel	Seeding density	Serum free DMEM	INTERFERin	Final Volume
6-well dish	150,000	200μL	8μL	2.2mL
25cm^2 Cell Culture Flask	400,000	400μL	15μL	4.4mL
75cm^2 Cell Culture Flask	1,000,000	500μL	40μL	10.5mL

Table 2.1 - siRNA Transfection Details
The three culture vessels used for all transfections are listed with the required initial seeding densities of the cells, the amount of serum free DMEM the siRNA oligonucleotides are diluted into and the amount of INTERFERin used per reaction.

Target Gene	Sequence
H1.2	5'-AAGAGCGUAGCGGAGUUUCUCTT-3' (21mer)
H1.X	5'-CCAAGAAGGUUCCGUGGUUTT-3' (19mer)
LUC	5'-CGUACGCGGAAUACUUCGATT-3' (19mer)

Table 2.2. List of siRNA oligonucleotides used for siRNA transfection.

2.2.7 Stably Transfected Cell Line Generation

To a labelled 1.5mL microcentrifuge tube, 98μL serum free DMEM and 3μL Fugene 6 transfection reagent (Roche) was added and mixed by gentle tapping. To this solution, 1μg of DNA was added and mixed gently by tapping, and left at room temperature for 15

minutes. This mixture was added to a well of a 6-well-plate containing 90% confluent cells in 2mL supplemented DMEM and placed in a humidified chamber. After 48 hours the cells were trypsinised as outlined in Section 2.2.3, the pellet resuspended in 10mL G418 DMEM and spread over three 10cm^2 Petri dishes containing G418 DMEM. The plates remained in a humidified chamber, with frequent media changes, for ~2 weeks to allow stably transfected isolated colonies to grow. Once colonies had begun to grow and contained ~150 cells they were scraped from the bottom of the Petri dish with a sterile 200μL pipette tip and transferred to a separate well in a 6-well plate containing G418 DMEM. The plates were placed in a humidified chamber and allowed to grow to 90% confluency before being transferred to a 75cm^2 cell culture flask. Individual colonies were assessed for transfection by Western blotting (Section 2.3) and immunofluorescence (Section 2.5) The flasks were kept in G418 DMEM to maintain a stable transfected population.

2.3 Protein Harvesting and Quantification

2.3.1 Mammalian Protein Extraction

Trypsinised cell pellets were washed with 5mL PBS and the resulting pellet resuspended in twice the cell pellet volume of RIPA buffer (50mM Tris/HCl pH7.5, 1mM EDTA, 150mM NaCl, 0.1% sodium dodecyl sulfate (SDS), 0.5% deoxycholic acid, 1% Igepal CA-360 (Mammalian Cell Lysis Kit, Sigma), and protease inhibitor cocktail (Roche)) and placed on ice for 20 minutes. The suspension was centrifuged at 13,000 rpm for 5 minutes at 4°C. The supernatant was carefully removed and placed into a fresh 1.5mL microcentrifuge tube.

Protein concentration was determined by the method of Bradford (Bradford, 1976), briefly, 1mL of 0.5x Bradford reagent was placed into a cuvette, to which 5μL of sample was added. Absorbance was read at 595nm using a Genova spectrophotometer against a standard curve (5-30μg bovine serum albumin (BSA)).

2.3.2 Sodium Dodecyl Sulphate Polyacrylamide Gel Electrophoresis

SDS-polyacrylamide gel electrophoresis (SDS-PAGE) gels for immuno-blotting were prepared with a resolving gel segment and an overlaying 3% stacking gel segment. The percentage of the resolving gel segment was 9%, 13% or 15% dependant on the molecular weight of the proteins to be resolved. The resolving gel was made up from 30% acrylamide Protogel (National Diagnostics), 375mM Tris/HCl pH8.8, 0.1% SDS, made to 5mL with water, and polymerised with 10% ammonium persulphate (APS) and tetramethylethylenediamine (TEMED). Four fifths of the resolving gel was poured and covered with isopropanol whilst the gel set. The isopropanol was removed and replaced with a stacking gel (3% polyacrylamide, 50mM Tris pH6.8, 0.1% SDS, made to 5mL with water and polymerised with 10% APS and TEMED). Combs were immediately added to the stacker gel and allowed to set. Once set, the gels were placed into an electrophoresis tank (BIORAD Mini), part filled with SDS running buffer (25mM Tris, 192mM glycine, 0.1% SDS) and the combs removed. Protein samples, typically 15μg, were diluted with 5x SDS loading buffer (65mM Tris/HCl pH8, 10% (v/v) glycerol, 2.3% (w/v) SDS, 0.01 bromophenol blue, 1% dithiothreitol (DTT)), denatured at $100^{o}C$ for 5 minutes and placed immediately on ice. The samples, including a protein ladder

were loaded into the wells of the gel and resolved at 150V for ~60 minutes until the loading dye approached the bottom of the gel.

2.3.3 Coomassie Staining and Drying of SDS-PAGE Gels

SDS-PAGE gels were stained using PageBlue (Fermentas). Briefly, the gel was placed in 20mL distilled water and heated until boiling point, the water was removed and replaced with fresh water. This was repeated twice more with the gel finally being boiled in 20mL PageBlue reagent. The gel was left on a rocker for approximately 20 minutes until banding had become clear, it was destained with several washes of distilled water.

The gel was dried by sandwiching it between filter paper and Saran wrap and vacuum dried at 80°C for 60 minutes on a Gel Master Gel Dryer Vacuum System (Welch).

2.3.4 Protein Transfer from SDS-PAGE to Polyvinylidene Fluoride Membrane

The SDS-PAGE gel was transferred to an adequately sized piece of polyvinylidene fluoride (PVDF) transfer membrane which had been activated by brief immersion in methanol. The membrane and gel were sandwiched between two sponges and filter paper and clamped into a transfer device which was placed into a transfer unit (Amersham). This was filled to the top with CAPS buffer (10mM CAPS pH 11, 10% methanol) and run at 230mA for 90 minutes at 4°C. The membrane was subsequently blocked using 5mL of 5% milk protein in PBS + 0.1% Tween (PBS/Tween) overnight at 4°C.

2.3.5 Western Blotting

The PVDF membrane was placed into a 50mL centrifuge tube (Falcon), with the protein bound side of the membrane facing inwards, containing 5mL of 5% milk protein in PBS/Tween and the primary antibody diluted as appropriate (Table 2.3). The centrifuge tube was placed on a tube rotator and incubated as appropriate (Table 2.3). The membrane was removed from the centrifuge tube and subjected to 3 x 5 minute washes in PBS/Tween. The membrane was again placed inside another 50mL centrifuge tube containing 5mL of 5% milk protein in PBS/Tween and the secondary antibody (Table 2.3) and placed on a tube rotator and incubated at room temperature for one hour. The membrane was removed from the centrifuge tube and subjected to a further 3 x 5 minute washes in PBS/Tween. After the washes the membrane was overlaid with ECLPlus reagent (Amersham Biosciences) for 5 minutes. Excess ECLPlus reagent was removed from the membrane and it was wrapped in Saran wrap, before exposure to autoradiography film (Kodak) for 30 seconds to 5 minutes dependant on the strength of the signal. Autoradiography films were then developed in an X-ray film developer (Konica Minolta).

Antibody	Species	Dilution	Application	Operating Conditions
Anti-H1.X[1]	Rabbit	1:1000	Western Blotting	1hr, room temp, 5% milk
Anti-H1.X[1]	Rabbit	4μg	Immunoprecipitation	Standard Protocol (2.19.4)
Anti-H1.2[1]	Rabbit	1:1000	Western Blotting	1hr, room temp, 5% milk
Anti-H2A.X[2]	Mouse	1:1000	Immunofluorescence	1hr, room temp, 2% FCS
Anti-bromodeoxyuridine[3]	Mouse	1:50	Flow Cytometry	0.5% normal goat serum, 0.5% Tween 20
Anti-FLAG[4]	Mouse	1:1000	Western Blotting	1hr, room temp, 5% milk
Anti-FLAG[4]	Mouse	1:1000	Immunofluorescence	1hr, room temp, 2% FCS
Anti-his[2]	Mouse	1:1000	Western Blotting	1hr, room temp, 5% milk
Anti-α-tubulin[1]	Rabbit	1:10000	Western Blotting	30 minutes, room temp, 5% milk
Anti-GFP[1]	Mouse	1:1000	Western Blotting	1hr, room temp, 5% milk
Anti-GFP[1]	Mouse	4μg	Immunoprecipitation	Standard Protocol (2.19.4)
Anti-H2A[5]	Rabbit	1:5000	Western Blotting	Overnight, 4°C, 5% milk
Anti-XRCC4[5]	Rabbit	1:1000	Western Blotting	1hr, room temp, 5% milk
Anti-DNA Ligase IV[6]	Goat	1:200	Western Blotting	1hr, room temp, 5% milk
Anti-Mouse-HRP[3]	Rabbit	1:5000	Western Blotting	1hr, room temp, 5% milk
Anti-Rabbit-HRP[3]	Goat	1:5000	Western Blotting	1hr, room temp, 5% milk
AlexaFluor 594[7]	Goat	1:1000	Immunofluorescence	1hr, room temp, 2% FCS
AlexaFluor 488[7]	Goat	1:50	Flow Cytometry	0.5% normal goat serum, 0.5% Tween 20

Table 2.3 - Table of antibodies, their dilutions and incubation times
Listed are all the antibodies used in this thesis. Other information provided includes the species the antibody was raised in, along with the specific application the antibody was used in, including the dilution for that application and the operating conditions. Antibody Sources. 1 – Abcam, 2 – Upstate, 3 – Dako, 4 – Sigma Aldrich, 5 – Made in house, 6 – Santa Cruz, 7 – Invitrogen.

2.4 Clonogenic Survival Assay

Transfected cells were grown in 75cm^2 cell culture flasks, as explained in 2.2.6, trypsinised as outlined in 2.2.3, counted using a haemocytometer and reseeded at 1x10^5 cells/mL. Cells were irradiated with 2, 4, 6 and 8 Gy of IR (Caesium 137 source), with one sample left un-irradiated. Cells were seeded out at 50, 100, 500, 1000, 5000 and 10000 cells per well into a 6-well plate for 0, 2, 4 and 6 Gy exposure. For 8 Gy exposure, 10000, 50000, 100000, 500000 and 1000000 cells were seeded out. The 6-well plate was placed in a humidified chamber and left for ~2 weeks until colonies of ~50 cells were visible. The media was aspirated and a few drops of crystal violet (0.4% crystal violet, 50% Methanol) were added to each well. This was agitated for a few seconds and washed off with distilled water. Colonies were counted in the wells that contained between 50 and 100 cells. The experiment was repeated in triplicate and the data statistically analysed using the students' two-tailed t-test.

2.5 Immuno-fluorescence

2.5.1 Fixation of Cells

Cells were grown in 6-well dishes containing a 22mm x 22mm coverslip (VWR, UK), sterilised under UV light for 30 minutes. At the point of fixation, the media was aspirated and the coverslip washed with PBS. To each coverslip 1mL of immuno-fluorescence lysis buffer was added (10mM PIPES pH 6.8, 300mM sucrose, 20mM NaCl, 3mM MgCl$_2$, 0.5% Triton X-100) and incubated on ice for 7 minutes. The slides were washed in PBS, and 1mL of 4%

paraformaldehyde (diluted in PBS) was added and left on ice for 10 minutes. The paraformaldehyde was aspirated and washed 3 times with PBS.

2.5.2 Immuno-probing

Ten percent FBS was added to the slides and incubated on a rocking platform for 1 hour at room temperature to aid blocking of non-specific proteins. FBS was removed and the slides washed with PBS. Subsequently, 100μL PBS supplemented with 2% FBS and primary antibody (Table 2.3) was added and incubated at 37°C for 1 hour on a rocking platform. The coverslip was washed with 3 x 5 minute PBS washes and replaced with 100μL PBS supplemented with 2% FBS and a fluorescently tagged secondary antibody (Table 2.3) and incubated at 37°C for 1 hour in the dark on a rocking platform. The coverslip was again washed with 3 x 5 minute PBS washes in the dark.

2.5.3 Mounting and Visualisation

The slides were mounted in Vectashield (Vector Laboratories, CA, USA) mounting media, containing 4',6-diamidino-2-phenylindole (DAPI), onto microscope slides (VWR). The slides were sealed with clear nail varnish and left at 4°C overnight before analysis. Slides were analysed with a Carl Zeiss microscope using a 100x objective and Smart Capture2 software.

2.6 γH2A.X Quantification

Transfected cells (Section 2.2.6) were grown in 6-well dishes containing a 22mmx22mm coverslip (VWR, UK), sterilised under UV light for 30 minutes. Cells were irradiated with 5 Gy of IR and placed in a humidified chamber. At 30 minutes and 24 hours post-irradiation the cells were fixed as outlined in Section 2.5.1, along with un-irradiated controls. Cells were immuno-probed as described in Section 2.5.2 with an antibody targeted towards γH2A.X. After mounting and visualisation (Section 2.5.3), a minimum of 50 nuclei per time point per sample were examined and γH2A.X foci per nuclei were counted using Photoshop Software (Adobe). The experiment was repeated in triplicate and the data statistically analysed using the students' two-tailed t-test.

2.7 Cytochalasin B Micronuclei Assay

The cytochalasin B micronuclei assay was adapted slightly from published protocols (Fenech, 2007, Fenech and Morley, 1985). Transfected cells (Section 2.2.6) were grown in 6-well dishes (Corning) containing a 22mmx22mm coverslip (VWR International, Lutterworth, UK), sterilised under UV light for 30 mins. Cells were irradiated with 5 Gy of IR and placed in a humidified chamber for 5 hours, along with un-irradiated controls. After 5 hours, cytochalasin B was added to the cells at 2μg/mL per well. At 24 and 48 hours post-irradiation, slides were fixed as outlined in 2.5.1. The slides were mounted as described in 2.5.3, 100 binucleate cells per time point per sample were examined and total nuclei and

total micronuclei were counted. The experiment was repeated in triplicate and the data statistically analysed using the students' two-tailed t-test.

2.8 Cell Cycle Flow Cytometry Assay

Transfected cells were grown in 75cm^2 cell culture flasks to ~60% confluency, as explained in 2.2.6. At this point 20μM bromodeoxyuridine (BrdU) was added to the flasks and left for 20 minutes in a humidified chamber. The cells were trypsinised as explained in Section 2.2.3 and resuspended in 10mL supplemented DMEM. This suspension was counted using a haemocytometer and the cells resuspended at a cell density of 3x10^5/mL with 2 aliquots for each cell line. One of each of these suspensions was irradiated with 5 Gy of IR, the other left un-irradiated as a control. One millilitre of this suspension was seeded out into 25cm^2 cell culture flasks allowing 4 hour time points over a 24 hour period. The flasks were placed in a humidified chamber until the designated time point. At each time point, including the cell suspension for time point zero, cells were trypsinised as explained in Section 2.2.3. The cell pellet was resuspended in 5mL PBS and centrifuged at 1,200 rpm for 5 minutes. The supernatant was removed and the cells resuspended in 2mL ice-cold ethanol whilst being vortexed to avoid cell clumping. The suspension was left at -20°C for at least 48 hours. The suspension was centrifuged at 1,200 rpm for 5 minutes, the pellet resuspended in 3mL PBS, followed by centrifugation at 1,200 rpm for 5 minutes and the pellet resuspended in 2mL 2M HCl containing 0.1% pepsin and left at room temperature for 20 minutes. Two millilitres PBS was added to the suspension and centrifuged at 1,200 rpm for 5 minutes. The pellet was resuspended in 3mL PBS and centrifuged at 1,200 rpm for 5 minutes, this PBS wash was

repeated a second time. The pellet was resuspended in 100μL PNT (PBS containing 0.5% normal goat serum and 0.5% tween) and anti-BrdU antibody (Table 2.3). This was left at room temperature for 60 minutes, after which 3mL PBS was added and the suspension vortexed, it was then centrifuged at 1,200 rpm for 5 minutes. The pellet was resuspended in 3mL PBS and centrifuged at 1,200 rpm for 5 minutes. The pellet was resuspended in 100μL PNT containing the secondary antibody, AlexaFluor 488 conjugated goat-anti-mouse secondary antibody (Table 2.3) and left in the dark for 60 minutes. Three millilitres PBS was added and the suspension vortexed, it was centrifuged at 1,200 rpm for 5 minutes. The pellet was resuspended in 3mL PBS and centrifuged at 1,200 rpm for 5 minutes. The pellet was resuspended in 0.5mL PBS containing 20μL/mL proidium iodide and analysed using a Coulter Elite flow cytometer using UV and 488nm lasers for excitation. The data obtained was analysed using FlowJo Flow Cytometry Analysis Software (Tree Star, Inc).

2.9 Plasmids

All plasmids used in this study are listed in Table 2.4. Their corresponding maps are shown in Figure 2.1 to Figure 2.4.

2.10 Bacteria

2.10.1 General Maintenance

Bacterial strains were maintained as glycerol stocks kept at -80°C, and were re-streaked onto fresh LB agar, supplemented with antibiotics as appropriate (Table 2.5), and incubated at 37°C overnight. Overnight cultures were grown by inoculating a single fresh colony into 5mL of LB broth, supplemented with antibiotics as appropriate (Table 2.5), and incubated in an orbital shaker at 37°C/220 rpm for 12-16 hours.

2.10.2 Image Clones

All image clones were ordered from Geneservice and are listed in Table 2.6.

2.10.3 Transformation

Typically, 2μL of ligation products were added to 20μL competent *Escherichia coli*, and left on ice for an hour. The mixture was placed at exactly 42°C for 1 minute, and then placed on ice for 2 minutes. SOC media (Invitrogen) was added to the mixture and placed in an orbital shaker, 220 rpm at 37°C, for 60 minutes. Following this recovery period, 125μL of this mixture was spread onto an LB agar plate supplemented with the appropriate antibiotic (Table 2.5) and incubated at 37°C overnight.

Plasmid	Description	Source
pGEM-T-Easy	Cloning of PCR generated DNA fragments. (Figure 2.1)	Promega
pFLAG-CMV-4	Generation of flag-tagged recombinant proteins for *in vivo* studies. (Figure 2.2)	Invitrogen
pET28-b	Generation of his-tagged recombinant proteins for use in protein purification. (Figure 2.3)	Novagen
pEGFP	Generation of EGFP-tagged recombinant proteins for *in vivo* studies. (Figure 2.4)	Clontech

Table 2.4 - List of plasmids used in this study.
All the plasmids used in this thesis are listed, along with their purpose of use and where the material was sourced from.

Antibiotic	Stock Concentration	Working Concentration	Plasmids
Ampicillin	50mg/mL in H_2O	50µg/mL	pGEM-T-Easy, pFLAG-CMV-4, pPCR-Script AMP SK (+)
Kanamycin	25mg/mL in H_2O	25µg/mL	pET28-b, pEGFP, pCR4-TOPO, pCR-BluntII-TOPO
Chloramphenicol	34mg/mL in ethanol	25µg/mL	pOTB7

Table 2.5 - Antibiotics used in this study.
The antibiotics used in this thesis are listed, along with the stock and working concentrations, along with the plasmids which carried the antibiotic resistance gene.

Gene Name	Accession Number	Source	Source Plasmid
H1.1	BC069492	Geneservice	pPCR-Script AMP SK (+)
H1.2	BC002649	Geneservice	pOTB7
H1.3	BC104874	Geneservice	pCR4-TOPO
H1.4	BC099632	Geneservice	pCR-BluntII-TOPO
H1.5	BC101581	Geneservice	pCR4-TOPO
H1.X	BC010435	Geneservice	pOTB7

Table 2.6 - List of Image Clones used in this study
Image clones were obtained for all linker histone genes used in this thesis. This table described where each image clone was sourced from and the accession number of each histone, along with the vector containing the gene.
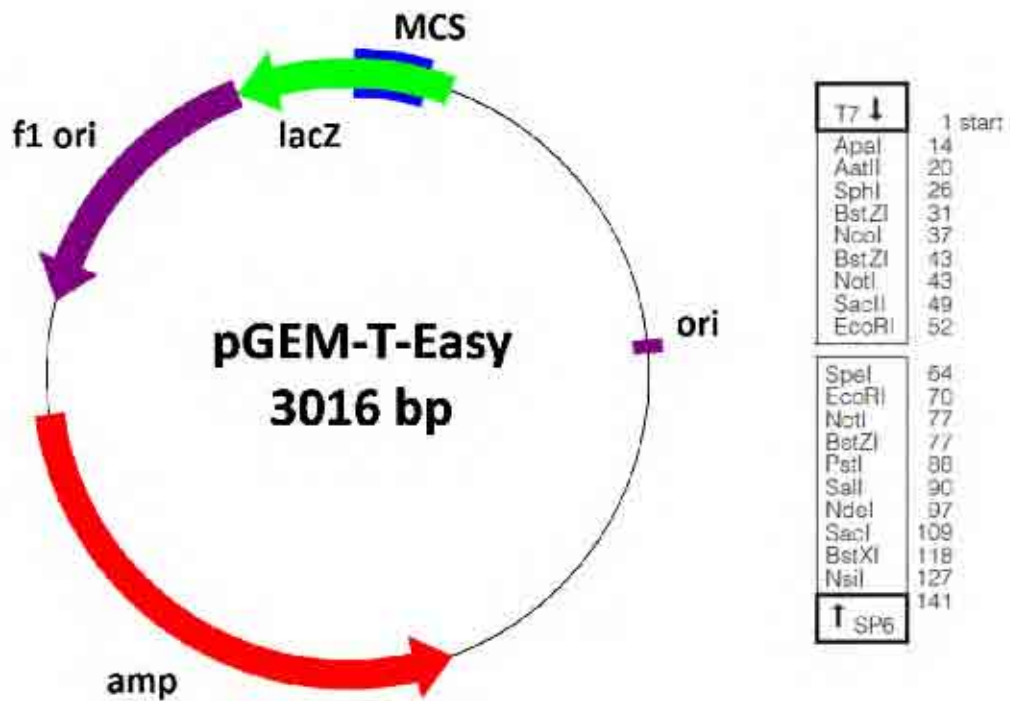
Figure 2.1 – Plasmid map of pGEM-T-Easy
pGEM-T-Easy is a plasmid used to clone A-tailed PCR fragments. The plasmid is supplied linear, and becomes circularised upon insertion and ligation of PCR products. The multiple cloning site (MCS) contains many restriction sites, including the double EcoRI site which, using a single digest will reveal any inserted DNA.
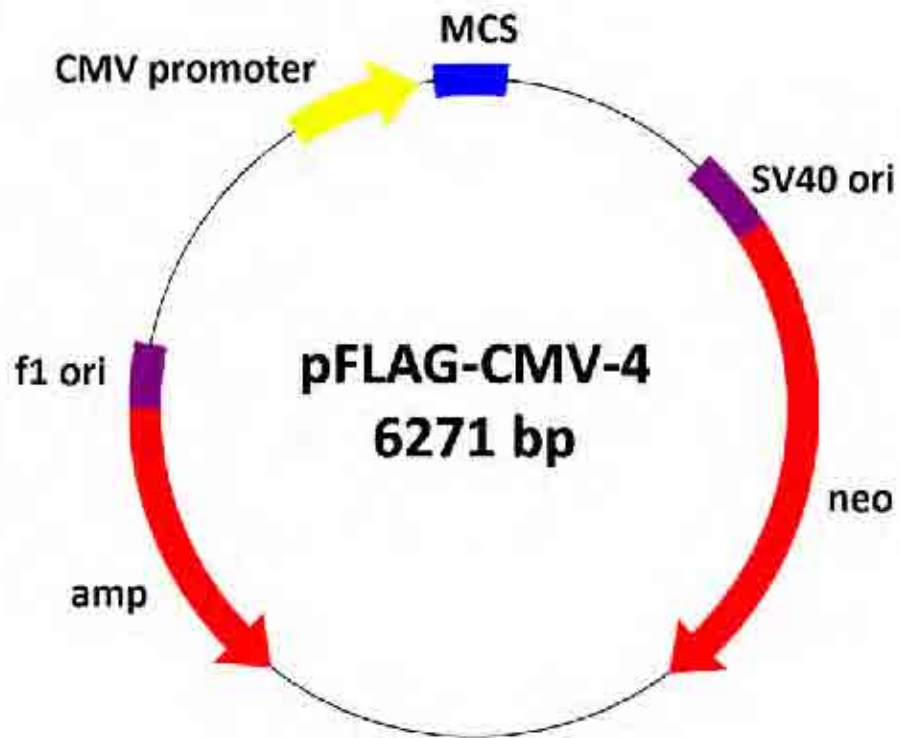
Figure 2.2 – Plasmid map of pFLAG-CMV-4
pFLAG-CMV-4 is a mammalian expression vector which adds the FLAG peptide sequence (DYKDDDDK, red filled box) at the amino terminus of the cloned gene. Linker histones were cloned into pFLAG-CMV-4 via the multiple cloning site (MCS) via the BglII and XbaI restriction sites. pFLAG-CMV-4 contains both an ampicillin resistance gene and a neomycin resistance gene for selection in both bacteria and mammalian cells respectively.
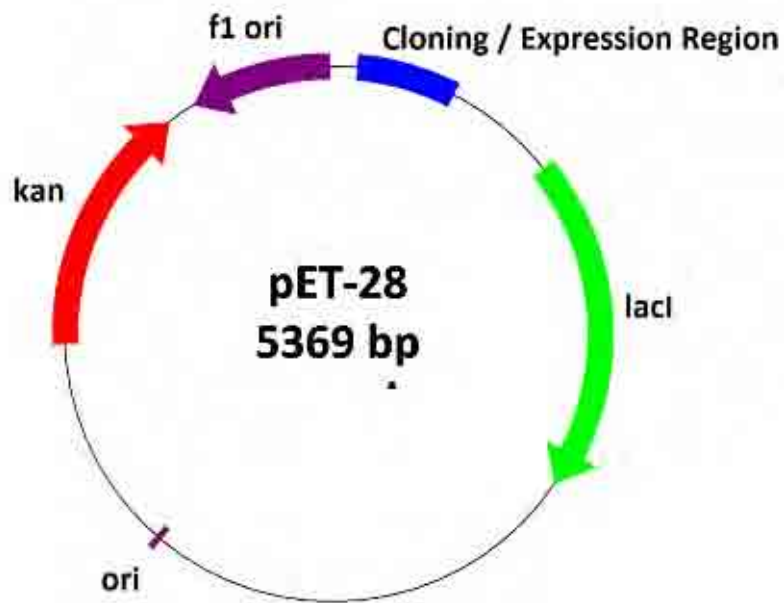
AGATCTCGATCCCGCGAAATTAATACGACTCACTATAGGGGAATTGTGAGCGGATAACAATTCCCCTCTAGAAATA

ATTTTGTTTAACTTTAAGAAGGAGATATACCATGGGCAGCAGCCATCATCATCATCATCACAGCAGCGGCCTGGTG

CCGCGCGGCAGCCATATGGCTAGCATGACTGGTGGACAGCAAATGGGTCGGGATCCGAATTCGAGCTCCGTCGACA

AGCTTGCGGCCGCACTCGAGCACCACCACCACCACCACTGAGATCCGGCTGCTAACAAAGCCCGAAAGGAAGCTGA

GTTGGCTGCTGCCACCGCTGAGCAATAACTAGCATAACCCCTTGGGGCCTCTAAACGGGTCTTGAGGGGTTTTTTG

Figure 2.3 – Plasmid map of pET28-b
pET28-b is a protein expression plasmid. Linker histone genes were cloned into the cloning/expression region (blue box on plasmid map, sequence data below). Highlighted are the T7 promoter and terminator regions (red box), the LacI operator (blue box), the ATG start site (red ATG), and the poly histidine tags (underlined). Note, linker histones were cloned so that the latter (3') his-tag was not expressed.
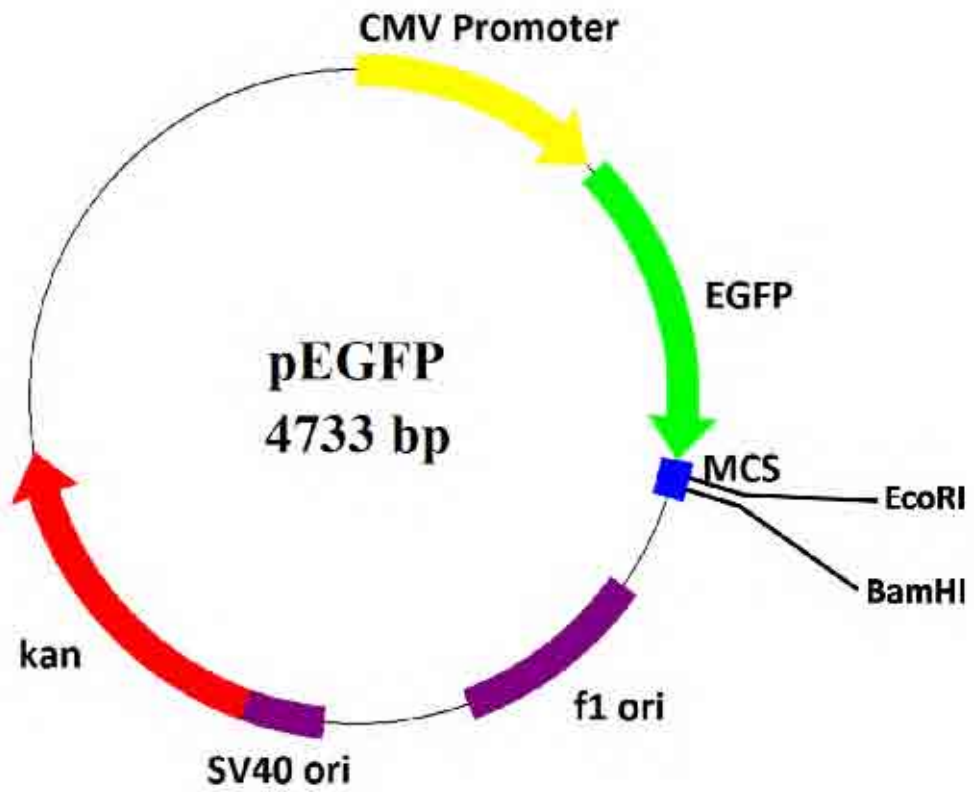
Figure 2.4 – Plasmid map of pEGFP

pEGFP is a mammalian expression vector which adds the GFP protein at the amino terminus of the cloned gene. Linker histone genes were cloned in to pEGFP via the multiple cloning site (MCS) and the EcoRI and BamHI restriction sites. pEGFP contains a kanamycin (kan) resistance gene which offers both bacterial and mammalian selection.

2.11 Agarose Gel Electrophoresis of DNA

Samples were typically resolved on an 1.5% agarose (Bioline), TBE (89 mM Tris-Base, 89 mM boric acid, 2mM EDTA) gel. This was heated until all the agarose had dissolved, allowed to cool before the addition of 0.5μg/mL ethidium bromide and poured into an electrophoresis tray (Anachem). The electrophoresis tray was placed inside an electrophoresis tank and the samples were loaded into the wells, each sample was loaded containing x10 DNA loading buffer (50% glycerol, 0.05% bromophenol blue). To determine the size of the fragments, 20μL of a 1kbPlus DNA ladder (Invitrogen) was also added to the gel. The products were resolved by applying 180V across the electrophoresis tank until the products had migrated 10 cm. Products were viewed and photographed under UV light.

2.12 DNA Extraction

2.12.1 DNA Extraction from Agarose Gels

DNA bands for extraction were excised from the agarose gel using a sharp scalpel and placed into a 1.5mL microcentrifuge tube. Excised bands were purified using the Qiagen QIAquick gel extraction kit following manufacturer instructions. Briefly, 300μl of QG buffer was added and heated to 60°C until the agarose fragment had dissolved. One hundred microlitres of isopropanol was added, after 1 minute the sample was transferred to a spin column provided and centrifuged at 13,000 rpm for 1 minute. The column was then washed twice with 750μL PE buffer and finally eluted with 50μL EB buffer (1.25M NaCl, 50mM Tris/HCl pH 8.5, 15% isopropanol (v/v)).

2.12.2 Small Scale Purification of Plasmid DNA, Miniprep.

Plasmid DNA was extracted from an overnight culture using the QIAprep Miniprep kit. Briefly, the bacterial cells from the overnight culture were pelleted by centrifugation at 13,000 rpm for 5 minutes in a 1.5mL microcentrifuge tube. The cells were resuspended in 250μL resuspension buffer P1 before the addition of 250μL of lysis buffer P2. The solution was mixed by several inversions and allowed to stand for 5 minutes. After lysis, 350μL neutralisation buffer, N3, was added and the solution mixed immediately by several inversions until the solution became cloudy. Cellular debris, including genomic DNA, was pelleted by centrifugation at 13,000 rpm for 10 minutes. The supernatant was aspirated and placed into a labelled QIAprep spin column and centrifuged for 1 minute at 13,000 rpm. The flow through was discarded and 500μL wash solution PB was added to the column and centrifuged for a further 1 minute at 13,000 rpm with the flow through being discarded. A second wash using 750μL of PE buffer was passed through the column by centrifugation at 13,000 rpm for 1 minute. The flow through was discarded and any residual buffer was washed away from the column by centrifugation at 13,000 rpm for 1 minute. The QIAprep column was then transferred to a labelled 1.5mL microcentrifuge tube, 50μL of elution buffer was added to the centre of the column and left to stand for 1 minute. The DNA was eluted by centrifugation at 13,000 rpm for 1 minute.

2.13 DNA Manipulation

2.13.1 Polymerase Chain Reaction

2.13.2 Standard Polymerase Chain Reaction

All polymerase chain reactions (PCR) were performed on a GeneAmp 9700 thermocycler (Perkin Elmer) using 2 units Taq DNA polymerase (Invitrogen), 1mM dNTP mix (Roche), 1.5mM MgCl2, 1mM forward and reverse primer (See Table 2.8 for primer list) and the appropriate amount of $10 \times$ PCR buffer (Invitrogen) unless otherwise stated. The amount of DNA template and PCR program used are listed in the relevant sections.   A general PCR program is shown in Table 2.7. In all cases an identical PCR reaction using distilled water instead of DNA was used as a negative control. Positive controls, which vary for each application, were always included.

Temperature	Time		Purpose
95°C	4 minute		Initial Melting
95°C	1 minute		Melting
$T_A{}^{\circ}$C	1 minute	35 cycles	Annealing
68°C	x minute		Extension
68°C	4 minute		Final Extension

Table 2.7 - Standard PCR Cycle
An annealing temperature (T_A°C) of 3-5°C below the melting temperature of the primers was used. The extension time (x minute) was calculated based on PCR product length and rate of extension of the polymerase used (according to the manufacturer's instructions).

2.13.3 Cloning Polymerase Chain Reaction

Cloning PCR reactions were performed on a GeneAmp 9700 thermocycler using 2.5 units Failsafe^{TM} DNA polymerase (CamBio), 2x buffer D (containing dNTPs and MgCl$_2$), 1mM forward and reverse primer (Table 2.8), 1µG plasmid DNA and topped to 50µL with nuclease free water. A general PCR program is shown in Table 2.7.

2.13.4 Colony Polymerase Chain Reaction

Colony PCR reactions were setup as outlined in Section 2.13.2 with the addition of 5µL of a fresh overnight bacterial culture. The PCR program used is shown in Table 2.7 with the initial melting step extended to 5 minutes to aid bacterial lysis.

Gene	Application	Sequence	Melting Temp	Extension Time
H1.1 Forward	All plasmids	GCAGAGATCTGATGTCTGAAACAGTGCCTCCCGCC	55°C	1 minute
H1.1 Reverse	All plasmids	GCAGTCTAGACTCGAGTTACTTTTTCTTGGGTGCCGC	55°C	1 minute
H1.2 Forward	All plasmids	GCAGAGATCTGATGTCCGAGACTGCTCCTGC	55°C	1 minute
H1.2 Reverse	All plasmids	GCAGTCTAGACTCGAGCTATTTCTTCTTGGGCGCCG	55°C	1 minute
H1.3 Forward	All plasmids	GCAGAGATCTGATGTCGGAGACTGCTCCACTTGCTCC	55°C	1 minute
H1.3 Reverse	All plasmids	GCAGTCTAGACTCGAGTCACTTTTTCTTCGGAGCTGCC	55°C	1 minute
H1.4 Forward	All plasmids	GCAGAGATCTGATGTCCGAGACTGCGCCTGCCGCG	55°C	1 minute
H1.4 Reverse	All plasmids	GCAGTCTAGACTCGAGCTACTTTTTCTTGGCTGCCGCCTTCTTTGGCTTGGCTG	55°C	1 minute
H1.5 Forward	All plasmids	GCAGAGATCTGATGTCGGAAACCGCTCCTGCCGAGA	55°C	1 minute
H1.5 Reverse	All plasmids	GCAGTCTAGACTCGAGCTACTTCTTTTTGGCAGCCG	55°C	1 minute
H1.X Forward	pFLAG Cloning	GCAGAGATCTGATGTCCGTGGAGCTCGAGGAGGCCC	55°C	1 minute
H1.X Reverse	pFLAG Cloning	GCAGTCTAGACTCGAGTCACTTGCGGCCCTTGGGCAC	55°C	1 minute
H1.X Forward	pET Cloning	GCAGGAATTCGATGTCCGTGGAGCTCGAGGAGGCCC	55°C	1 minute

H1.X Reverse	pET Cloning	GCAGAAGCTTTCACTTGCGGCCCTTGGGCAC	55°C	1 minute
pGEM Sequencing Forward	pGEM Sequencing	CCCAGTCACGACGTTGTAAAACG	50°C	10 seconds
pGEM Sequencing Reverse	pGEM Sequencing	AGCGGATAACAATTTCACACAGG	50°C	10 seconds

Table 2.8 - List of primers used in this thesis.
Primers sequences used in this thesis along with the application for the primers, their melting temperature and extension times.

2.13.5 Restriction Digests

Restriction digestions were routinely set up in 25μL reaction volumes which consisted of 18μg miniprep DNA, 20 units of each restriction endonuclease, 10x buffer and where applicable 10x BSA, topped up with distilled water. Reactions were left at 37°C for 4 hours to allow complete digestion. Digested products were then visualised on an agarose gel as explained in Section 2.11.

2.13.6 Ligation

Ligation reactions were routinely set up in 10μL reaction volumes using the LigaFast Rapid Ligation System (Promega). Briefly, 1μg vector DNA, 3μg insert DNA, 3 units T4 DNA Ligase and 2X rapid ligation buffer, made up to 10μL with distilled water was incubated overnight at room temperature.

2.13.7 pGEM-T-Easy Cloning

Primers were designed to accommodate restriction sites either side of the linker histone genes allowing direct in-frame sub-cloning into expression vectors (Table 2.8). DNA was amplified from miniprep DNA (Section 2.12.2) obtained from linker histone image clones (Section 2.10.2) using PCR (2.13.1). PCR products were ligated into the pGEM-T-Easy (Promega) vector following manufacturer's instructions. This involved mixing 1μg PCR product, 3 units T4 DNA Ligase, 50ng pGEM-T-Easy linear vector, 2x ligation buffer and made

up to 10μL with distilled water. The ligation mix was left overnight at room temperature. The ligation products were transformed into *E. coli* bacteria as described in Section 2.10.3 and spread onto an LB agar plate supplemented with the appropriate antibiotic (Table 2.5) along with 0.1M isopropyl thiogalactoside (IPTG) and 40μg/μL 5-bromo-4-chloro-3-indolyl-beta-D-galactopyranoside and incubated overnight at 37°C.

2.13.8 DNA Sequencing

2.13.8.1 Sequencing Polymerase Chain Reaction

Sequencing PCR was routinely set up in 20μL reaction volumes, consisting of 1μL Big Dye (Applied Biosystems), 1mM sequencing primer (Table 2.8), 2μg plasmid DNA and 5x sequencing buffer. PCR reaction conditions are shown in Table 2.9.

Temperature	Time		Purpose
95°C	4 minutes		Initial Melting
95°C	20 seconds		Melting
50°C	10 seconds	35 cycles	Annealing
60°C	4 minutes		Extension
60°C	7 minutes		Final Extension

Table 2.9 - Standard Sequencing PCR Cycle

2.13.8.2 Ethanol Precipitation of DNA Products

Ethanol precipitation was used to purify the DNA from the sequencing reaction. To the PCR reaction, 3μL 1.5M Sodium Acetate – EDTA and 100μL 95% ethanol were added and allowed

to stand at room temperature in the dark for 20 minutes. DNA products were then pelleted by centrifugation at 14,000 rpm at 4°C for 30 minutes. The supernatant was carefully removed by inversion, before the addition of 200µL 100% ethanol. This was again centrifuged at 14,000 rpm for 30 minutes at 4°C. The supernatant was again carefully removed by inversion and the DNA pellet allowed to air dry for 30 minutes.

2.13.8.3 Sample Preparation for Sequencing Analysis

The DNA pellet was resuspended in 10µL Hi-Di formamide loading buffer (Applied Biosystems). The DNA was denatured at 95°C for 4 minutes before being placed on ice for 2 minutes. Samples were loaded on to the ABI Prism 3700 according to manufacturers' instructions. DNA sequences were analysed by using BioEdit Sequence Alignment Editor.

2.14 Protein Purification

2.14.1 Cloning of Linker Histone Genes in to the pET28-b Vector

Genes coding for the linker histone variants with ligateable ends were excised from pGEM-T-Easy vector (H1.X, Figure 2.1) or from pFLAG-CMV-4 (H1.1 to H1.5, Figure 2.2, Section 2.19.1) using EcoRI/HindIII and EcoRI/XhoI restriction enzymes respectively (Section 2.13.5). Products were resolved on an agarose gel (Section 2.11), the relevant products were excised and the DNA extracted from the agarose (Section 2.12.1). These products were ligated into pET28-b expression vector (Section 2.13.6) which had been linearised with the same restriction enzymes listed above to allow compatible ends and the genes to be inserted in-

frame and with an amino-terminal poly-histidine tag. Ligated products were transformed into competent *E. coli* (Section 2.10.3) capable of protein expression (BL21(DE3)pLysS; Promega) and plated out onto LB agar containing kanamycin and left at 37°C overnight (Section 2.10.1). Overnight cultures were obtained from individual colonies and these were assessed for the presence of the inserted gene by colony PCR (Section 2.13.4). Those positive colonies were used to generate recombinant protein.

2.14.2 Induction of Recombinant Proteins.

An overnight culture was transferred into 50mL of LB broth containing kanamycin (Table 2.5) and incubated at 37°C in an orbital shaker until the OD$_{600}$ reached 0.6-1.0. Protein expression was typically induced by the addition of 1.0mM IPTG and was allowed to continue for 3 hours. The bacterial culture was pelleted by centrifugation at 4,000 rpm for 10 minutes, this pellet was placed at -20°C overnight. Where necessary, the amount of IPTG used for induction, along with the induction time was changed.

2.14.3 Extraction and Purification of Recombinant Proteins.

The pellet was thawed with the addition of his-tag lysis buffer (50mM Tris/HCl pH 7.5, 750mM NaCl, 0.02mM EDTA, 0.02mM ethylene glycol tetraacetic acid (EGTA), 1% Triton, 0.06% ß-mercaptoethanol, 1mM benzamidine, 0.2mM phenylmethylsulfonyl fluoride (PMSF) and protease inhibitor cocktail (Roche)). Bacteria were further lysed by sonication, three 15 second pulses whilst on ice, followed by end-over-end rotation at 4°C for 30 minutes. The

lysate was centrifuged at 15,000 rpm at 4°C for 30 minutes and the soluble fraction (supernatant) was mixed with TALON metal affinity resin (Clontech), pre-equilibrated in his-tag lysis buffer, by end-over-end rotation for 30 minutes to allow the his-tagged proteins to bind the beads. The flow-through was discarded as this contained unbound proteins and the column was washed with 10x column volumes of his-tag high salt buffer (50mM Tris/HCl pH 7.5, 500mM NaCl, 0.02mM EDTA, 0.02mM EGTA, 0.03% Brij 35, 20mM imidazole, 0.06% ß-mercaptoethanol, 1mM benzamidine, 0.2mM PMSF). The column was subsequently washed with 10x column volumes of his-tag low salt buffer buffer (50mM Tris/HCl pH 7.5, 150mM NaCl, 0.02mM EDTA, 0.02mM EGTA, 0.03% Brij 35, 20mM imidazole, 0.06% ß-mercaptoethanol, 1mM benzamidine, 0.2mM PMSF). Proteins were then eluted in his-tag elution buffer (his-tag low salt buffer + 300mM imidazole, pH 7.5) in 250μl fractions, each fraction was then analysed by SDS-PAGE (Section 2.3.2) and the fraction containing the protein of interest was used for further experimentation.

Where necessary, the NaCl concentration of the his-tag lysis buffer and subsequent washes was changed.

2.14.4 Dialysis of Recombinant Proteins.

Protein solutions were placed inside a dialysis chamber of a custom made dialysis apparatus. Proteins were dialysed against TNB buffer (10 mM Tris, 50mM NaCl, 1mM β-mercaptoethanol, pH 8.0) overnight at 4°C.

2.15 Protein Kinase Assay

Typically, 5μg purified DNA-PK (Promega) was incubated with kinase buffer (25mM HEPES pH 7.5, 10mM MgCl$_2$, 1mM DTT, 0.1% Nonidet P-40, 20% glycerol) in the presence of 5mg dsDNA cellulose (Amersham Bioscience) and incubated at 4°C for 30 minutes with end-over-end rotation. The dsDNA cellulose was washed to remove any unbound DNA-PK with kinase buffer. Purified calf thymus linker histone H1 (Roche) or individually purified linker histone variants (Section 2.14) were added to the reaction mixture along with 4mM ATP, and 30nCi of [γ-^{32}P]ATP and incubated for 20 minutes at 30°C. The reaction was terminated by the addition of 5x SDS loading buffer. Products were resolved on an SDS-PAGE gel as described in Section 2.3.2. The gel was stained and dried as detailed in Section 2.3.3. The gel was exposed to a storage phosphor screen (Molecular Dynamics) for 60 minutes, the screen was scanned using a STORM Phosphorimager (Molecular Dynamics) and the images analysed using ImageQuant software (GE Healthcare).

2.16 Phospho-peptide Mapping

Purified recombinant linker histone variants were phosphorylated as described in Section 2.15, with the exclusion of [γ-^{32}P]ATP. Products were resolved on an SDS-PAGE gel as explained in Section 2.3.2 using pre cast 4-20% gradient gels (Bio-Rad). The gel was stained as explained in Section 2.3.3, but not dried, and bands of interest were excised and analysed by mass spectrometry to identify proteins, and any post translational modifications. Mass

spectrometry analysis was carried out by Functional Genomics Unit, University of Birmingham and the results returned in Microsoft Excel format.

2.17 In Vitro Ligation

2.17.1 dsDNA End Labelling

Two micrograms of DNA was incubated with 20 Units of shrimp alkaline phosphatase and 10X buffer in a total reaction mix of 20μL at 37°C for 1 hour. The reaction was terminated with a 5 minute incubation at 65°C and placed on ice for a further 5 minutes. To this mixture, 5mM DTT and 5% polyethylene glycol were added, heated at 75°C for 10 minutes and chilled on ice for 5 minutes. Following this, 10 units of T4 polynucleotide kinase, 10X buffer and 60μCi [γ-^{32}P]-ATP were added and incubated at 37°C for 2 hours. The DNA products were then precipitated from the reaction mix with Pellet Paint CoPrecipitant (Novagen). DNA was pelleted by centrifugation at 13,000 rpm for 10 minutes and the supernatant was removed carefully. The DNA pellet was washed twice with 70% ethanol and finally dissolved in 100μL elution buffer (Qiagen).

2.17.2 Ligation Assay

Reactions were set up in 20μL reaction volumes consisting of 70fmol [γ-^{32}P]-ATP labelled DNA, x10 ligation buffer (66 mM Tris/HCl pH 7.5, 5 mM MgCl$_2$, 1 mM DTT, 1mM ATP, 0.5mg/mL BSA) and the stated amount of purified linker histone. This mixture was incubated on ice for 10 minutes before the addition of 200ng recombinant purified LX complex

(purified in house by Dr. Boris Kysela). Reactions were placed inside a Thermomixer (Eppendorf), mixed briefly then incubated at 37°C for 10 minutes, before being placed on ice for 5 minutes. The reaction was terminated by the addition of 0.6mg/mL Proteinase K in 0.6% SDS at 37°C for 15 minutes. The DNA products were then precipitated from the reaction mix with Pellet Paint CoPrecipitant. DNA was pelleted by centrifugation at 13,000 rpm for 10 minutes and the supernatant was removed carefully and the remaining DNA pellet allowed to air dry. The products were dissolved in elution buffer and non-specific DNA products were separated by a 3 minute period at 95°C followed by a 3 minute period on ice. DNA loading buffer was added to the samples and they were loaded on a 0.8% agarose gel without the addition of ethidium bromide, outlined in Section 2.11, and resolved by applying 150V across the gel for 45 minutes. The gel was vacuum dried at 50°C for 120 minutes, then exposed to a storage phosphor screen for 60 minutes. The screen was scanned using a STORM Phosphorimager and the images analysed using ImageQuant software.

2.18 Electrophoresis Mobility Shift Assay

Electrophoresis mobility shift assay (EMSA) reactions were set up in 20μL reaction volumes consisting of 70fmol [γ-^{32}P]-ATP labelled DNA, x10 EMSA buffer (66 mM Tris/HCl pH 7.5, 1 mM DTT, 1mM ATP, 0.5mg/mL BSA) and the required amount of purified linker histone, and incubated on ice for 10 minutes. Where appropriate, 200ng purified LX complex was added and incubated for a further 10 minutes on ice. DNA loading buffer (excl bromophenol blue) was added to the samples and they were loaded on a 0.8% agarose gel without the addition of ethidium bromide, outlined in Section 2.11, and resolved by applying 30mA across the gel

for 3 hours. The gel was vacuum dried at $50^{o}C$ for 120 minutes, then exposed to a storage phosphor screen for 60 minutes. The screen was scanned using a STORM Phosphorimager and the images analysed using ImageQuant software.

2.19 Co-Immunoprecipitation

2.19.1 Cloning of Linker Histone Genes in to the pFLAG-CMV-4 Vector

Genes coding for the linker histone variants with ligateable ends were excised from the pGEM-T-Easy vector (Section 2.13.7) using XbaI/BglII (H1.2) or XbaI/EcoRI (H1.X) restriction enzymes (Section 2.13.5) along with empty pFLAG-CMV-4 vector (Figure 2.2). Products were resolved on an agarose gel (Section 2.11), the relevant products were excised and the DNA extracted from the agarose (Section 2.12.1). Excised gene fragments along with linearised pFLAG-CMV-4 vector were ligated together (Section 2.13.6) enabling the linker histone genes to be inserted in-frame and with an amino-terminal FLAG peptide sequence (Asp-Tyr-Lys-Asp-Asp-Asp-Asp-Lys). Ligated products were transformed into competent *E. coli* (Section 2.10.3) and plated out onto LB agar containing ampicillin and left at $37^{o}C$ overnight (Section 2.10.1). Overnight cultures were obtained from individual colonies and these were assessed for the presence of the inserted gene by colony PCR (Section 2.13.4). From the positive colonies, mini-prep DNA was extracted (Section 2.12.2) which was used to generate stably transfected cell lines (Section 2.2.7).

2.19.2 Cloning of Linker Histone Genes in to the pEGFP Vector

Genes coding for the linker histone variants with ligateable ends were excised from the pFLAG-CMV-4 vector (Figure 2.2) using BamHI/EcoRI restriction enzymes (Section 2.13.5) along with empty pEGFP vector (Figure 2.4). Products were resolved on an agarose gel (Section 2.11), the relevant products were excised and the DNA extracted from the agarose (Section 2.12.1). Excised gene fragments along with linearised pEGFP vector were ligated together (Section 2.13.6) enabling the linker histone genes to be inserted in-frame and with an amino-terminal GFP fusion protein. Ligated products were transformed into competent *E. coli* (Section 2.10.3) and plated out onto LB agar containing ampicillin and left at 37°C overnight (Section 2.10.1). Overnight cultures were obtained from individual colonies and these were assessed for the presence of the inserted gene by colony PCR (Section 2.13.4). From the positive colonies mini-prep DNA was extracted (Section 2.12.2) which was used to generate stably transfected cell lines (Section 2.2.7).

2.19.3 Protein Extraction

Trypsinised cell pellets were washed with 5mL PBS and the resulting pellet resuspended in 300μL ice-cold IP lysis buffer (50mM Tris/HCl pH 7.5, 1mM EGTA, 1mM EDTA, 50mM sodium fluoride, 5mM sodium pyrophosphate, 1mM sodium orthovanadate, 0.27M sucrose, 1% Triton X-100, 0.1% β-mercaptoethanol, and protease inhibitor cocktail), vortexed for 10 seconds and placed on ice for 10 minutes. Cellular debris was pelleted by centrifugation at 13,000 rpm for 10 minutes at 4°C. The supernatant was carefully removed and placed into a

fresh 1.5mL microcentrifuge tube. Protein concentration was determined as outlined in Section 2.3.1.

2.19.4 Co-Immunoprecipitation

Protein G slurry (10μL) was washed twice with ice-cold IP wash buffer (IP lysis buffer excluding protease inhibitor cocktail). Extracted protein, typically 500μg, was added to the protein G beads and left for one hour with end-over-end rotation. Protein G beads were pelleted by centrifugation at 3,000 rpm for 2 minutes and the supernatant was removed and placed in a fresh 1.5mL microcentrifuge tube. Primary antibodies (Table 2.5) were added to the protein lysate and placed in a Thermomixer at max speed overnight at 4°C. A further 10μL protein G slurry was washed twice in ice-cold IP wash buffer, the lysate/antibody mixture was added, and the mixture placed in a Thermomixer at max speed for 3 hours at 4°C. Protein G beads were pelleted by centrifugation at 3,000 rpm for 2 minutes and the supernatant discarded. The beads were resuspended in 250μL ice-cold IP wash buffer and transferred to a labelled spinX centrifuge tube filter (Costar, 0.45μm pore size). The spinX column was centrifuged at 7,000 rpm for 1 minute and the flow through discarded. A further 250μL ice-cold IP wash buffer was added, centrifuged and discarded. Proteins were eluted with the addition of 35μL 1X sample buffer (Biorad) and placed at 70°C for 5 minutes, followed by centrifugation at 7,000 rpm for 1 minute.

2.19.5 Interacting Protein Partners Determination

To discover interacting partners following co-immunoprecipitation, the co-immunoprecipitation eluate was resolved on an SDS-PAGE gel as explained in Section 2.3.2 using pre cast 4-20% gradient gels (Bio-Rad). The gel was stained as explained in Section 2.3.3, but not dried, and bands of interest were excised and analysed by mass spectrometry to identify proteins. Mass spectrometry analysis was carried out by Functional Genomics Unit, University of Birmingham and the results returned in Microsoft Excel format

To confirm protein interactions, co-immunoprecipitation eluates were resolved on an SDS-PAGE gel and transferred to PVDF membrane as outlined in Section 2.3.4. Antibodies raised against potential interacting partners were used in Western blotting (Section 2.3.5).

CHAPTER THREE: MAPPING PHOSPHORYLATION SITES IN

THE SOMATIC LINKER HISTONE VARIANTS

3.1 Introduction and Overview

Vast networks of signal transduction cascades amplify and relay signals from the site of a DSB to the repair, cell-cycle and apoptotic machineries. The most heavily studied of these cascades is that of phosphorylation, however interesting data is surfacing on other modifications such as acetylation (Sun et al., 2009) and ubiquitylation (Stewart et al., 2009). Following a DSB there is a rapid phosphorylation of ATM on serine 1981, activating it and enabling it to phosphorylate its many targets (Bakkenist and Kastan, 2003). Some of these targets include p53 (serine 15), MDM2 (serine 395) and CHK2 (threonine 68), and phosphorylation of these proteins and subsequent effects leads to cell cycle arrest in the G1 phase of the cell cycle (Banin et al., 1998, Canman et al., 1998, Chehab et al., 2000, Matsuoka et al., 2000, Maya et al., 2001). Phosphorylation of BRCA1 (serine 1387) , FANCD2 (serine 222), NBS1 (serines 343, 397 and 615) and SMC1 (serines 957 and 966) by ATM leads to S-phase arrest (Cortez et al., 1999, S. T. Kim et al., 2002, Lim et al., 2000, Taniguchi et al., 2002, Wu et al., 2000b, Xu et al., 2002, B. B. Zhou et al., 2000), whereas cell cycle arrest at the G2 to M checkpoint can involve phosphorylation of hRAD17 (serines 635 and 645) and BRCA1 (serine 1423) (S. Bao et al., 2001, Xu et al., 2001). Phosphorylation of these targets is important in halting the cell cycle to allow the DNA damage to be correctly repaired.

Another target of ATM is the histone variant H2A.X which is specifically phosphorylated on a highly conserved residue, serine 139. Histone H2A.X is a crucial phosphorylation target in the repair of DSB with its phosphorylation status widely being used as a marker for sites of DSBs. Following DSBs, H2A.X molecules are phosphorylated anywhere up to 1Mb from the site of

the DSB (Burma et al., 2001). This propagation amplifies the signal which is expected to aid the recruitment and retention of DNA repair proteins.

DNA-PK also plays an active part in the phosphorylation cascade induced by a DSB, although many targets remain to be validated *in vivo*. DNA-PK phosphorylates p53 on serine 15 and serine 37 following IR, disrupting its interaction with MDM2 (Lees-Miller et al., 1992, Shieh et al., 1997). MDM2 itself is also phosphorylated on serine 17 by DNA-PK, further disrupting the p53-MDM2 interaction, although this phosphorylation event has only been studied *in vitro* (Mayo et al., 1997). Phosphorylation of poly(ADP-ribose) polymerase (PARP), a component of the base excision repair pathway, by DNA-PK has also been shown *in vitro*. This phosphorylation event does not seem to have any *in vivo* effect on its function however (Ariumi et al., 1999).

DNA-PK has also been shown to phosphorylate several members of the NHEJ pathway including the KU complex, XRCC4, XLF and Artemis *in vitro* and *in vivo* (Cao et al., 1994, Douglas et al., 2005, Ma et al., 2002, Yu et al., 2008, Yu et al., 2003c). Using site directed mutagenesis, putative phosphorylation sites in XRCC4 and XLF were removed, however, there was no loss-of-NHEJ-function (Yu et al., 2008, Yu et al., 2003c). Interestingly however, the phosphorylation activity of DNA-PK has been shown to be crucial for NHEJ activity, highlighting the importance in discovering phosphorylation targets *in vivo* (Kurimasa et al., 1999).

Autophosphorylation of DNA-PK has been shown to be the only crucial DNA-PK phosphorylation target for the rejoining of DSBs *in vivo* (Chan et al., 2002). Although there are many phosphorylation sites on DNA-PK, the phosphorylation of a cluster of residues around amino acid 2609 result in the dissociation of DNA-PK from DNA (Uematsu et al., 2007). This cluster is a site of autophosphorylation, however, other kinases are reported to also phosphorylate this 2609 cluster. One study reports that the phosphorylation event is dependent on ATM (B. P. Chen et al., 2007), whereas another study shows there is no requirement for the presence of ATM, but that the cluster can be phosphorylated in the absence of a functional DNA-PKcs kinase, suggesting the involvement if other kinases (Meek et al., 2007). A third study has shown that the 2609 cluster can be phosphorylated by ATR following UV damage, although the involvement of ATR in NHEJ is still unclear (Yajima et al., 2006). Either way, the phosphorylation of the 2609 cluster causes DNA-PKcs to leave the immediate site of the DSB allowing the processing and ligation of DNA ends (Uematsu et al., 2007).

Phosphorylation of p53, MDM2, CHK2, BRCA1, FANCD2, NBS1, SMC1, hRAD17 and H2A.X all occur at the ATM/DNA-PK consensus sequence (P/M/Y/G/F)-X-(S/A/D/E)-S/T-Q. The only strict requirement of the consensus sequence is that a glutamine residue is positioned directly after the phosphorylatable serine or threonine (S. T. Kim et al., 1999). Other proteins can be phosphorylated by DNA-PK at other regions, for example, RPA in response to UV irradiation (Zernik-Kobak et al., 1997).

DNA-PK can also phosphorylate the linker histone family *in vitro*. A commercially available mix of linker histones extracted from calf thymus tissue was phosphorylated by DNA-PK, *in vitro*, to a greater degree than the control p53 peptide. Purified phosphorylated linker histones were shown to remove the inhibition of LX mediated ligation which is seen with non-phosphorylated linker histones (Kysela et al., 2005).

3.2 Aims

In the previous published experiments, it was determined that the phosphorylation of linker histone variants has a functional impact on NHEJ (Kysela et al., 2005). The exact composition of the linker histone mix used in these studies is not known, therefore the exact target for DNA-PK phosphorylation could be any one or a combination of the 7 somatic linker histone variants (Section 1.2.3).

This chapter aims to identify DNA-PK phosphorylation sites in the individual linker histone variants by:

1. Identifying which individual linker histone variants are phosphorylated by the kinase DNA-PK, *in vitro*.

2. Identifying the DNA-PK phosphorylation sites in the linker histone variants.

3.3 Results

3.3.1 Identification of putative ATM/DNA-PK phosphorylation sites.

As previously mentioned, the ATM/DNA-PK phosphorylation consensus sequence has been identified as S/T-Q (S. T. Kim et al., 1999). All somatic linker histone variants were examined by sequence analysis to determine if any of these contained putative S/T-Q sites. Only two of the linker histone variants, H1.0 and H1.X, contained an SQ motif (Figure 3.1, underlined in red). Interestingly, the serine residue of the SQ motif in H1.0 is conserved throughout all the linker histone variants with the exception of H1.X, whereas, the serine residue of the SQ motif in H1.X is conserved in all linker histones variants. In both cases the glutamine residue following the serine residue is not conserved at all.

Conservation of these SQ sites in H1.X and H1.0 were then studied across different species. The SQ site in H1.X is conserved from *Homo sapiens* through to *Gallas gallas*, along with a surrounding 15 amino acid region (Figure 3.2). However, the site is not conserved in *Danio rerio* with the glutamine residue being replaced by a lysine residue. The full length H1.X protein is conserved 94% and 91% with *Pan troglodytes* and *Bos taurus* respectively, however it is much less conserved with other species (Figure 3.2). The SQ site in H1.0 is conserved in all species studied, excluding *G. gallas* where the serine residue is replaced with a leucine residue (Figure 3.3).

```
               10        20        30        40        50        60        70        80
       ----|----|----|----|----|----|----|----|----|----|----|----|----|----|----|----|
H1.1   ----MSETVPPAPAASAAPEKPLAGKKAKKPAKA-AAASKKKPAGPSVSELIVQAASSSKERGGVSLAALK-KALAAAGY
H1.2   ----MSETAPAAPAAAPPAEKAPVKKKAAKKAG--GTP--RKASGPPVSELITKAVAASKERSGVSLAALK-KALAAAGY
H1.3   ----MSETAPLAPTIPAPAEKTPVKKK-AKKAG--ATAGKRKASGPPVSELITKAVAASKERSGVSLAALK-KALAAAGY
H1.4   ----MSETAPAAPAAPAPAEKTPVKKKARKSAG--AAK--RKASGPPVSELITKAVAASKERSGVSLAALK-KALAAAGY
H1.5   ----MSETAPAETATPAPVEKSPAKKKATKKAAG-AGAAKRKATGPPVSELITKAVAASKERNGLSLAALK-KALAAGGY
H1.0   ----MTENSTSAPAAKPK------RAKASKKST----------DHPKYSDMIVAAIQAEKNRAGSSRQSIQ-KYIKSHYK
H1.X   MSVELEEALPVTTAEGMAKKVTKAGGSAALSPSKKRKNSKKKNQPGKYSQLVVETIRRLGERNGSSLAKIYTEAKKVPWF
                                                          *

               90       100       110       120       130       140       150       160
       ----|----|----|----|----|----|----|----|----|----|----|----|----|----|----|----|
H1.1   DVEKNNSRIKLGIKSLVSKGTLVQTKGTGASGSFKLNKKASSVETKPGASKV--ATKTKATGASKKLKKATGAS--KKSV
H1.2   DVEKNNSRIKLGLKSLVSKGTLVQTKGTGASGSFKLNKKAASGEAKPKVKKAGGTKPKKPVGAAKKPKKAAGGATPKKSA
H1.3   DVEKNNSRIKLGLKSLVSKGTLVQTKGTGASGSFKLNKKAASGEGKPKAKKAGAAKPRKPAGAAKKPKKVAGAATPKKSI
H1.4   DVEKNNSRIKLGLKSLVSKGTLVQTKGTGASGSFKLNKKAASGEAKPKAKKAGAAKAKKPAGAAKKPKKATGAATPKKSA
H1.5   DVEKNNSRIKLGLKSLVSKGTLVQTKGTGASGSFKLNKKAASGEAKPKAKKAGAAKAKKPAGAT--PKKAKKAAGAKKAV
H1.0   VGENADSQIKLSIKRLVTTGVLKQTKGVGASGSFRLAKSDEPKKSVAFKKTKKEIKKVATPKKASKPKKAASKAPTKKPK
H1.X   DQQNGRTYLKRYSIKALVQNDTLLQVKGTGANGSFKLNRKKLEGGGE---RRGAPAAATAPAPTAHKAKKAAPGAAGSRRA
             *

               170       180       190       200       210       220       230
       ----|----|----|----|----|----|----|----|----|----|----|----|----|----|----|----
H1.1   K-TPKKAKKPAATR---KSSKNPKKPKTV-KPKKVAKSPAKAKAVKPKAAKARVTKPKTAKPKKAA-----PKKK----
H1.2   KKTPKKAKKPAAATVTKKVAKSPKKAKVA-KPKKAAKS--AAKAVKPKAAKPKVVKPKKAAPKKKANAYFNPKGSFQSH
H1.3   KKTPKKVKKPATAAGTKKVAKSAKKVKTP-QPKKAAKSPAKAKAPKPKAAKPKSGKPKVTKAKKAA-----PKKK----
H1.4   KKTPKKAKKPAAAAGAKK-AKSPKKAKAA-KPKKAPKSPAKAKAVKPKAAKPKTAKPKAAKPKKAA-----AKKK----
H1.5   KKTPKKAKKPAAAG-VKKVAKSPKKAKAAAKPKKATKSPAKPKAVKPKAAKPKAAKPKAAKPKAAKAKKAAAKKK----
H1.0   ATPVKKAKK--------KLAATPKKAKKP---KTVKAKP--VKASKPKKAKP--VKPKAKSSAKRAG-----KKK----
H1.X   DKKPARGQKPEQRS--HKKGAGAKKDKGG----KAKKTAAAGGKKVKKAAKP--SVPKVPKGRK---------------
```

Figure 3.1 – Amino acid sequence alignment of human linker histones.
Linker histones were analysed to see if they contained putative ATM/DNA-PK phosphorylation sites. Two possible sites were found, one in H1.0 and the other in H1.X (boxed in red and highlighted by an asterix). Alignment of the linker histones illustrates the conservation of these sites amongst the somatic linker histones. Sequences were aligned using ClustalW program (www.ebi.ac.uk). Genbank accession numbers for protein sequences used are given in Table 2.6 and Appendix B. Key - Alanine, Tyrosine and Phenylalanine, Glycine, Proline, Serine and Threonine, Aspartic acid and Glutamine acid, Tryptophan, Histidine, Lysine and Arginine, Isoleucine, Leucine, Methionine and Valine, Asparagine and Glutamine and Cysteine.

Figure 3.2 – Amino acid sequence alignment of H1.X putative SQ site in humans and the orthologues in different species.
Amino acid sequences of H1.X, or similar to H1.X (*P. troglodytes and B. taurus*), aligned to show conservation of the putative SQ phosphorylation site. The SQ site is highlighted with a red box showing conservation in all species excluding *D. rerio*. Percentages shown in brackets represent the % identity to *H. sapiens* full length protein. Sequences were aligned using ClustalW program (www.ebi.ac.uk). Genbank accession numbers for protein sequences used are given in Appendix B. Key - Alanine, Tyrosine and Phenylalanine, Glycine, Proline, Serine and Threonine, Aspartic acid and Glutamine acid, Tryptophan, Histidine, Lysine and Arginine, Isoleucine, Leucine, Methionine and Valine, Asparagine and Glutamine and Cysteine.

Figure 3.3 - Amino acid sequence alignment of H1.0 putative SQ site in humans and the orthologues in different species.
Amino acid sequences of H1.0, or hypothetical sequence (*P. troglodytes*), aligned to show conservation of the putative SQ phosphorylation site. The SQ site is highlighted with a red box showing conservation in all species excluding *G. gallus*. Percentages shown in brackets represent the % identity to *H. sapiens* full length protein. Sequences were aligned using ClustalW program (www.ebi.ac.uk). Genbank accession numbers for protein sequences used are given in Appendix B. Key - Alanine, Tyrosine and Phenylalanine, Glycine, Proline, Serine and Threonine, Aspartic acid and Glutamine acid, Tryptophan, Histidine, Lysine and Arginine, Isoleucine, Leucine, Methionine and Valine, Asparagine and Glutamine and Cysteine.

3.3.2 Phosphorylation mapping of linker histone variants.

To identify potential DNA-PK phosphorylation sites on linker histone variants, a linker histone mix from calf thymus was used as a substrate for DNA-PK in an *in vitro* kinase assay (Section 2.15). Proteins were resolved on an SDS-PAGE gel (Section 2.3.2) and stained with PageBlue (Section 2.3.3). The linker histone bands were excised from the SDS-PAGE gel and phospho-peptide mapped by Functional Genomics (University of Birmingham). The collision induced dissociation technique was used to isolate PTM's of the linker histone variants. Whilst this technique confirms the presence of a modification, it does not necessarily determine which residue is modified (Sweet et al., 2006). Therefore all phosphorylatable residues within a peptide will be listed as a potential site of phosphorylation.

Peptides from all of the somatic linker histone variants were identified (H1.0-H1.5 and H1.X). Phosphorylation sites were seen that correspond with sites previously reported for H1.1, H1.2, H1.3 and H1.4 (Garcia et al., 2004, Wisniewski et al., 2007; Table 3.1). These are typically serine 2 and threonine 4, or those that reside within the RKASGPPVSELITKA peptide. These sites were seen before phosphorylation by DNA-PK, suggesting that these are phosphorylated residues which have arisen in the calf thymus cells and not specifically by DNA-PK. Several novel non DNA-PK-mediated phosphorylated residues were also identified namely; serine 55 or serine 58 of H1.2, H1.3 (serine 56 and serine 59) and H1.4, along with threonine 77, threonine 78 or threonine 84 within H1.0.

All linker histone variants except H1.5 were phosphorylated by DNA-PK (Table 3.1). Novel phosphorylation by DNA-PK of serine 89, serine 92, threonine 85 or threonine 99 was found in H1.1. Phosphorylation of the same residues has already been identified in H1.2 and H1.3, however, since the matched peptide is the same across all three variants it is impossible to ascertain which of the three variants is actually phosphorylated (Garcia et al., 2004). Novel DNA-PK phosphorylation was also seen in: H1.1, serine 149 or threonine 152; H1.3, threonine 164 or threonine 168; H1.0 threonine 77, threonine 78 or threonine 84; and H1.X, tyrosine 48, serine 49 or threonine 55.

Protein	Modification	Peptide	Source	Cell Line or Tissue
H1.1	pS-2	**pS**ETVPPAPAASAAPEKPLAGK	(Wisniewski et al., 2007)	HeLa, Mouse heart, kidney, seminal vesicle, testis.
	pT-4	**pS**E**pT**APVAQAASTATEKPAAAK	(Wisniewski et al., 2007)	Mouse testis
	pS-43	KPAGPSV**pS**ELIVQAVSSSK	(Wisniewski et al., 2007)	
	pS-89, pS-92, pT-85 or pT-99	KpSLVpSKGpTLVQpTKG	This Study	
	pS-149 or pT-152	KKpSVKpTPKK	This Study	
H1.2	pS-2	**pS**ETAPAAPAAAPPAEK	(Wisniewski et al., 2007)	HeLa, Mouse heart, seminal vesicle
	pS-2 or pT-4	MpSEpTAPAAPAAAPPAEKA	This Study	
	pT-31	KAAKKAGG**pT**PR	(Garcia et al., 2004)	HeLa
	pS-36	KA**pS**GPPVSELITK	(Garcia et al., 2004, Wisniewski et al., 2007)	MCF7, HeLa, Mouse brain, kidney, muscle, seminal vesicle, spleen
	pS-36, pS-41 or pT-45	RKApSGPPVpSELIpTKA	This Study	
	pS-41	ASGPPV**pS**ELITK	(Wisniewski et al., 2007)	Mouse spleen
	pS-55 or pS-58	pSGVpSLAALK	This Study	
	pS-86	LGLK**pS**LVSK	(Wisniewski et al., 2007)	Mouse kidney
	pS-86, pS-89 or pT-92	KpSLVpSKGpTLVQpTKG	This Study	
	pT-146	KAAGGA**pT**PKK	(Garcia et al., 2004, Wisniewski et al., 2007)	HeLa, Mouse spleen
	pT-154	KSAKK**pT**PK	(Garcia et al., 2004)	HeLa

	pT-165	KPAAA**pT**VTKK	(Wisniewski et al., 2007)	MCF7
	pS-173	KVAK**pS**PK	(Garcia et al., 2004, Sarg et al., 2006, Wisniewski et al., 2007)	HeLa, HLTC
H1.3	pT-18	SETAPLAPTIPAPAEK**pT**PVK	(Wisniewski et al., 2007)	MCF7, HeLa, Mouse testis, spleen
	pS-37	KA**pS**GPPVSELITK	(Garcia et al., 2004, Wisniewski et al., 2007)	MCF7, HeLa, Mouse brain, kidney, muscle, seminal vesicle, spleen
	pS-42	ASGPPV**pS**ELITK	(Wisniewski et al., 2007)	Mouse spleen
	pS-37, pS-42 or pT-46	RKApSGPPVpSELIpTKA	This Study	
	pS-56 or pS-59	pSGVpSLAALK	This Study	
	pS-87	LGLK**pS**LVSK	(Wisniewski et al., 2007)	Mouse kidney
	pS-87, pS-90, pT-93 or pT-97	KpSLVpSKGpTLVQpTKG	This Study	
	pT-147	KVAGAA**pT**PKK	(Garcia et al., 2004, Wisniewski et al., 2007)	MCF7, HeLa, Mouse spleen
	pT-155	KSIKK**pT**PK	(Garcia et al., 2004)	HeLa
	pT-164 or pT-168	KKVKKPApTAAGpTKK	This Study	
	pT-180	KVK**pT**PQPK	(Garcia et al., 2004)	HeLa
	pS-189	KAAK**pS**PAKAKAPKPK	(Garcia et al., 2004, Sarg et al., 2006)	HeLa, HLTC
H1.4	pS-2	**pS**ETAPAAPAAPAPAEK	(Garcia et al., 2004, Wisniewski et al.,	HeLa, Mouse spleen, heart

			2007)	
	pT-4	**pS**E**pT**APAAPAAPAPAEKT	(Garcia et al., 2004, Wisniewski et al., 2007)	HeLa, Mouse spleen
	pT-18	SETAPAAPAAPAPAEK**pT**PVK	(Garcia et al., 2004, Wisniewski et al., 2007)	MCF7, HeLa, Mouse testis, liver
	pS-2, pT-4 or pT-18	pSEpTAPAAPAAPAPAEKpTPVK	This Study	
	pS-27	KARK**pS**AGAAKR	(Garcia et al., 2004)	HeLa
	pS-36	RKA**pS**GPPVSELITKA	(Wisniewski et al., 2007)	MCF7, HeLa, Mouse heart, lung, muscle, spleen
	pS-41	TSGPPV**pS**ELITK	(Wisniewski et al., 2007)	Mouse kidney, lung
	pS-36, pS-41, pT-45	RKApSGPPVpSELIpTKA	This Study	
	pS-55 or pS-58	pSGVpSLAALK	This Study	
	pS-86	LGLK**pS**LVSK	(Wisniewski et al., 2007)	Mouse kidney
	pT-146	KATGAA**pT**PKK	(Garcia et al., 2004)	HeLa
	pS-172	KAK**pS**PK	(Garcia et al., 2004, Sarg et al., 2006)	HeLa, HLTC
	pS-187	KAPK**pS**PAK	(Garcia et al., 2004, Sarg et al., 2006, Wisniewski et al., 2007)	MCF7, HeLa, HLTC, Mouse spleen
H1.5	pS-2	**pS**ETAPAETATPAPVEK	(Wisniewski et al., 2007)	MCF7, Mouse heart, seminal vesicle
	pT-4	**pS**E**pT**APAETATPAPVEK	(Wisniewski et al., 2007)	HeLa
	pT-11	Not given	(Sarg et al., 2006)	HTLC
	pS-18	SETAPAETATPAPVEK**pS**PAK	(Sarg et al., 2006,	MCF7, HeLa, Mouse brain, kidney, liver, muscle,

			Wisniewski et al., 2007)	seminal vesicle, spleen, testis, HLTC
	pT-138	KPAGA**pT**PKK	(Garcia et al., 2004, Sarg et al., 2006, Wisniewski et al., 2007)	MCF7, HeLa, HLTC
	pT-155	KAVKK**pT**PK	(Garcia et al., 2004, Sarg et al., 2006)	HeLa, HLTC
	pT-173	Not given	(Sarg et al., 2006)	HLTC
	pS-188	Not given	(Sarg et al., 2006)	HLTC
H1.X	pS-31	AGGSAAL**pS**PSK	(Garcia et al., 2004, Wisniewski et al., 2007)	HeLa
	pY-48, pS-49 or pT-55	K<u>p</u>Y<u>p</u>SQLVVE<u>pT</u>IRRL	This Study	
	pS-154	AKKAAPGAAG**pS**R	This Study	
H1.0	pT-77, pT-78 or pT-84	LV<u>pTp</u>TGVLKQ<u>pT</u>K	This Study	

Table 3.1 – Phosphorylation Mapping of Linker Histones identified in this chapter, compared to published results.

Linker histones were phosphorylated by DNA-PK and analysed by mass spectrometry. Due to the nature of the mass spectrometry only peptides, and not specific phosphorylation sites, were mapped. All phosphorylation sites are preceded with a lower case p, ambiguous phosphorylation sites are underlined and identified phosphorylation sites are listed in bold. Along with results identified in this chapter are previously published phosphorylated residues with the tissue/cell line they were isolated in. Red identifies phosphorylation sites in the absence of DNA-PK which have previously been recorded. Blue identifies novel phosphorylation sites in the absence of DNA-PK. Green identifies novel DNA-PK mediated phosphorylation sites.

3.3.3 Purification of individual linker histones variants from *E.coli*.

To confirm whether the DNA-PK mediated phosphorylation sites seen in H1.X and H1.0 are phosphorylated *in vitro*, recombinant proteins were prepared in *E. coli* and reconstituted into the *in vitro* kinase assay (Section 2.15). Following induction of protein expression, prominent bands were clearly visible which represent the individual linker histone variants (Figure 3.4A, red boxes). Following lysis, the linker histone bands are still present, and in some cases, extremely prominent (Figure 3.4B). Eluates of the linker histone variants showed a prominent main band which corresponded to the predicted protein size (35kDa-40kDa), however all but H1.X showed varying degrees of protein degradation (Figure 3.5).

Attempts were made to reduce the amount of degradation seen in linker histone variants H1.1 to H1.5. These included changing the bacteria in which the proteins were produced, varying the amounts of IPTG used for induction and the induction time itself, varying the constituents of the lysis buffer, removing the sonication step and changing the wash conditions. All of these had no significant impact on the amount of degradation seen (data not shown).
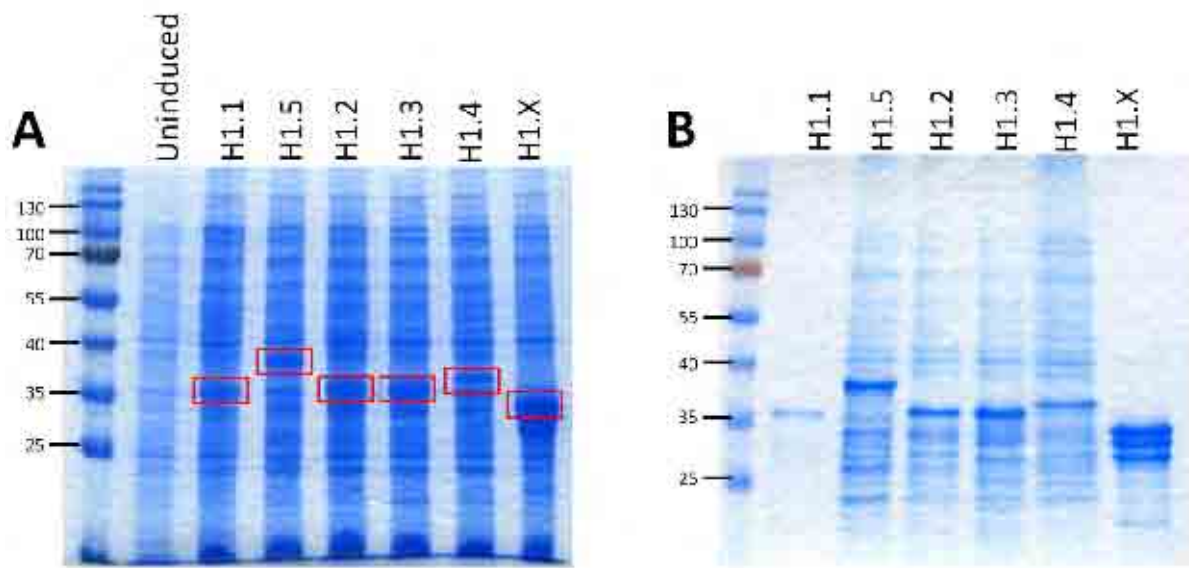
Figure 3.4 – Recombinant linker histone variant purification in *E. Coli*.
A. Bacteria containing the pET28-b expression vector with linker histone variant genes cloned into the multiple cloning site were induced to produce protein with the addition of IPTG. Linker histone variants H1.1-H1.5 and H1.X show a clear over-expressed protein band, boxed in red, compared to the un-induced controls.
B. After salt lysis the over-expressed histone bands have been solubilised and are clearly visible.
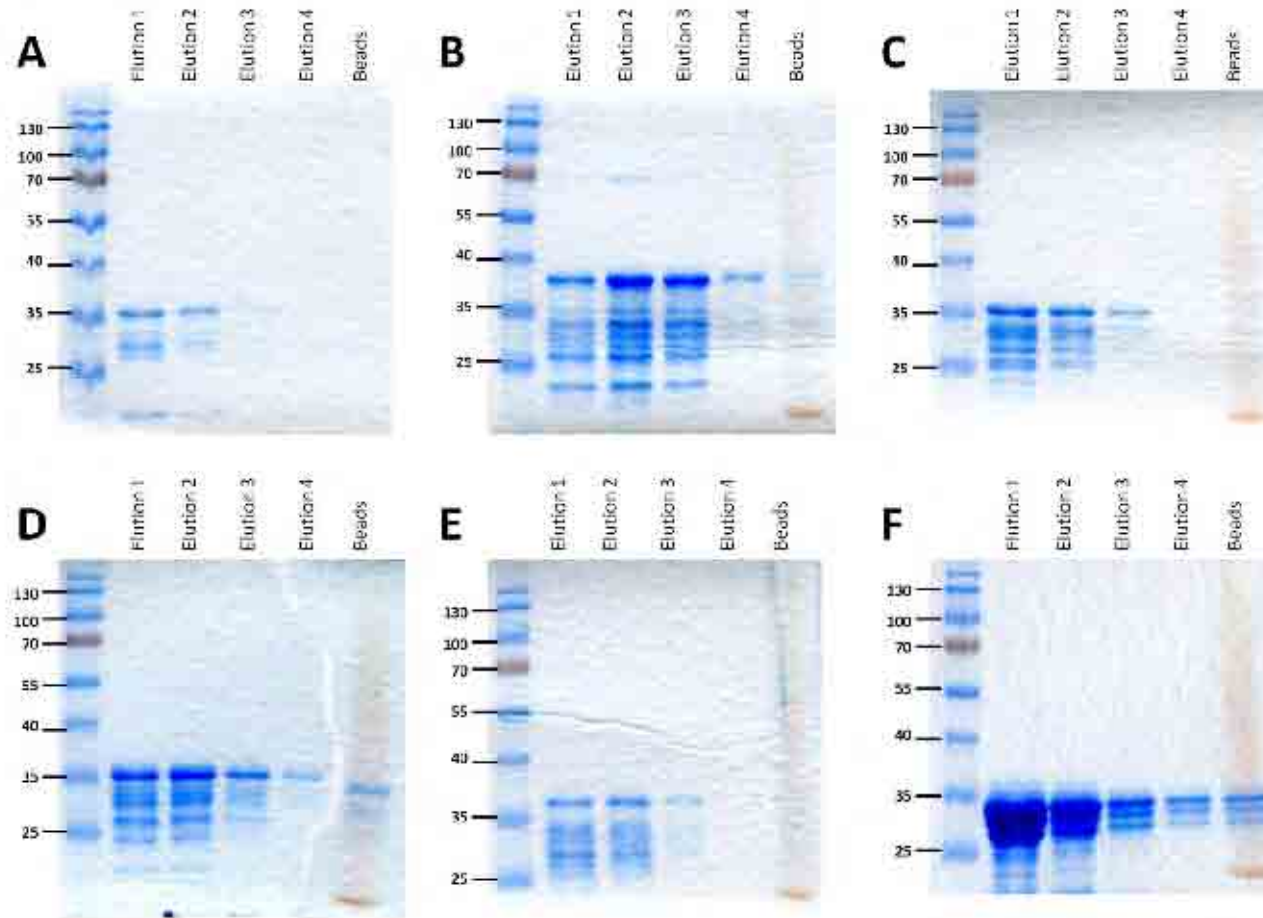
Figure 3.5 – Elution of affinity purified linker histone variants.
Each linker histone variant (A-H1.1, B-H1.5, C-H1.2, D-H1.3, E-H1.4, F-H1.X) was eluted in 250uL aliquots from affinity beads with imidazole. In the majority of cases the first elution provides the most protein, and where it does not then the second elution provides the most protein. Varying amounts of purified proteins can be seen, along with degradation products. After 4 elutions very little protein remained on the beads.

Attempts were also made to over-express and purify some of the linker histone variants in the baculovirus over-expression system. Cellular extracts of over expressed H1.2 protein from SF9 insect cells were produced (personal communication with Dr. Chris Bruce, procedure outlined in Riballo et al., 2001). Using the standard lysis buffer, H1.2 protein remained in the insoluble fraction (Figure 3.6A). The lysis buffer was subsequently changed to resemble that used in the bacterial cell lysis (Section 2.14.3), and this also was unable to solubilise H1.2 from insect cells (Figure 3.6B).
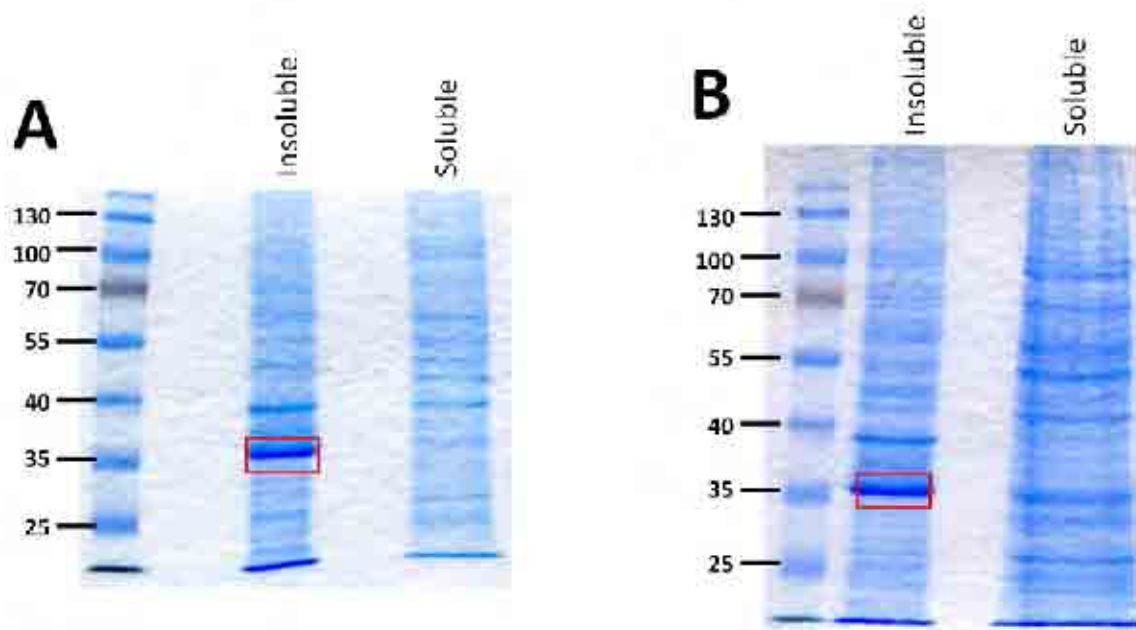
Figure 3.6 – Purification of mammalian H1.2 from SF9 insect cells.
Over-expressed H1.2 protein was produced in SF9 insect cells. Under normal lysis conditions, the proteins remain insoluble (A), using similar lysis conditions to those used in bacterial lysis the protein remained insoluble (B).

3.3.4 Phosphorylation of linker histone variants by DNA-PK.

Purified recombinant linker histone variants H1.1, H1.2, H1.3, H1.4, H1.5, H1.X, and purified H1.0 (a gift from Prof. Jeffrey Hansen, Colorado State University) were examined using the *in vitro* kinase assay with DNA-PK as the kinase (Section 2.15). All the linker histone variants were phosphorylated by DNA-PK (Figure 3.7A). However, the linker histone variants which showed large amounts of degradation, H1.1-H1.5, also showed large amounts of phosphorylated degradation products (Figure 3.7A). Although H1.X and H1.0 both contain the ATM/DNA-PK SQ phosphorylation motif, H1.X was phosphorylated to a greater extent than H1.0 which has an extremely faint band. All linker histones were loaded equally (Figure 3.7B).
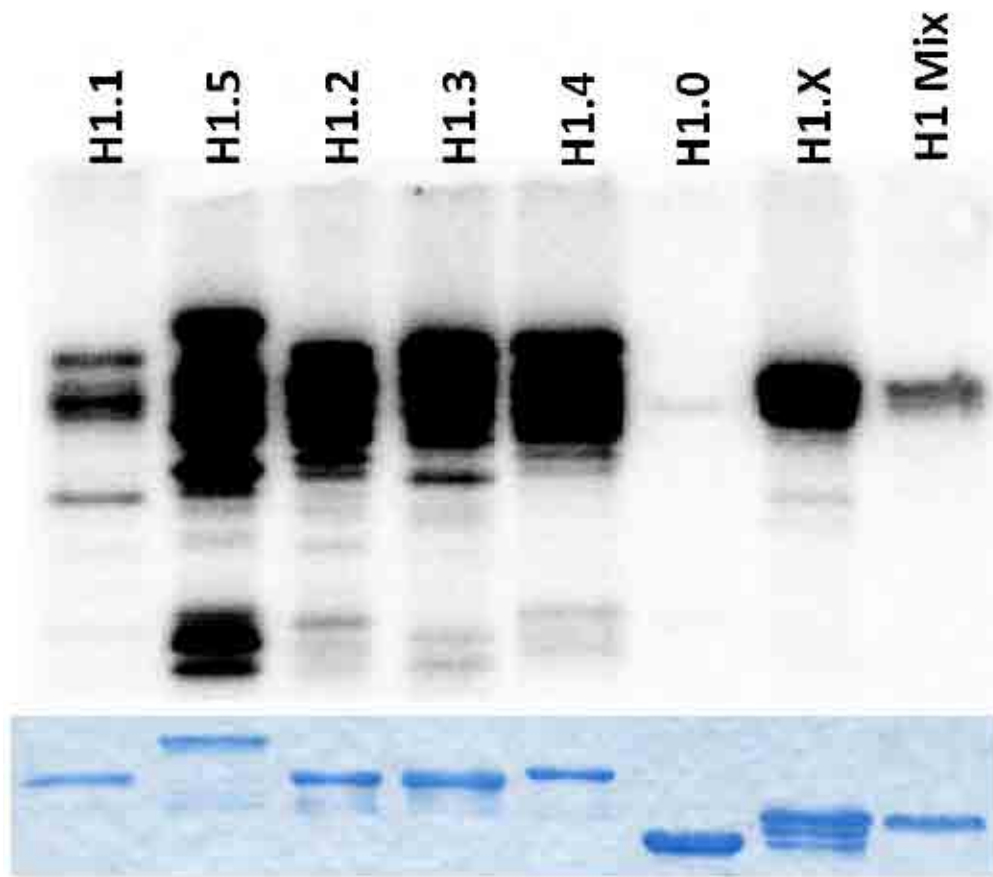
Figure 3.7 – DNA-PK phosphorylation of recombinant linker histone variants.
Recombinant linker histone proteins were incubated with DNA-PK and [γ-^{32}P]ATP. Dried SDS-PAGE gels were exposed to a storage phosphor screen and imaged on a Typhoon Phosphorimager. Linker histone variants H1.1 – H1.5 show phosphorylation of the full length protein, but also of the degraded protein. H1.0 shows extremely low phosphorylation, and H1.X exhibits good phosphorylation of the full length product. H1.X also displays the least amount of phosphorylated degradation products due to its cleaner purification. H1 Mix contains linker histone variants purified from calf thymus which shows phosphorylation.
The lower panel shows PageBlue staining of the linker histones used in the kinase assay to show equal loading of proteins.

3.4 Discussion

The aim of this chapter was to identify potential phosphorylation sites on the linker histone variant proteins. Using *in silica* analysis we show that the replication dependent somatic linker histone variants do not contain a putative ATM/DNA-PK phosphorylation site. However, the less characterised H1.0 and H1.X both contain putative SQ sites. Aligning all somatic linker histone variants (Figure 3.1), we reveal significant homology surrounding these SQ sites but crucially, the required glutamine is absent. The SQ sites in both H1.0 and H1.X are also conserved in *P. troglodytes, B. taurus, M. musculus and Rattus norvegicus*.

Table 3.1 shows that the phosphorylation of the H1.2, H1.3 and H1.4 proteins could be observed at the RKASGPPVSELITKA site prior to incubation with DNA-PK. This supports other studies in HeLa and MCF7 human cell lines, along with different mouse tissues, which suggest these phosphorylation events occur during normal cycling of the cell and are not limited to the response to DNA damage in the form of DSBs (Garcia et al., 2004, Wisniewski et al., 2007). Phosphorylation of serine 2 and threonine 4 in the amino terminus of H1.1 and H1.4 was also seen, which supports studies where it has been previously seen in mouse tissues and HeLa cells (Garcia et al., 2004, Wisniewski et al., 2007). It is suggested that phosphorylation of these residues occurs during the cell cycle. During interphase the CTD is primarily phosphorylated, and during mitosis the NTD also becomes phosphorylated (Gurley et al., 1995). As the linker histones were commercially sourced it is impossible to determine whether they were cycling or not.

Novel phosphorylation sites were identified prior to incubation with DNA-PK for H1.2, H1.3 and H1.4 on the SGVSLAALK peptide. The first serine residue is not conserved in H1.1, H1.5, H1.X or H1.0, suggesting that it may be this residue that is preferentially phosphorylated as it is unique to H1.2, H1.3 and H1.4. This peptide is part of the central conserved domain of the linker histones and is conserved in mice. Novel phosphorylation was also seen in H1.X at serine-154, a residue not conserved in any other linker histone, nor in mouse H1.X.

Of particular interest was the identification of novel DNA-PK phosphorylation sites. Several novel sites of phosphorylation in the linker histone variants H1.1, H1.3 and H1.X were identified following incubation with DNA-PK, none of which were detected in previous studies of HeLa, MCF7 or lymphoblastic T-cell human cell lines, or mouse tissue (Garcia et al., 2004, Sarg et al., 2006, Wisniewski et al., 2007).

Phosphorylation of the KKSVKTPKK peptide, identified in H1.1, is particularly interesting as it contains a residue, threonine 152, which is proposed to facilitate high affinity binding between the linker histone and the DNA. Mutations in this residue, and/or serine 183, result in the reduced mobility of the linker histone variant H1.1 on DNA, as measured by FRAP analysis (Hendzel et al., 2004). If threonine 152 is a target of DNA-PK phosphorylation, it would imply that following DNA damage, DNA-PK phosphorylates linker histone variant H1.1 at threonine 152, and potentially the other replication dependent linker histone variants as this residue is conserved. This would result in weaker binding of the linker histone variants to the DNA, aiding their release from the DNA, allowing the NHEJ repair proteins access to the site of the DSB (Dou et al., 2002, Lever et al., 2000).

Phosphorylation of the KKVKKPATAAGTKK peptide at positions threonine 164 or threonine 168, identified in H1.3, has not been shown before in cell lines or mouse tissue. These residues are very poorly conserved between the other linker histones with only threonine 168 conserved in H1.2, and both threonine residues not being conserved at all in mouse H1.3.

Phosphorylation of the KYSQLVVETIRRL peptide in H1.X contains three potential phosphorylatable residues. Conservation of these residues shows the tyrosine residue is only conserved in H1.0, the threonine residue is not conserved at all and the serine residue is conserved in all linker histones. The glutamine residue which immediately follows in H1.X conforms to the DNA-PK SQ consensus motif, this residue is not conserved amongst the somatic linker histones, suggesting it could be an important unique linker histone capable of phosphorylation by DNA-PK.

Although the S/T-Q motif is generally thought to be the target for DNA-PK phosphorylation (Y. R. Chen et al., 1991), more recently proteins lacking these motifs have been shown to be phosphorylated by DNA-PK (Chan et al., 1999, Zernik-Kobak et al., 1997). Mass spectroscopy has shown that serine or threonine sites can be phosphorylated when immediately followed by a hydrophobic amino acid (Meek et al., 2004). This chapter demonstrates that the majority follow this rule but there is one exception where a threonine residue is followed by a glycine residue in H1.0 (Table 3.1).

To determine the importance of the potential individual phosphorylation sites identified they would have to be knocked out by site-directed mutagenesis and re-assessed using the *in vitro* kinase assay. However, the potential impact of these sites *in vivo* would also need to be tested. Studies knocking out DNA-PK phosphorylation sites in XRCC4 (Yu et al., 2003c) and XLF (Yu et al., 2008) have resulted in no impact on NHEJ. This suggests that although the native proteins can be phosphorylated, their phosphorylation has no detrimental effect on NHEJ.

In order to study the phosphorylation sites in more detail, recombinant proteins were produced. Although linker histone variants were purified from *E. coli* using the pET vector system, with the exception of H1.X, they were highly degraded. A study which aimed to purify rat H1.3 also encountered similar problems and the authors suggest that the degradation is due to the high lysine and arginine content found in the CTD of the linker histone (Bharath et al., 1998). This group also tried to express the linker histone H1.3 as a fusion protein with GST using the pGEX-2T vector but the fusion protein was unable to bind the GST affinity matrix, something also observed when attempting to purify linker histone variants using this system (data not shown). To overcome the problem of degradation the group used an alternative vector, pTrc99A, which places the poly-histidine tag at the carboxyl-terminus of the protein, as opposed to the amino-terminus in the pET vector system. An alternative approach would be to tag the protein at each end and employ a tandem purification approach which would result in optimal yield with minimum degradation.

Another approach to purify linker histone H1.2 was to use the baculovirus expression system. Although the system adequately expressed linker histone H1.2, the protein was insoluble and remained insoluble despite using several different lysis buffers. Further work to find the correct lysis buffer to solubilise H1.2 is required.

Using the purified linker histone variants reconstituted in the *in vitro* kinase assay, it was seen that H1.1, H1.2, H1.3, H1.4, H1.5 and H1.X are all phosphorylated and H1.0 had very minimal phosphorylation. As previously discussed, phosphorylation of H1.1 to H1.5 must be at a non-SQ site as these linker histone variants do not contain this site. As the products are also not pure, the possible phosphorylation of contamination products cannot be ruled out. H1.0 and H1.X are the only two linker histone variants to contain the SQ-site and of these two, H1.X is seen to be phosphorylated to a greater extent *in vitro*.

CHAPTER FOUR: *IN VIVO* CHARACTERISATION OF H1.X'S

ROLE IN DOUBLE STRAND BREAK REPAIR

4.1 Introduction and Overview

H1.X is the most recently identified of the linker histone family (Yamamoto and Horikoshi, 1996). The expression profile of H1.X demonstrates expression across many tissues in a non cell cycle dependant manner, in contrast to the rest of the linker histone variants H1.1, H1.2, H1.3, H1.4 and H1.5 (Happel et al., 2005).

Structurally, H1.X contains the typical tripartite structure comprising of a central globular domain, flanked by a short basic NTD and a long basic CTD, as seen in other linker histone variants (Figure 1.11). However, H1.X shares much less sequence homology with the other linker histones. The globular domain (underlined in purple in Figure 4.1) shows striking conservation between linker histones H1.1 to H1.5, however, there is only 38% identity between H1.X and H1.1 to H1.5. Outside of the globular domain, in the basic NTD and CTD there is also little conservation.

There are three key lysine residues (Figure 4.1, red asterisks) within the globular domain which are postulated to be important for contact with DNA. These three lysine residues are conserved between all linker histone variants. Two amino acids that are considered to be important for the high-affinity binding of linker histones to chromatin *in vivo*, threonine 152 and serine 183 in H1.1, are not conserved in H1.X (Hendzel et al., 2004). The importance of these residues can be seen when comparing H1.2, which has these conserved sites, and H1.X, which does not. Using GFP-tagged linker histone proteins and analysing their binding kinetics using FRAP, H1.2 remains more tightly bound than H1.X (Takata et al., 2007).

H1.X also has a different localisation pattern to other linker histone variants which have an overall nuclear localisation and do not appear to be accumulated in the nucleoli. H1.X primarily locates to the nucleoli during the G1 phase of the cell cycle, however, it is not required for the maintenance of nucleolar structure (Stoldt et al., 2007, Takata et al., 2007). Olsen *et. al.* (2002) suggest a role for the nucleoli whereby it serves as a storage centre for the temporary inactivation of regulatory proteins (Olson et al., 2000). This theory seems even more interesting when considering some of the proteins which have been reported to be present in the nucleoli: RAD51, involved in HR (Section 1.1.3; De et al., 2006); BRCA1 (Section 1.1.2.7), involved in HR, checkpoint control and DNA repair (De et al., 2006, Tulchin et al., 2010).

Depletion of H1.X in HeLa cells results in defective spindle formation, leading to misaligned chromosomes and activation of the spindle checkpoint resulting in delayed mitosis (Takata et al., 2007). Interestingly, the presence of micronuclei following successful mitotic division was also detected. The presence of micronuclei can indicate that the protein may have an involvement in DNA repair. Micronuclei are unrepaired DSBs that result in an acentric chromosome fragment being created. Micronuclei are also seen when depleting the levels of KU70, or inhibiting the kinase function of DNA-PK$_{CS}$ (Chernikova et al., 1999, Y. Zhang et al., 2008).
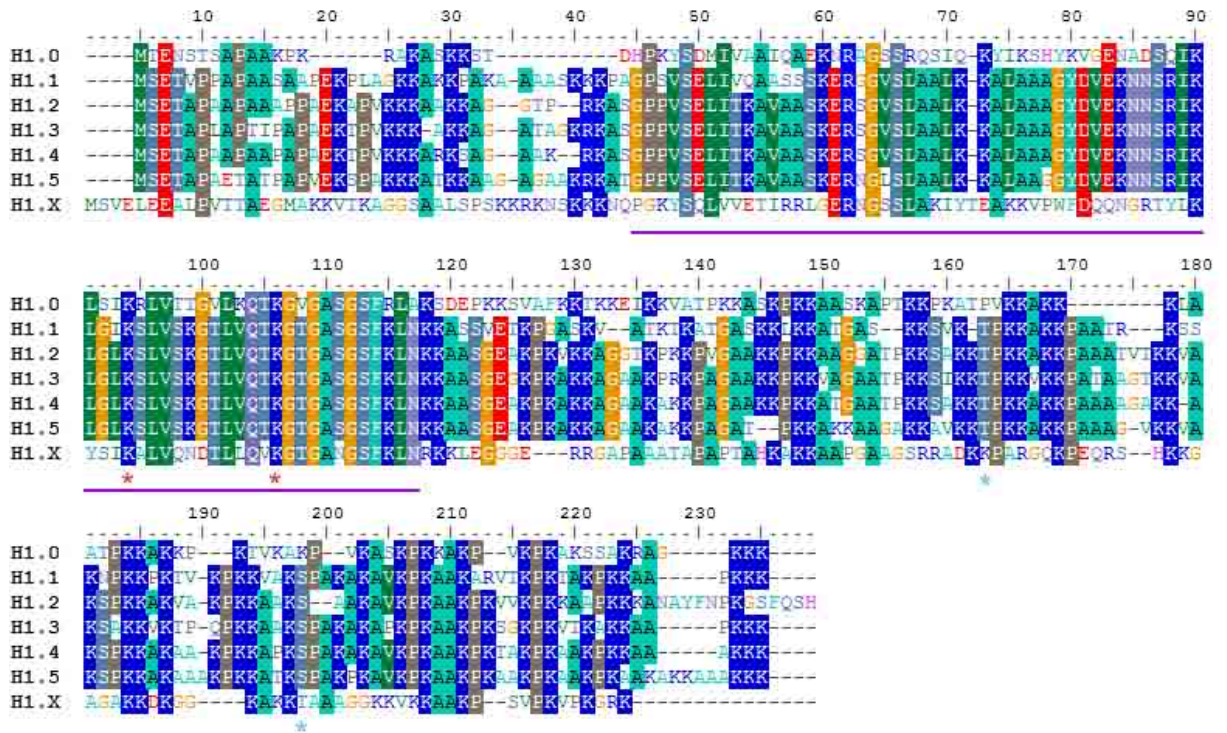
Figure 4.1 - Sequence alignment of linker histone variants
Multiple alignment of the primary sequences of human somatic linker histone variants. The globular domain sequence is underlined in purple. Lysine residues thought to be important for contact with DNA are highlighted with red asterisks, and the two amino acids postulated to be important for chromatin interactions are highlighted with blue asterisks. Key - Alanine, Tyrosine and Phenylalanine, Glycine, Proline, Serine and Threonine, Aspartic acid and Glutamine acid, Tryptophan, Histidine, Lysine and Arginine, Isoleucine, Leucine, Methionine and Valine, Asparagine and Glutamine and Cysteine.

4.2 Aims

The previous chapter explains that although all the linker histone variants examined are able to be phosphorylated by DNA-PK *in vitro*, H1.X contains an SQ site which could be phosphorylated *in vivo* by DNA-PK. This observation suggests that H1.X might be a true physiological target for DNA-PK *in vivo*, and as such, it may be involved in DNA-PK mediated DNA damage responses in human cells. In order to investigate the functional role of H1.X *in vivo* this chapter will:

1. Investigate H1.X function by depleting cells of H1.X protein and then:

    a. Assessing cell survival and growth using the clonogenic survival assay.

    b. Assessing the ability of cells to repair DSBs by the γH2A.X foci assay.

    c. Assessing changes to cell cycle kinetics by flow sorting.

2. Further characterise H1.X function by examining the localisation of H1.X following exposure to IR.

4.3 Results

4.3.1 siRNA targeted knockdown of H1.X

Using small RNA oligonucleotides targeted towards the globular domain of H1.X, protein levels were reduced by 95% 24 hours post transfection, and lasted for a minimum of 5 days (Figure 4.2). α-tubulin was used as a loading control, and immuno-probing for the linker histone variant H1.2 will assess the specificity of the siRNA. H1.2 does not contain an SQ

phosphorylation motif and has been reported as being the most highly expressed of all linker histones (Kratzmeier et al., 1999). Immuno-probing for the core histone H2A will also highlight any changes in core histone protein levels due to H1.X depletion. Levels of all of these proteins remain the same as the pre-siRNA samples (0 hours) showing that the depletion of H1.X had no effects on other linker histones nor core histones. Using siRNA targeted towards H1.2, H1.2 protein levels were reduced by 96% after 24 hours and the following 5 days. Levels of H1.X, H2A and α-tubulin remained constant during this time course. siRNA targeted towards the firefly luciferase (LUC) gene was used a control for transfection. The α-tubulin levels are constant and there is no noticeable reduction of H2A levels over the 5 day time course, however, after 24 hours both H1.X and H1.2 protein levels were reduced by 80% and 95% respectively. These levels do return to their un-transfected level after 48 hours however and remain at that for the next 72 hours. Due to this all experiments were carried out 48 hours post transfection when the levels of all un-targeted proteins are at their normal levels.
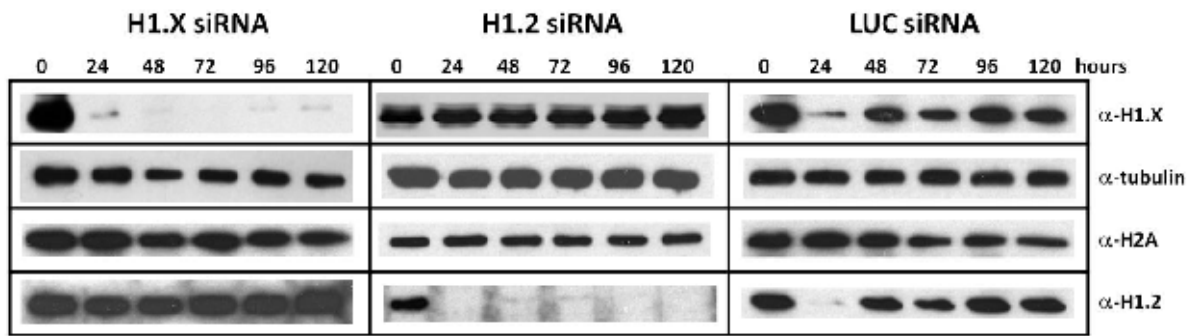
Figure 4.2 - siRNA depletion of H1.X, H1.2 and LUC
MRC5VA cells were treated with siRNA targeted towards H1.X, H1.2 and LUC and examined over a 120 hour period. All siRNA transfections were assessed with antibodies directed towards H1.X, H1.2, H2A and α-tubulin. H1.X siRNA reduced H1.X proteins levels by 95% over the 120 hour period with no significant changes seen in the expression levels of H2A and H1.2. H1.2 siRNA reduced H1.2 protein levels by 96% over the 120 hour period with no significant changes seen in the expression levels of H1.X and H2A. Control LUC siRNA reduced the protein levels of H1.X and H1.2 by 80% and 95% respectively after the first 24 hours. From 48 hours onwards the expression levels returned to pre-siRNA levels. Levels of H2A remained consistent throughout the 120 hour period. Protein quantification was determined with ImageJ imaging software (NIH).

4.3.2 siRNA mediated depletion of H1.X renders cells sensitive to ionising radiation

To determine whether H1.X had a role in survival following exposure to IR, MRC5VA cells were exposed to increasing doses of IR and their survival rates analysed (Figure 4.3). Over the 8 Gy dose range H1.X siRNA cells are consistently more sensitive than the untransfected, LUC siRNA or H1.2 siRNA transfected cells (Figure 4.3). Using the students' two tailed t-test, the difference between H1.X depleted cells and control cells is statistically significant with a p-value of at least < 0.05 for 2, 4 and 6 Gy (Figure 4.3, gold stars), at 8 Gy the p-value becomes < 0.001 (Figure 4.3, red star). Interestingly there is a slight resistance to IR for the H1.2 depleted cells when cells are exposed to 8 Gy (p < 0.05, Figure 4.3, black star).
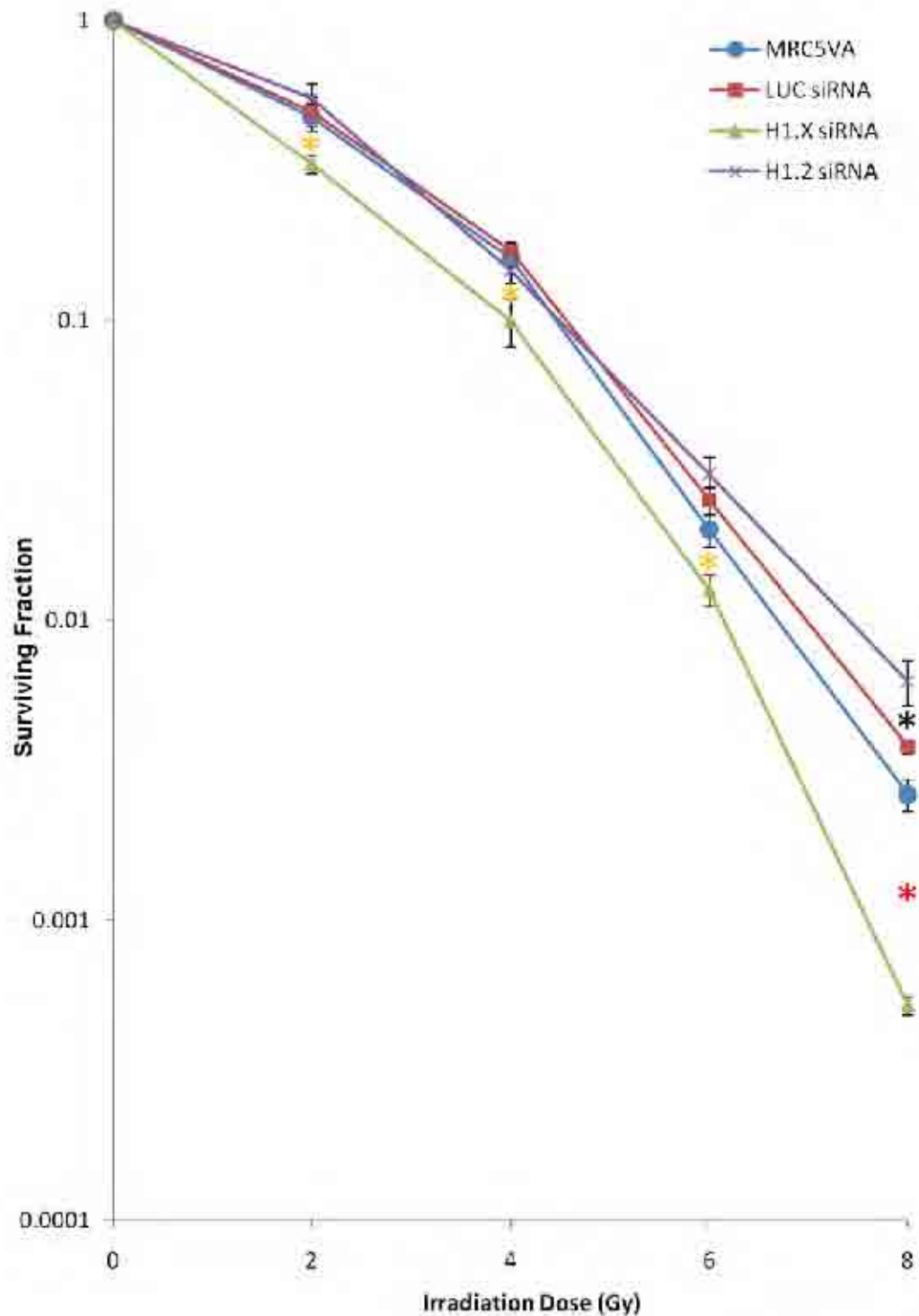
Figure 4.3 - siRNA mediated depletion of H1.X renders cells sensitive to ionising radiation
Over increasing doses of IR, cells depleted of H1.X by siRNA are more sensitive than the control un-transfected cells, LUC siRNA control cells and cells depleted of H1.2 by siRNA. At 8Gy, the difference between cells depleted in H1.X is at its greatest, it is also at this dose where cells depleted in H1.2 show a mild resistance to IR when compared to the un-transfected and LUC siRNA control cells. Gold and black stars represent a statistically significant difference of $p < 0.05$ and red stars a difference of $p < 0.001$ as measured by the students' two tailed t-test. (n=3 independent experiments, each in triplicate; error bars represent ± standard error of the mean)

4.3.3 siRNA depletion of H1.X leads to elevated levels of unrepaired double strand breaks as revealed by γH2AX staining

As cells depleted in H1.X are more radiosensitive, it would suggest that the repair of DSBs is compromised. To examine the effects of H1.X depletion on DSB repair, the levels of γH2A.X were studied in un-irradiated cells to determine the background level, 30 minutes following IR to determine the maximum amount of DNA damage, and 24 hours post-irradiation when, under normal conditions, the majority of DSBs should be repaired (Section 1.1.2.4).

Figure 4.4 shows the foci seen in the untransfected MRC5VA and LUC siRNA and H1.2 siRNA transfected control cells along with the H1.X siRNA transfected cells. At 0 hours the nuclei in all conditions contain comparably low amounts of γH2A.X foci, MRC5VA, LUC siRNA and H1.X siRNA having 7, 5 and 6 foci (±3), and H1.2 siRNA having slightly more with 10 foci on average. At 30 minutes post IR they all contain comparably high amounts of γH2A.X foci, an average of 60 per nuclei for MRC5VA, LUC siRNA and H1.X siRNA, and an average of 65 of H1.2 siRNA. Twenty four hours post-irradiation, the majority, if not all of the γH2A.X foci have disappeared in the MRC5VA and LUC siRNA transfected control cells, with 10 and 8 foci on average respectively. Cells depleted in H1.2 again have a marginally higher amount of γH2A.X foci after 24 hours, on average 13 foci remain. This suggests that depletion of H1.2 has no effect on DSB repair. Cells depleted in H1.X have a greater number of γH2A.X foci after 24 hours than seen in the controls, on average 19 foci remain.

Plotting the number of unrepaired breaks as a percentage of the total breaks seen at 30 minutes, termed the residual foci, clearly shows the difference between cells depleted in H1.X and the controls (Figure 4.5). The control MRC5VA, LUC siRNA and H1.2 siRNA cells all display, on average, 5% residual foci, compared to H1.X siRNA which display 28% residual foci. The gold star representing a statistically significant difference between cells depleted in H1.X and the controls, MRC5VA, LUC siRNA and H1.2 siRNA ($p<0.01$, students' two tailed t-test).
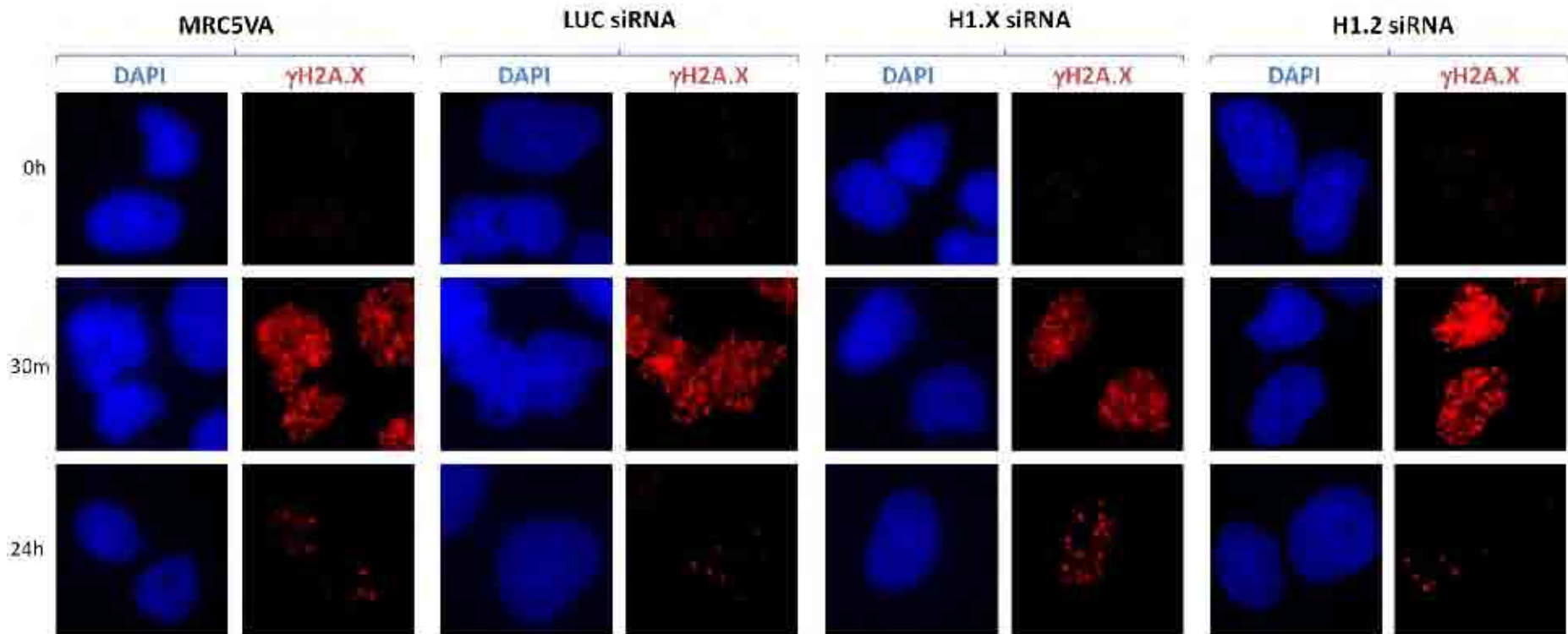
Figure 4.4 - γH2A.X foci are elevated following a 24 hour repair period in cells depleted for H1.X

The panel labelled MRC5VA shows the un-transfected control cells. Un-IR (0h) cells show no, or very low, γH2A.X foci which are representative of a DSB. The maximum γH2A.X signal can be seen 30 minutes post IR, with the majority of these being repaired 24 hours post IR. A very similar story is seen in control LUC siRNA and cells depleted in H1.2. Cells depleted in H1.X again show very comparable levels of γH2A.X foci at 0 hour and 30 minutes, however, there are considerably more foci remaining 24 hours post IR.
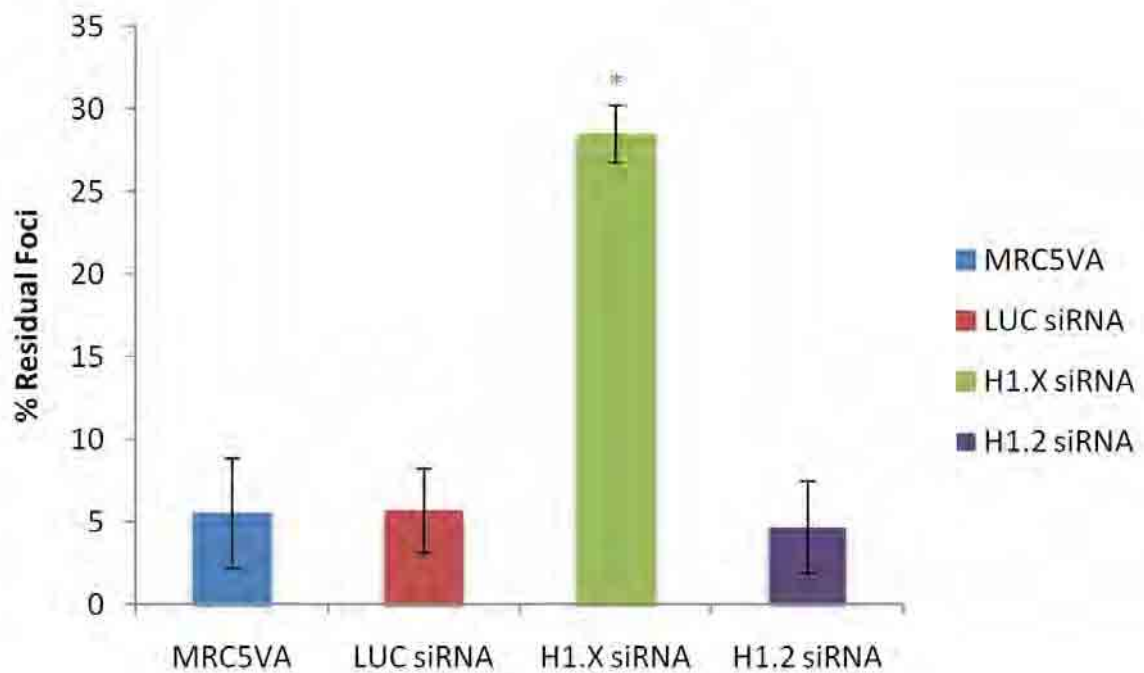
Figure 4.5 - Residual γH2A.X foci 24 hours post-irradiation
Foci counted at 30 minutes and 24 hours post -irradiation were normalised against the un-irradiated counts. Residual foci were calculated as the percentage of foci remaining after 24 hours against the foci counted at 30 minutes post-irradiation. The un-transfected MRC5VA cells, control LUC siRNA cells and cells depleted in H1.2 all displayed comparable levels of residual foci at, on average 5%. Cells depleted in H1.X displayed a much higher amount of residual foci at 28%. Gold star represents a statistically significant difference of $p < 0.01$ compared to all controls, as measured by the students' two tailed t-test. (n=3 independent experiments; error bars represent ± standard error of the mean)

4.3.4 Cells depleted in H1.X show a delay in the G2 to M cell cycle progression following ionising radiation

Results described in Section 4.3.3 show that γH2A.X foci persist in cells depleted in H1.X, 24 hours post-irradiation. The elevated number of unrepaired breaks seen in H1.X siRNA cells is generally accompanied by a longer lasting G2 block, reflecting the presence of DNA damage (Walworth et al., 1993). To determine whether the delay in dephosphorylation of the γH2A.X signal is linked to a delay in the cell cycle, cell cycle kinetics were examined using bivariate cell cycle analysis. Cells were examined over a 24 hour period with sampling every 4 hours. Following flow cytometry analysis, dot plots were plotted with DNA content on the horizontal axis, and BrdU content on the vertical axis. Each plot is representative of 70,000 cells (Figure 7.2 - Figure 7.7, Appendix C). The BrdU labelled population of cells can be split in to specific defined regions (Figure 7.1, Appendix C): R1 is a measure of the total BrdU labelled population; R2 a measure of the BrdU labelled population in the G1 phase of the cell cycle having a DNA copy number of 1; R3 a measure of the BrdU labelled population currently synthesising DNA, the S-phase of the cell cycle; and R4 a measure of the BrdU labelled population in the G2/M phases of the cell cycle, having a DNA copy number of 2.

Following the BrdU pulse-labelling in all samples, the majority of the cells are in S-phase (R3, Figure 7.1, Appendix C). At subsequent time points this population moves towards the G2/M phase of the cell cycle (R4, Figure 7.1, Appendix C). MRC5VA, LUC siRNA and H1.X siRNA un-irradiated populations all show a re-appearance in G1 (R2, Figure 7.1, Appendix C) after 8 hours (Figure 7.2 - Figure 7.4, red box, Appendix C). In contrast, following IR, MRC5VA and

LUC siRNA populations show a re-appearance in G1 after 12 hours, 4 hours longer than the corresponding un-irradiated samples (Figure 7.5 & Figure 7.6, red box, Appendix C). Cells depleted in H1.X show a re-appearance in G1 after 16 hours, 8 hours longer than the corresponding un-irradiated samples and 4 hours longer than the irradiated controls (Figure 7.7, red box, Appendix C).

The duration of the G2/M phase can be estimated by plotting the entry of BrdU positive cells into the G1 phase of the cell cycle (R2/R1, Figure 7.1, Appendix C). By extrapolating the regression line from the most linear part of the curve to the x-axis one can estimate the G2 to M delay. All un-irradiated samples show a duration in G2/M of approximately 5 hours, with no differences seen between all samples (Figure 4.6 & Figure 4.7, filled markers). Irradiated MRC5VA and LUC siRNA samples show an extended duration in G2/M of approximately 12 hours, with no differences seen between the two samples (Figure 4.6 & Figure 4.7, open markers). The regression line for H1.X depleted cells is much shallower and never resumes cycling therefore it is difficult to ascertain the duration of time in G2/M (Figure 4.6 & Figure 4.7).
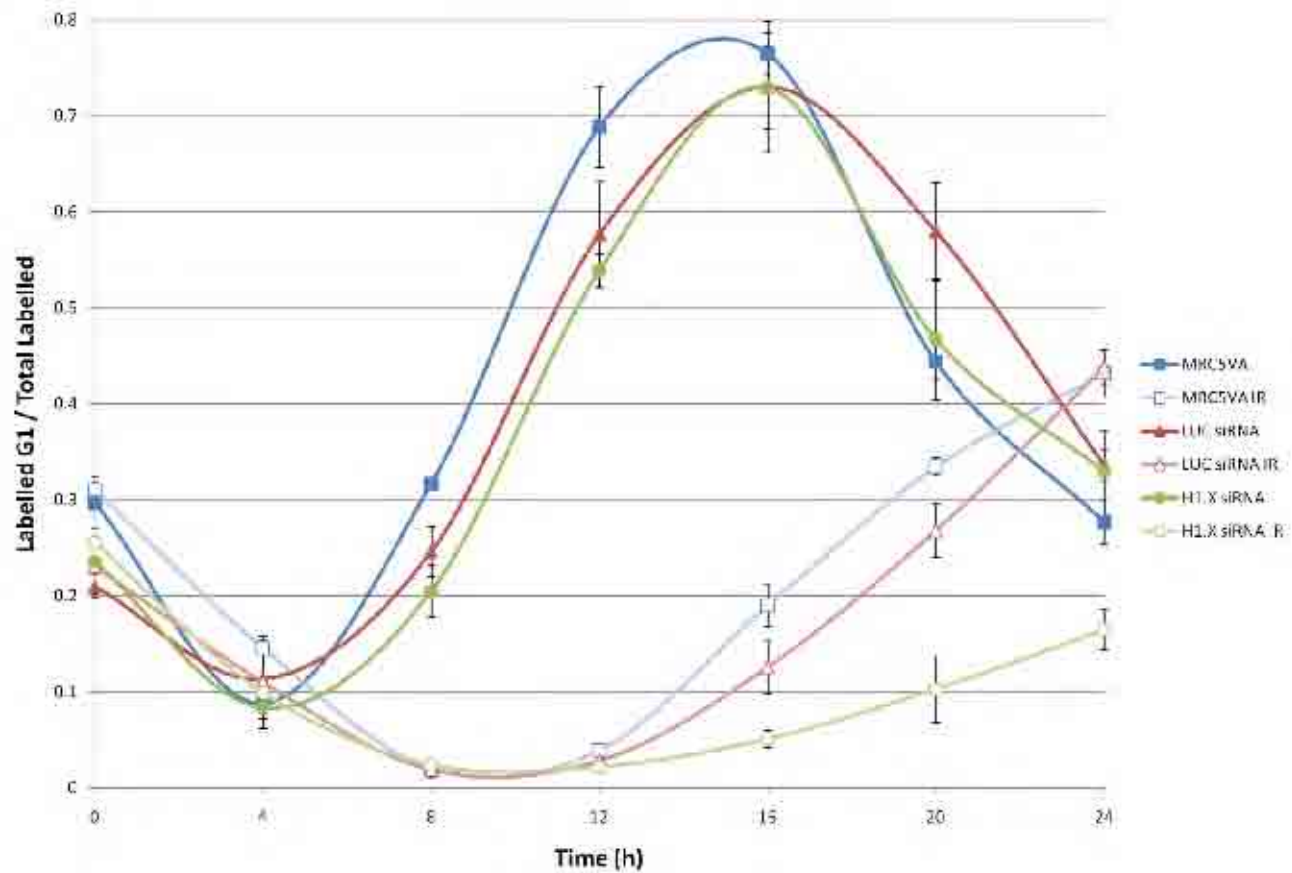
Figure 4.6 – Measurement of G2/M delay over 24 hours
Exponentially growing, BrdU labelled cells were measured for their entry back in to G1 after a successful mitotic division. Filled markers represent those samples which remained un-irradiated and the un-filled markers represent those samples which were exposed to 5 Gy IR. By extrapolating the regression line of the linear part of the curve, the G2/M delay can be estimated. The un-irradiated samples all exhibit a 5±1 hour delay, whereas the irradiated samples are delayed much longer. Control MRC5VA and LUC siRNA cells exit G2/M after 12±1 hours, whereas it is difficult to determine the delay for H1.X siRNA cells. (n=3 independent experiments; error bars represent ± standard error of the mean)
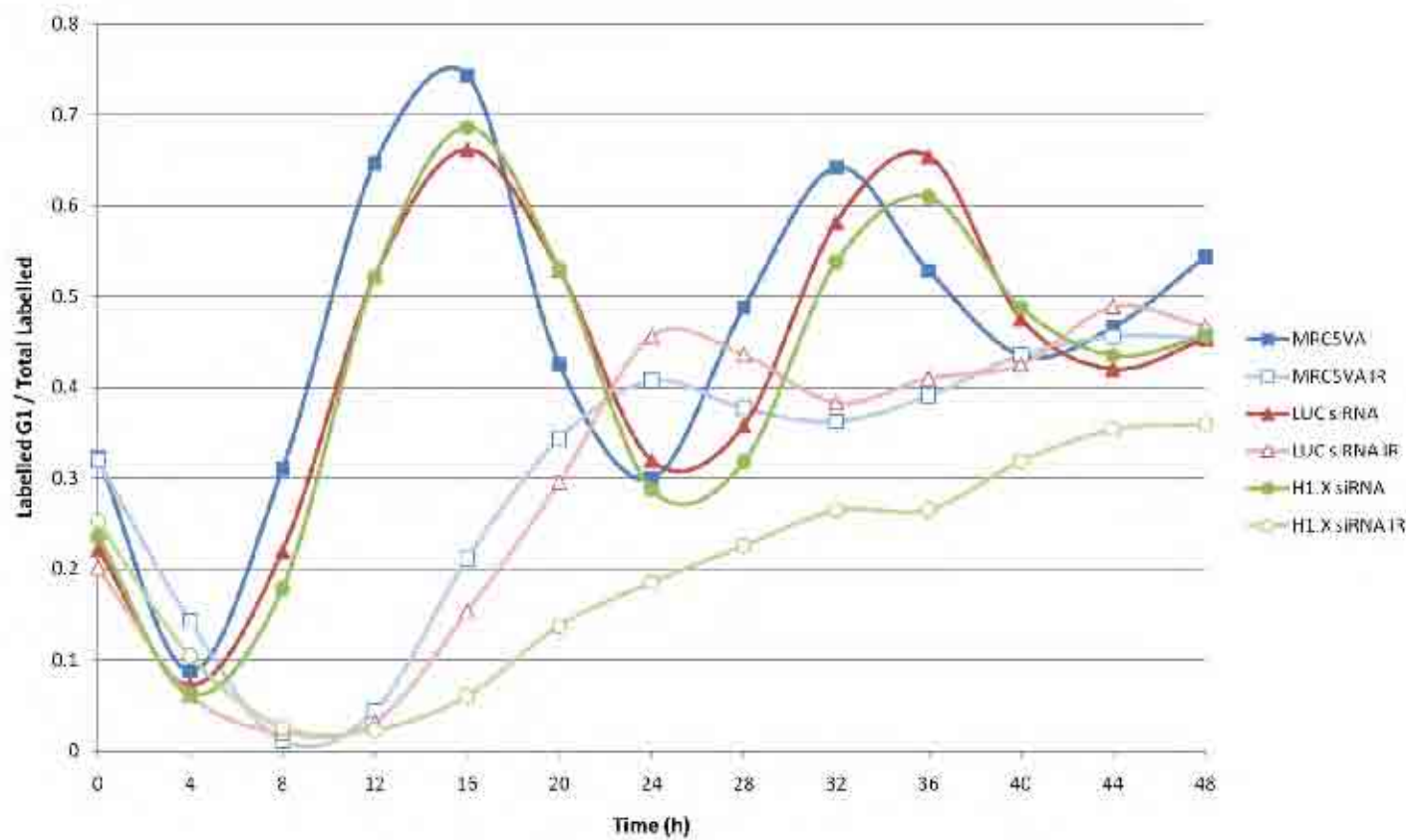
Figure 4.7 - Measurement of G2/M delay over 48 hours
Exponentially growing, BrdU labelled cells were measured for their entry back in to G1 after a successful mitotic division. Filled markers represent those samples which remained un-irradiated and the un-filled markers represent those samples which were exposed to 5 Gy IR. By extrapolating the regression line of the linear part of the curve, the G2/M delay can be estimated. The un-irradiated samples all exhibit a 5±1 hour delay, whereas the irradiated samples are delayed much longer. Control MRC5VA and LUC siRNA cells exit G2/M after 12±1 hours, whereas it is difficult to determine the delay for H1.X siRNA cells. (n=1 independent experiment)

4.3.5 siRNA depletion of H1.X leads to a delay in the appearance of micronuclei following ionising radiation

It was noted in a recent paper that, following mitosis, micronuclei formed when cells were depleted in H1.X (Takata et al., 2007). Micronuclei form during defective repair following a DSB, whereby the unrepaired chromosomal fragment is excluded from the nucleus and forms a smaller nuclear body. Cells that are un-irradiated are absent of any micronuclei, irrespective of siRNA depletion (data not shown). Following irradiation, cells were analysed for their number of micronuclei per binucleate cell after 24 and 48 hours. After 24 hours post-irradiation, the MRC5VA, LUC siRNA and H1.2 siRNA transfected control cells all exhibited, on average, approximately 0.8 to 1 (± 0.05) micronucleus per binucleate cell, whereas in H1.X siRNA transfected cells this number was substantially lower with an average of approximately 0.2 micronuclei per binucleate cell (Figure 4.8 & Figure 4.9; p<0.01, students' two-tailed t-test). After 48 hours the MRC5VA, LUC siRNA and H1.2 siRNA transfected cells all had approximately 1 micronucleus (± 0.05) per binucleate cell, however, in H1.X siRNA transfected cells the number of micronuclei per binucleate cell had increased significantly to approximately 1.3 (± 0.02; Figure 4.8 & Figure 4.9; p<0.05, students' two-tailed t-test).
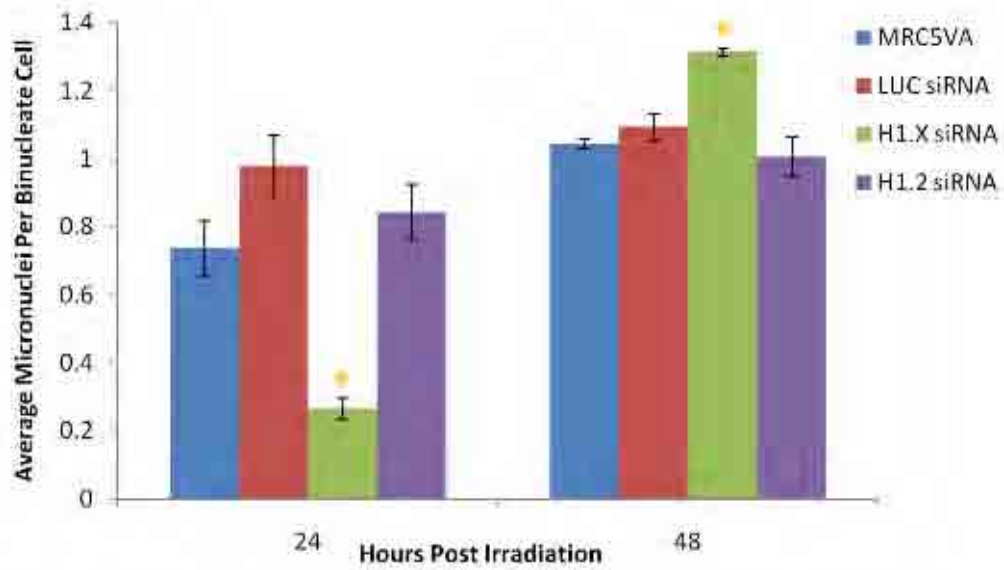
Figure 4.8 – Cells depleted in H1.X have less micronuclei 24 hours post-irradiation
Cells were exposed to 5 Gy IR, incubated for 5 hours after which cytochalasin B was added and cells were incubated for a further 24 and 48 hours. Following this period the number of micronuclei were counted in binucleate cells and plotted as the number of micronuclei per binucleate cell. Levels of micronuclei were significantly lower in the H1.X siRNA cells than the controls 24 hours post irradiation. After 48 hours the levels of micronuclei were significantly higher in the H1.X siRNA cells than in the controls. Gold stars represent statistically significant difference between H1.X siRNA and the MRC5VA, LUC siRNA and H1.2 siRNA controls ($p < 0.01$ for 24 hours and $p < 0.05$ for 48 hours, students' two tailed t-test). (n=3 independent experiments; error bars represent ± standard error of the mean)
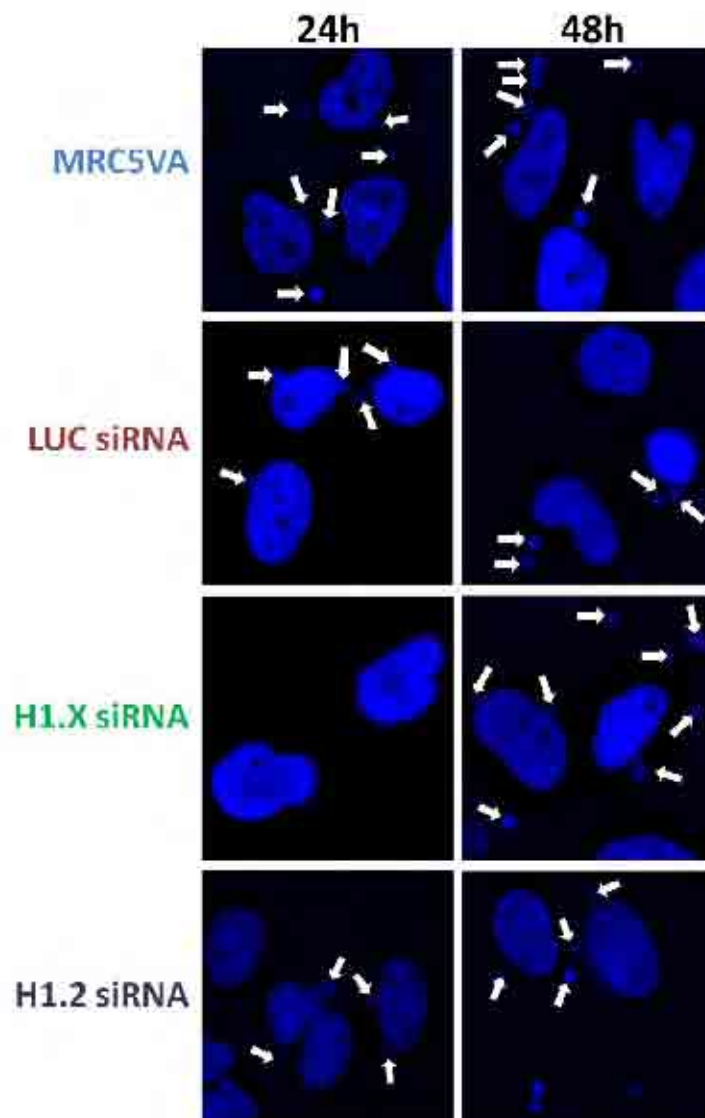
Figure 4.9 - Micronuclei seen at 24 and 48 hour post-irradiation
Micronuclei (labelled with white arrows) are highlighted in all samples at 24 and 48 hours post-irradiation. In the MRC5VA, LUC siRNA and H1.2 siRNA control cells there are micronuclei observed 24 hours post-irradiation. Cells depleted of H1.X show an absence of micronuclei 24 hours post-irradiation, with them appearing 48 hours post-irradiation.

4.4 Discussion

4.4.1 H1.X depletion results in cellular sensitivity to IR

The initial aim of this chapter was to successfully reduce cellular levels of H1.X protein in MRC5VA cells. Using INTERFERin as a transfection reagent, extremely small amounts, 10nM, of siRNA was used to achieve specific and efficient knock down. Using other transfection reagents, larger amounts of siRNA were needed to be used, which can lead to off-target effects whereby the expression of genes involved in cell cycle regulation and apoptosis amongst others, have been show to be altered (Semizarov et al., 2003). The expression of H1.X was reduced by 99% for a minimum of 5 days, with no noticeable effects on control linker and core histones. Further, using siRNA targeted towards LUC there was a noticeable decrease in H1.X and H1.2 protein levels after 24 hours, however these returned to normal after 48 hours. For this reason all resulting experiments were performed 48 hours post transfection with Western blots confirming proteins levels for each experiment (data not shown).

Cells depleted in H1.X were assessed for their response to IR using the clonogenic survival assay. The clonogenic survival assay aims to determine the ability of a cell to proliferate indefinitely (Munshi et al., 2005). Using increasing doses of IR it is possible to determine whether the depletion of a certain protein is important for cellular proliferation and survival. Cells depleted in H1.X are significantly more sensitive than the control MRC5VA and LUC siRNA treated cells. Although the decreased survival seen is not as great as that seen in ATM

(Taylor et al., 1975) and XRCC4 (Grawunder et al., 1998) deficient cell lines, it is comparable with cells depleted in MDC1 by siRNA (J. Zhang et al., 2005). Chicken DT40 cells with H1.R (a chicken specific linker histone variant) knocked out do not show sensitivity to IR. However they are sensitive to MMS treatment, which results in stalled replication forks, invoking the HR repair pathway (Hashimoto et al., 2007). Interestingly, cells depleted in H1.2 show a slight but statistically significant increase in survival at the 8 Gy dose. This is supported by another study which shows that using embryonic stem cells deficient in H[234] show marked resistance to IR, along with MMS and hydroxyurea treatment (Murga et al., 2007). This suggests that depletion of H1.2 offers protection to the cell, either by not allowing the promotion of an H1.2-stimulated, slower, backup pathway (B-NHEJ; Rosidi et al., 2008), or by preventing H1.2-stimulated apoptosis (Konishi et al., 2003).

As cells depleted in H1.X show a marked sensitivity to IR, it was important to ascertain whether this had any implications with regards to γH2A.X foci which are formed following IR (Section 1.1.2.4). It is known that cells deficient in ATM are unable to form γH2A.X foci (Burma et al., 2001), however, along with the control cells, cells depleted in H1.X are able to form γH2A.X foci showing that H1.X exerts its effect further downstream than the phosphorylation of γH2A.X by ATM (Burma et al., 2001). After 30 minutes all cells showed a very similar level of γH2A.X, therefore H1.X does not promote nor inhibit the propagation of the γH2A.X signal. Interestingly, H[234] cells show an elevated intensity of γH2A.X following IR which was not directly measured in this study, although the γH2A.X foci counts in cells depleted in H1.2 are the same as the control cells in this study (Murga et al., 2007).

Furthermore, 53BP1, MDC1, BRCA1 and RAD51 have also been shown to be successfully recruited to the sites of DSBs in cells depleted in H1.X (Personal communication, Dr. Grant Stewart). This suggests that the initial stages of DSB recognition and protein recruitment remain intact in the absence of H1.X.

Following IR, a 24 hour period should be enough time for all DSBs to be repaired under normal circumstances, which is seen in the control MRC5VA and LUC siRNA cells. Cells depleted in H1.X, however, still retain an elevated level of γH2A.X foci 24 hours post irradiation. Other proteins which form foci which co-localise with γH2A.X: 53BP1, MDC1, BRCA1 and RAD51 also remain at an elevated level (Personal communication, Dr. Grant Stewart). This suggests that although DSB recognition and protein recruitment remain intact, the DSB is either not getting repaired, or the γH2A.X signal is not being dephosphorylated, as seen in cells depleted in protein phosphatase 6 (Douglas et al., 2010). To determine whether the breaks are actually being repaired, DNA breaks can be quantified by using either pulsed field gel electrophoresis (Whitaker and McMillan, 1992), or the neutral COMET assay (Olive et al., 1990).

4.4.2 H1.X depletion invokes the G2 to M cell cycle checkpoint

Following IR and DSB induction, the cell cycle checkpoints will be activated, allowing the cell to repair the damage before it is propagated to the daughter cell. Following the successful repair of the DSB the γH2A.X signal is removed which is essential for the recovery from the

DNA damage induced cell cycle checkpoint (Chowdhury et al., 2005, Keogh et al., 2006, Nakada et al., 2008).

Upon exposure to IR, the control MRC5VA and LUC siRNA cells show a G2 to M delay of 12 hours, a delay typically representative of the time required to repair the DNA DSBs (Konig and Baisch, 1980). Cells depleted in H1.X however show an extended delay following IR. The increased amount of γH2A.X foci and the extended delay in G2/M would be consistent with a failure to repair the DSBs incurred. Interestingly, over a 48 hour period, cells depleted in H1.X fail to synchronise, unlike the MRC5VA and LUC siRNA populations (data representative of one experiment), suggesting that small populations of cells are escaping the G2 to M block without the successful repair of the DSB, a phenomenon seen in *S. cerevisiae* (S. E. Lee et al., 2001). In the MRC5VA, LUC siRNA and H1.X siRNA cells, phosphorylation of CHK2 on tyrosine 68 is observed, therefore the activation of the G2 checkpoint remains intact in all populations, suggesting that the depletion of H1.X does not affect cell cycle checkpoint initiation (personal communication, Dr. Grant Stewart). Unfortunately, cells depleted in H1.2 were not examined so it is impossible to determine whether the G2 to M delay is truly linked with H1.X depletion, or to general linker histone depletion.

A recent study which characterised H1.X as having a role in mitosis, also revealed the appearance of micronuclei following mitosis in cells depleted in H1.X (Takata et al., 2007). The cells used in the study were human HeLa cells under no genotoxic stress. Micronuclei are a marker of unrepaired double strand breaks, therefore, based on the evidence so far, it would be expected that cells depleted in H1.X would show elevated levels of micronuclei.

Elevated levels were seen, but the micronuclei appeared after 48 hours, 24 hours later than they appeared in the controls. It is expected that the delay in appearance of micronuclei is due to the extended delay in the cell cycle. Elevated levels of micronuclei are also seen in cells depleted for KU70 and RPA (Balajee and Geard, 2004, Vandersickel et al., 2010).

CHAPTER FIVE: THE ANALYSIS OF THE MECHANISM OF

ACTION OF H1.X IN DSB REPAIR

5.1 Introduction and Overview

The final stage of repair in the NHEJ pathway is performed by the LX complex, in conjunction with the recently discovered XLF protein (outlined in more detail in Section 1.1.3.2.3; Ahnesorg et al., 2006, Buck et al., 2006, L. Chen et al., 2000).

DNA end ligation by DNA ligase IV has been shown to be significantly stimulated by XRCC4 and XLF in the *in vitro* reconstituted ligation reaction (Gu et al., 2007b). Whereas, the KU complex is inhibitory when multiple heterodimers are bound to the DNA, however when one or two KU heterodimers are bound, the DNA ligase IV mediated ligation reaction is stimulated (Kysela et al., 2003). This observation suggests that strict stoichiometric control is necessary to achieve stimulation. Previous work has also shown that linker histones also inhibit ligation, whereas the packaging of DNA in to nucleosomes with purified core histones showed no inhibition at all (Kysela et al., 2005, Rosidi et al., 2008, Yamanaka et al., 2002). DNA-PK, on its own, has also been shown to inhibit ligation in a dose-dependent manner. In the presence of linker histones and under phosphorylation permissive conditions in the presence of ATP, inhibition by DNA-PK is alleviated allowing DNA ligase IV ligation. The linker histones incorporated in to the *in vitro* ligation assay are efficiently phosphorylated and their overall DNA binding capacity is significantly reduced (Kysela et al., 2005).

Linker histones, along with the core histones, are generally considered to be a barrier preventing access to DNA. There are reports which highlight the effect of phosphorylation of the CTD of linker histone variants and the effect this can have on their ability to bind DNA.

Altering phosphorylation sites to render the sites un-phosphorylatable (Serine-Alanine), or global inhibition of phosphorylation using staurosporine or 5,6-dichloro-1-β-D-ribofuranosylbenziminidazole increase the linker histones affinity to DNA (Dou et al., 2002, Lever et al., 2000). This suggests a model whereby, un-phosphorylated linker histones have a high affinity towards DNA which is alleviated when the linker histones are phosphorylated.

5.2 Aims

It has been previously shown that H1.X has an important impact *in vivo* during NHEJ (Chapter 4), however the mechanism behind this remains to be elucidated. The initial stages of NHEJ, including γH2A.X phosphorylation and the recruitment of 53BP1, MDC1 and BRCA1 to the site of the DSB remain intact, suggesting H1.X is more likely to act further downstream in the repair pathway (personal communication, Dr. Grant Stewart). Previous results have shown that somatic linker histones have a general inhibitory effect on NHEJ, therefore it is not intuitively obvious as to why the absence of H1.X would decrease the efficiency of DSB repair and cell survival after exposure to IR. The established *in vitro* reconstitution techniques have been employed to dissect the functional impact of H1.X on DSB repair and its potential interactions with components of the NHEJ machinery.

This chapter aims to:

1. Use an *in vitro* reconstituted DNA ligation assay to determine the impact of H1.X on LX-mediated ligation.

2. Examine the binding properties of H1.X and H1.X/LX on DNA using EMSA to elucidate if the interaction between LX and DNA is stabilised in the presence of H1.X.

3. Determine if H1.X can specifically interact with any members of the NHEJ machinery.

5.3 Results

5.3.1 H1.X stimulates LX mediated ligation of double stranded DNA

To test whether the presence of H1.X affects the rate of dsDNA ligation, recombinant H1.X was added to the ligation system reconstituted *in vitro* as described previously (Section 2.17) (Kysela et al., 2003). As shown in Figure 5.1, the addition of H1.X markedly enhanced the rate of LX-mediated DNA ligation when compared to LX alone. LX alone is able to produce some high order ligation products (Figure 5.1A Lane 2), however, the addition of H1.X dramatically increased the amount of ligated products (Figure 5.1A Lanes 3-16). Amounts of H1.X exceeding 157nM begin to decrease the stimulation of ligation, although these are still higher than those seen with LX alone (Compare Figure 5.1A lanes 10 and 2). With increasing amounts of H1.X up to, and including, 67nM the stimulation increased linearly (Figure 5.1C). At the point of stimulation between 34 and 67nM H1.X, approximately equimolar concentrations of H1.X, LX and DNA ends are present (Figure 5.1 lanes 8 and 9).
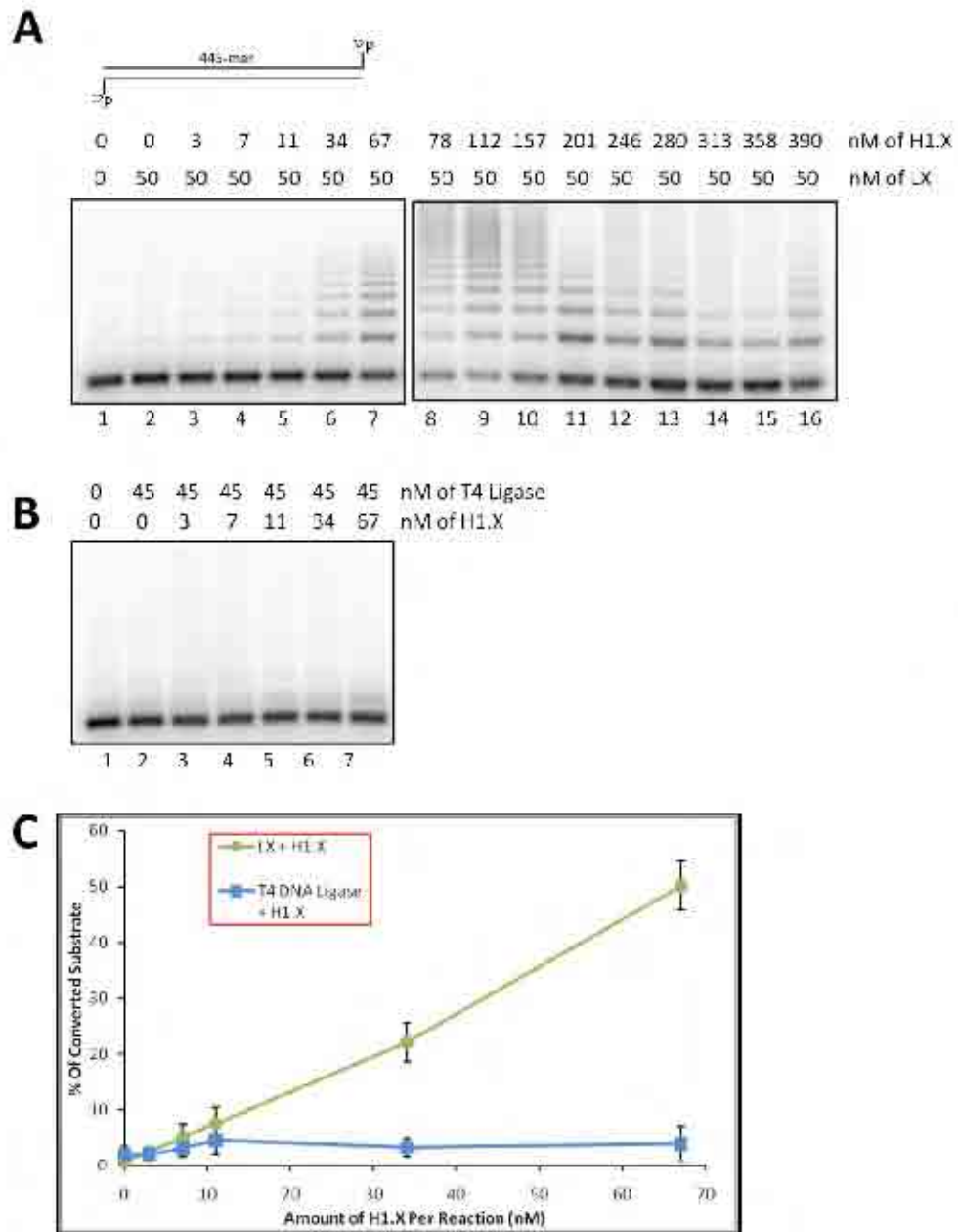
Figure 5.1 – Recombinant linker histone H1.X stimulates LX-mediated ligation.
A. Schematic of radio-labelled DNA substrate. Purified recombinant linker histone H1.X was incubated, in increasing amounts, with purified LX complex. Increasing amounts of H1.X (lanes 3-16) result in the increasing amount of higher order fragment when compared to DNA alone (lane 1), or LX and DNA alone (lane 2). 157nM of H1.X (lane 10) results in the majority of ligated products and ligation decreases from 201nM – 390nM (lanes 11-16), although ligation products remain greater than those seen in the controls (lanes 1 & 2).
B. Purified recombinant linker histone H1.X was incubated, in increasing amounts, with commercially available T4 DNA ligase. T4 DNA ligase alone was unable to ligate DNA fragments (lane 2), and the addition of H1.X failed to stimulate ligation (lanes 3-7).
C. Graphical representation of A, lanes 1-7 and B, lanes 1-7. Converted substrate was calculated as the amount of DNA present in ligated products as a percentage of the total DNA present. Stimulation of LX mediated ligation by H1.X is clearly linear using these amounts of proteins, whereas T4 DNA ligase shows very minimal ligation.

To determine whether H1.X mediated stimulation was specific to DNA Ligase IV, ligation experiments were repeated, replacing the LX complex with T4 DNA Ligase. T4 DNA Ligase alone was not able to stimulate end ligation (Figure 5.1B Lane 2), and with the addition of H1.X the stimulation of ligation was not seen (Figure 5.1B Lanes 3-7 and Figure 5.1C).

To determine whether H1.X itself possessed DNA ligase activity on its own, ligation experiments were repeated omitting the LX complex. H1.X was shown to possess no DNA ligase activity (Figure 5.2 Compare lanes 1 and 2 to lanes 3 and 4).

The original studies, which showed that a somatic linker histone mix inhibited ligation, used an increased amount of LX complex, 125nM, coupled with an incubation time of 3 hours (Kysela et al., 2005). To confirm that H1.X did not act in an inhibitory manner, its activity was assessed under these conditions. Figure 5.3, lanes 2-4, show ligation under stimulatory conditions (50nM LX, 30 minute incubation), whereas Figure 5.3, lanes 12-14, show ligation under the conditions described previously (125nM LX, 3 hour incubation). Figure 5.3 lanes 5-11 show the other permutations of incubation times and amount of LX and also show ligation. These include 125nM LX complex for 30 minutes (Figure 5.3 lanes 5-7) and 50nM LX complex for 3 hours (Figure 5.3 lanes 9-11).
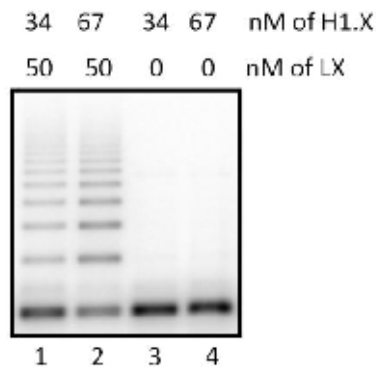
Figure 5.2 – Linker histone H1.X does not possess DNA ligase activity.
Purified recombinant linker histone H1.X was incubated with LX in the presence of DNA resulting in increasing amounts of ligated DNA. In the absence of LX, H1.X was unable to ligate fragments of DNA showing it does not possess DNA ligase activity on its own.
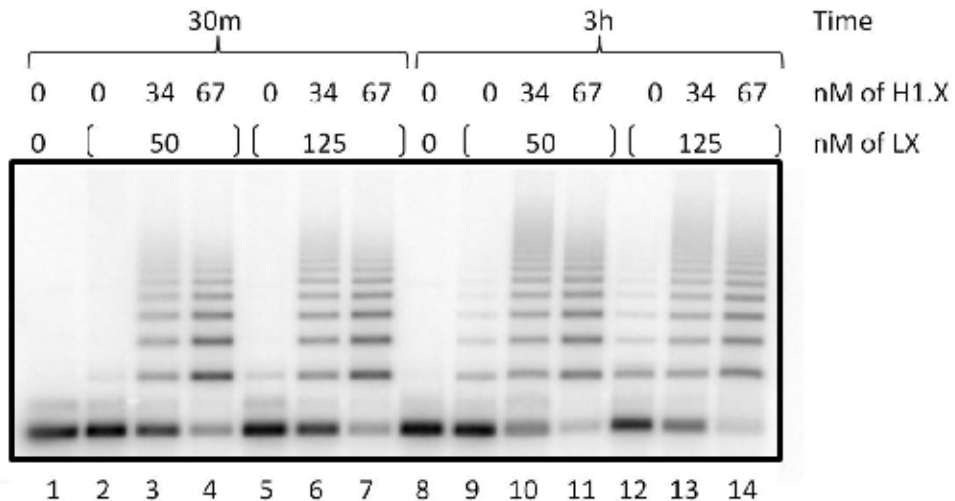
Figure 5.3 - H1X stimulates ligation under conditions previously shown to inhibit ligation
Typical stimulatory conditions for ligation require 50nM of LX to be incubated for 30mins. Conditions used in the study where a linker histone mix inhibited ligation required 125nM LX to be incubated for 3 hours. To assess whether H1.X stimulated ligations under all conditions, it was assessed under all permutations. Ligation was seen for all permutations (lanes 4, 7, 11 and 14 compared to lanes 1 & 8), with enhanced ligation when incubated for 3 hours (lanes 11 & 14 compared to 4 & 7). This demonstrates that under the same conditions which H1 inhibited ligation (125nM of LX for 3 hours), H1.X was still able to stimulate the reaction.

5.3.2 H1.X cannot rescue H1-mediated inhibition of ligation

The commercially available linker histone mix, previously shown to contain H1.0 – H1.5 and H1.X (Section 3.3.2), is able to inhibit LX-mediated ligation quite dramatically (Figure 5.4 Lane 3) whereas H1.X alone clearly stimulates ligation (Figure 5.4 Lane 2). To determine whether H1.X was able to rescue the inhibitory phenotype displayed by the linker histone mix, H1.X was added to the reaction containing radio-labelled substrate DNA before (Figure 5.4 Lanes 4-6), after (Figure 5.4 Lanes 7-9), or at the same time (Figure 5.4 Lanes 10-12) as the H1 linker histone mix. In all cases DNA ligation was still inhibited showing that under these experimental conditions H1.X is unable to rescue H1-mediated inhibition of DNA ligation.
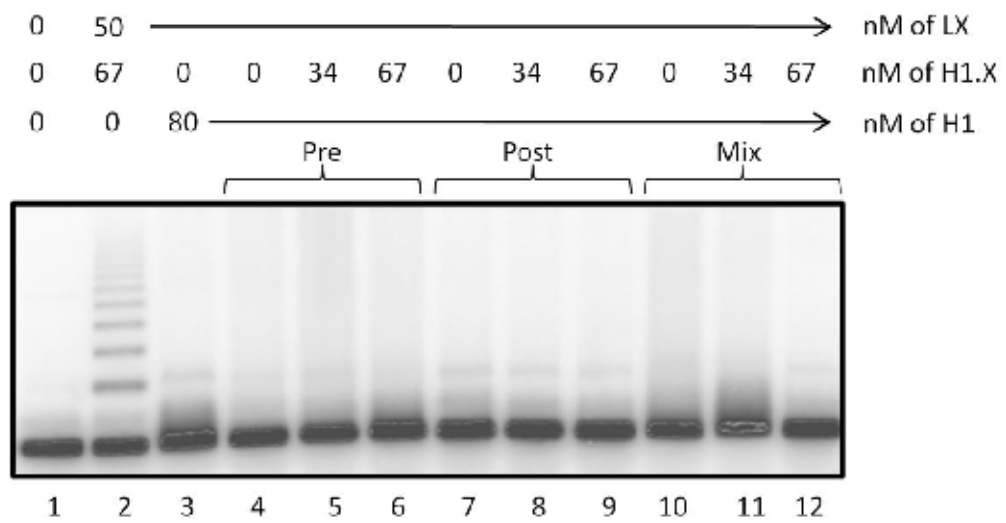
Figure 5.4 - H1.X does not have the ability to rescue H1 mediated inhibition of ligation.
Purified recombinant linker histone H1.X is able to stimulate LX mediated ligation (compare lane 2 to 1), whereas a commercially available linker histone mixture inhibits ligation by LX (compare lane 3 to lane 2). H1.X was unable to rescue ligation inhibition by H1 when it was added to the reaction before H1 (lanes 4-6), after H1 (lanes 7-9) or when added at the same time as H1 (lanes 10-12).

5.3.3 H1.X and DNA Ligase IV/XRCC4 form protein-DNA complexes.

H1.X and LX complex were incubated together in the presence of DNA and the absence of MgCl$_2$, to stop DNA ligation, and DNA-protein complexes were analysed using EMSA. Alone, neither protein was able to form stable DNA-protein complexes (Figure 5.5 lanes 2-9 and lane 10). However, two stable DNA-protein complexes are formed when both the LX complex and H1.X are present (Figure 5.5 lanes 16-18, indicated by arrows). The lower band appears in the presence of 22nM H1.X (Figure 5.5 lane 14) and increases in intensity as the amount of H1.X increases (Figure 5.5 lanes 15-18). The higher band appears in the presence of 44nM of H1.X (Figure 5.5 lane 16), and also increases in intensity as the amount of H1.X increases (Figure 5.5 lanes 17 & 18). It is unclear from the data as to what these bands contain.

5.3.4 H1.X interacts with the DNA Ligase IV/XRCC4 complex

Enhanced stimulation of ligation and the formation of band shifts by H1.X could be due to an interaction with either DNA ligase IV or XRCC4. To address the question whether H1.X functionally interacts with the LX complex only on a DNA complex, or if it possibly performs a complex *in vivo* co-immuno-precipitation studies using GFP-tagged H1.X proteins were used. GFP-H1.X was shown to co-immuno-precipitate endogenous XRCC4 proteins, providing evidence for an interaction between H1.X and XRCC4 which is not seen when using GFP alone or a control antibody (Figure 5.6). This is not dependent on, or induced by DNA

damage since no differences were observed between cells exposed to 30 Gy and un-irradiated controls (Figure 5.6).

To verify the interaction with endogenous native proteins in a non-over-expressed background, co-immuno-precipitation experiments were repeated. Co-immuno-precipitation of endogenous proteins with either anti-H1.X or anti-DNA ligase IV antibodies co-immuno-precipitated the reciprocal protein, suggesting there is an interaction between endogenous H1.X and DNA ligase IV which is not seen when using a control antibody (Figure 5.7).

Since both proteins are capable of binding to DNA, albeit with low efficiency, it had to be determined if the interaction detected could be the result of both proteins being bound to the same DNA fragments present in the lysate, a false positive interaction. To exclude this possibility, the intercalating agent, ethidium bromide, was added to the co-immuno-precipitation buffers (Section 2.19.4) and the endogenous co-immuno-precipitation repeated (Lai and Herr, 1992). Increasing concentrations of ethidium bromide were unable to disrupt the interaction between H1.X and DNA ligase IV verifying the interaction as a true protein-protein interaction, not mediated by DNA (Figure 5.8).
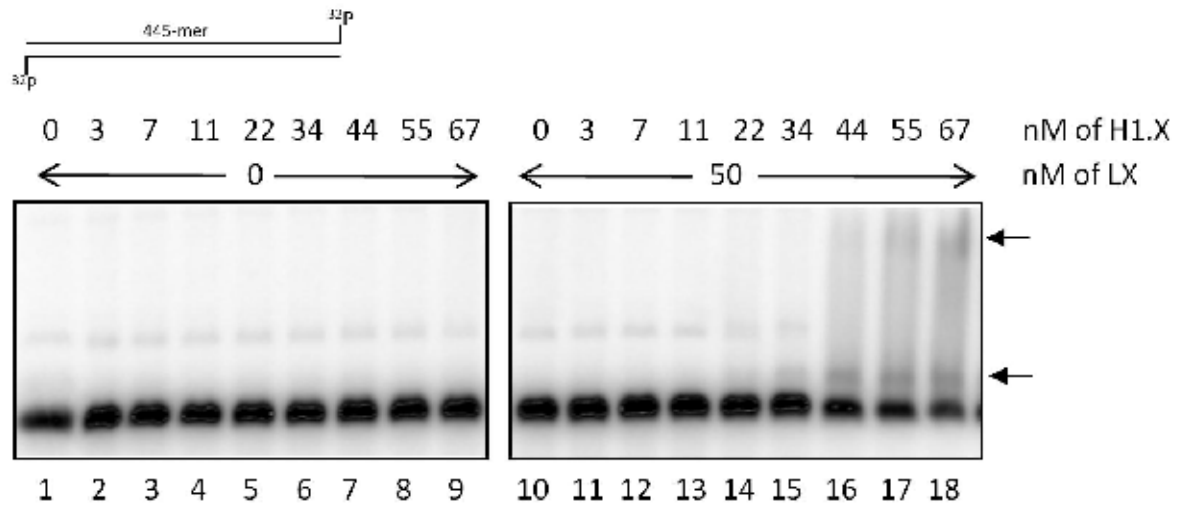
Figure 5.5 - H1.X stabilises LX on dsDNA ends.
Schematic of radio-labelled DNA substrate. Purified recombinant linker histone H1.X was incubated with radio-labelled substrate DNA, in the absence of $MgCl_2$, and analysed by EMSA. In the absence of LX (lanes 1-9) no band-shift was observed when incubated with H1.X up to and including 67nM. In the presence of LX and 22nM of H1.X a low band shift becomes apparent (lane 14; lower arrow). As the amount of H1.X increases, as does the intensity of this band (lanes 15-18; lower arrow), along with the appearance of a new band shift (lanes 16-18; higher arrow).
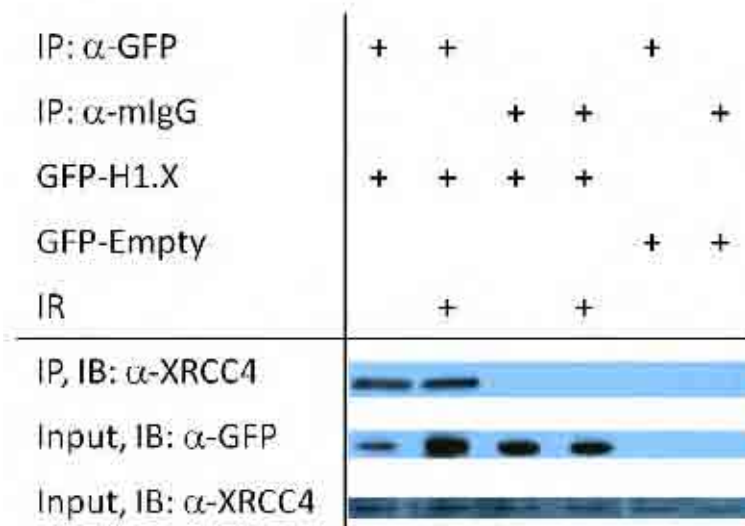
Figure 5.6 - Co-immuno-precipitation of XRCC4 with GFP-H1.X
MRC5VA cells were stably transfected with GFP tagged H1.X. Co-immuno-precipitation experiments show that GFP-H1.X interacts with endogenous XRCC4 with and without exposure to 30Gy IR. Co-immuno-precipitation experiments using non-specific antibodies do not co-immuno-precipitate any endogenous XRCC4 protein. Co-immuno-precipitation experiments using cells stably transfected with empty GFP vector do not co-immuno-precipitate any endogenous XRCC4 protein. IP = Co-immuno-precipitation; IB = Western Blot
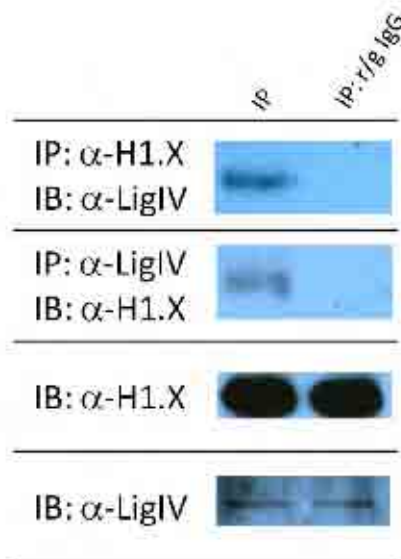
Figure 5.7 - Co-immuno-precipitation of DNA Ligase IV with endogenous H1.X
Co-immuno-precipitation of endogenous DNA ligase IV and H1.X from MRC5VA cells using the reciprocal antibody shows the two proteins do interact with one another. Control (r/g IgG, either rabbit or goat, depending on the antibody used for the co-immuno-precipitation) co-immuno-precipitation experiments failed to pull down either H1.X or XRCC4 despite their presence in the lysate. IP = Co-immuno-precipitation; IB = Western Blot
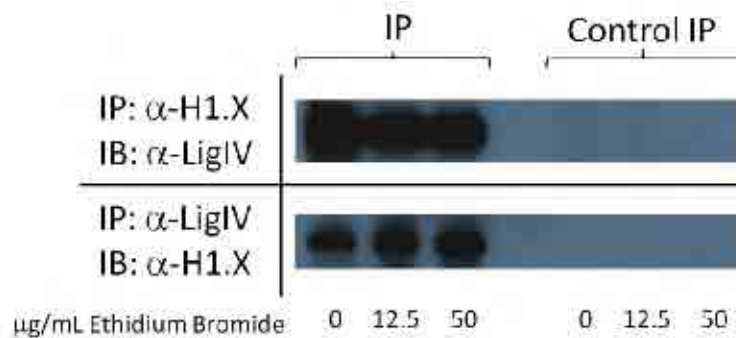
Figure 5.8 - Interaction between H1.X and DNA ligase IV is not disrupted with the addition of ethidium bromide.
Co-immuno-precipitation of endogenous DNA ligase IV and H1.X from MRC5VA cells using the reciprocal antibody in the presence of the DNA- intercalator ethidium bromide. Increasing amounts of ethidium bromide does not affect the interaction between H1.X and DNA ligase IV, nor does it promote the pull down of DNA ligase IV when using a non-specific antibody control. IP = Co-immuno-precipitation; IB = Western Blot

5.3.5 H1.X interacts with nucleolin following exposure to IR

Recombinant H1.X has been shown to interact with two members of the NHEJ pathway, DNA ligase IV and XRCC4 and stimulate ligation. It has also been shown that recombinant H1.X forms stable complexes with DNA in the presence of LX. The exact location of H1.X on the DNA substrate is unknown, however, to interact and stimulate LX-mediated ligation it means that H1.X must be close to the site of the DSB. This opens the possibility that H1.X could interact with other members of the NHEJ pathway.

To ascertain if there are any other interacting partners for H1.X, co-immuno-precipitation experiments were used to immuno-precipitate bound proteins (Section 2.19). Co-immuno-precipitated proteins were resolved on an SDS-PAGE gel (Section 2.3.2) and bands of interest were excised and the protein content analysed by mass spectrometry (Section 2.19.5).

Table 5.1 shows the mass spectrometry results obtained that are of specific interest. Interestingly, both DNA-PK$_{CS}$ and KU70 are present in the table, both key members of the NHEJ pathway. Also, a 14-3-3 protein is also listed. 14-3-3 proteins interact with CDC25C and sequester it to the cytoplasm during the G2-M phase arrest (Dalal et al., 1999; Section 1.1.1.3).

The highest scoring interacting protein was that of nucleolin. Nucleolin is a nucleolar protein, along with H1.X, therefore it is not unsurprising that these two could interact (Lapeyre et al., 1987). To validate this interaction, GFP-H1.X interacting proteins were co-immuno-

precipitated, in the presence of ethidium bromide, and, using Western blotting, directly probed for nucleolin (Figure 5.9). Interestingly, the interaction was only seen following IR, suggesting that the interaction occurs following DNA damage.

Coverage	Peptides	Score	Protein
38.31	58	1239.10	Nucleolin
1.81	1	60.70	ATP-dependent DNA helicase 2 subunit 1 (KU70)
1.16	3	55.76	DNA-dependent protein kinase catalytic subunit
8.24	2	45.13	14-3-3 protein epsilon

Table 5.1 - GFP-H1.X interacting partners as determined by mass spectrometry
GFP-H1.X and interacting partners were co-immuno-precipitated and analysed by mass spectrometry. Proteins identified of particular interest are listed here and include nucleolin, KU70, DNA-PK$_{CS}$ and 14-3-3 protein epsilon.
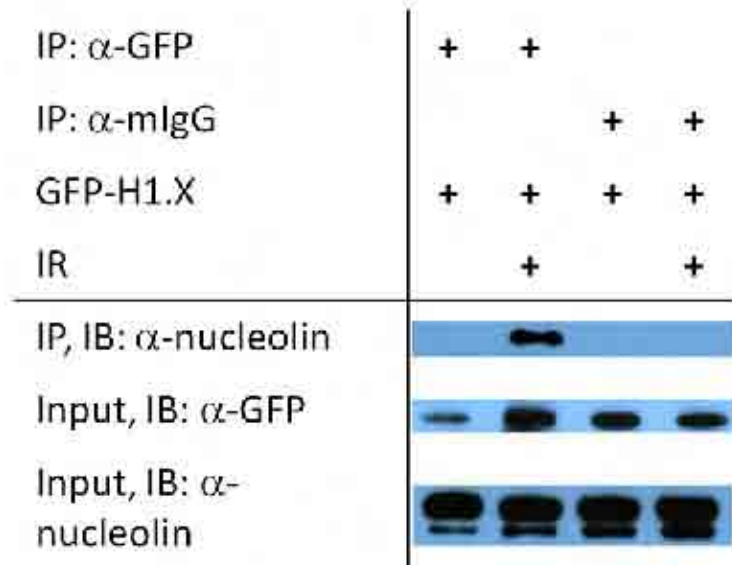
Figure 5.9 - Co-immuno-precipitation of nucleolin with GFP-H1.X

MRC5VA cells were stably transfected with GFP tagged H1.X. Co-immuno-precipitation experiments show that GFP-H1.X interacts with endogenous nucleolin in response to exposure to 30Gy IR. Co-immuno-precipitation experiments using non-specific antibodies do not co-immuno-precipitate any endogenous nucleolin protein. IP = Co-immuno-precipitation; IB = Western Blot

5.4 Discussion

Previous work has shown that linker histone variants are inhibitory to LX-mediated ligation, the final step of NHEJ (Kysela et al., 2005). The linker histones used in these experiments were a mixture of all the somatic linker histone variants (H1.0 – H1.5 and H1.X). Therefore, it is impossible to ascertain whether this effect is contributable to an individual linker histone, or the complex interplay between several linker histone variants.

Previous work in this thesis opposes the suggested inhibitory role of linker histones as the depletion of H1.X causes a profound impact on DSB repair and cellular survival to IR. Using *in vitro* mechanistical analysis we have provided an important insight in to the possible mechanism of action of H1.X in the NHEJ pathway.

Inhibition of LX-mediated ligation was seen both in this study and in other studies when a linker histone mix is added to the *in vitro* reconstitution ligation assay (Kysela et al., 2005). Purified recombinant linker histone H1.X, however, stimulates LX-mediated ligation from as little as 7nM to as much as 390nM purified recombinant H1.X under the same experimental conditions. H1.X is also found in the linker histone mixture used in the previous studies so it would suggest that one or more of the other linker histones are able to mask its stimulation. Experiments to determine if the formation of H1.X-LX or H1.X-DNA complexes could abrogate the inhibitory effect on ligation following the addition of linker histones were unsuccessful. This suggests that there is a complex interplay between the individual linker histones at the DNA ends of the DSB.

The amount of H1.X used in the *in vitro* reconstituted ligation assay is important for the amount of stimulation observed. The greatest stimulation was achieved at approximately equimolar concentrations of H1.X to LX complex, with approximately 20 H1.X molecules per molecule of DNA. Amounts exceeding 157nM recombinant H1.X, although still stimulating the ligation, decrease the stimulation observed. At this concentration of H1.X, there are approximately 44 H1.X molecules per DNA molecule. This suggests that amounts of H1.X above 157nM could 'coat' the DNA in too much protein thereby reducing the accessibility of the DNA to the LX complex. This data suggests that there is a stoichiometric relationship between H1.X and the LX complex that determines the optimum ligation efficiency, something also suggested with the linker histone mix (Rosidi et al., 2008).

Unfortunately, due to problems encountered purifying the other linker histone variants (Section 3.3.3), it is impossible to ascertain whether H1.X is unique in its role of stimulating the *in vitro* reconstituted ligation assay. However, commercially available H1.2 and H1.3 have been recently shown to inhibit LX-mediated ligation over the same range at which H1.X stimulates the reaction (personal communication, Dr. Boris Kysela).

Ideally, it would be interesting to see what effect all the linker histone variants have on the *in vitro* reconstituted ligation assay as only then would it be possible to draw conclusions regarding the complex interplay which would take place at the DNA ends between the linker histone variants. This is highlighted by H1.X stimulating ligation of DNA ligase IV in the

conventional NHEJ pathway, whereas H1.2 simulates ligation in the proposed DNA ligase III backup pathway (Rosidi et al., 2008).

Linker histone variants have been shown to form stable complexes with the KU complex in the presence of DNA (Kysela et al., 2005), and in this chapter, H1.X has formed stable complexes with LX in the presence of DNA. Interestingly, H1.X is unable to form a stable DNA complex alone. This is likely due to linker histone variants having a shorter residence time on DNA than other chromatin binding proteins, such as transcription factors (Lever et al., 2000, Misteli et al., 2000, Phair et al., 2004). Also, H1.X lacks the conserved serine and threonine residues found in other linker histone variants, which are postulated to enhance DNA binding (Hendzel et al., 2004).

The enhanced ligation stimulation and the presence of stable complexes in the presence of DNA suggests an interaction between recombinant H1.X and the LX complex. Interestingly, H1.X co-immuno-precipitated both DNA ligase IV and XRCC4 implying that this interaction occurs *in vivo*. Using mass spectrometry, H1.X is also suspected to interact with both KU70 and DNA-PK$_{CS}$, although not confirmed by co-immuno-precipitation studies. This data highlights H1.X having a significant role in DSB repair, interacting with the protein kinase DNA-PK$_{CS}$ and the ligation machinery, LX, to enhance the final ligation step. It would be interesting to assess whether H1.X's interaction with DNA-PK$_{CS}$ results in H1.X phosphorylation as it has already been determined that H1.X can be phosphorylated by DNA-PK$_{CS}$ *in vitro* (Section 3.3.4).

Unfortunately, it is impossible to determine from the co-immuno-precipitation experiments as to whether the interaction between LX and recombinant H1.X is direct, or mediated through other protein(s). To ascertain this, proteins would need to be produced with different tags for purification and assessed using standard pull-down techniques, as both H1.X and the LX complex are histidine tagged. Far western blotting could also be used, whereby a PVDF membrane is probed with recombinant protein, allowing it to bind to potential interacting proteins. The protein is either radio-labelled, or probed with antibodies to allow its detection, highlighting proteins which interact. The only potential pitfall of this technique as that the proteins on the PVDF membrane will have been denatured and lost their tertiary structure which could be important for potential interactions.

Nucleolin was also identified as an interacting partner for H1.X, however, unlike the LX complex, this interaction was only detected following DNA damage induced by IR. Nucleolin is predominantly a nucleolar protein, although it can be found in the nucleus, the cytoplasm and the cell membrane (Borer et al., 1989, Hovanessian et al., 2000). Interestingly, nucleolin has already been linked with other types of repair. Nucleolin can accelerate oligonucleotide binding, including oligonucleotides which contain mismatches (Hanakahi et al., 2000). Nucleolin has also been shown to interact with PCNA, and following exposure to UV, the interaction is enhanced having an inhibitory effect on nucleotide excision repair (C. Yang et al., 2009). Nucleolin has also been proposed to bind to RAD51 and regulate HR (De et al., 2006). Also, down-regulation of nucleolin following DNA damage increases the translation of p53, helping to initiate the G1 phase checkpoint (De et al., 2006). Further work is required to

fully characterise these complex interactions and dissect the role of H1.X and nucleolin in response to IR.

CHAPTER SIX: DISCUSSION

6.1 Linker Histone Variant, H1.X, and its Role in Double Strand Break Repair

Fundamentally, this project has added to the growing body of evidence showing that linker histones are not just structural components of chromatin, and that they have many implications in cellular function, specifically DNA repair (Hashimoto et al., 2007, Kysela et al., 2005, Rosidi et al., 2008). In 1990 a model was proposed that during NHEJ, an alignment protein would exist which would bind broken DNA ends to align them, facilitating the end joining. It is also proposed that this alignment protein would support and stimulate end joining (Thode et al., 1990). One of those end binding proteins, the KU complex, has already been characterised in NHEJ (Griffith et al., 1992, Suwa et al., 1994, Taccioli et al., 1994). From the evidence provided in this thesis, it is plausible that the linker histone variant, H1.X, could act in a similar manner.

Initial studies by Kysela *et. al.* (2005), proposed that linker histone variants were inhibitory to LX-mediated ligation, with the inhibition being relieved following phosphorylation by DNA-PK (Kysela et al., 2005). Subsequently, the work presented here suggests that although some linker histone variants may be inhibitory to LX-mediated ligation, H1.X actually acts to stimulate ligation in an *in vitro* reconstituted assay.

Interestingly, Rosidi et. al. (2008) have also presented a stimulatory role for a linker histone variant, H1.2, however stimulating DNA ligase III ligation in the alternative B-NHEJ pathway, rather than DNA ligase IV during NHEJ (Rosidi et al., 2008). B-NHEJ has a slower function

than NHEJ, is inhibited by DNA-PK and utilises DNA ligase III and PARP (Audebert et al., 2004, Perrault et al., 2004, H. Wang et al., 2005a). This observation also suggests that individual linker histone variants may fulfil different roles in different pathways of DSB repair, and DNA repair generally.

Data in this thesis also suggests that H1.X has a specific role in DSB repair in the NHEJ pathway. Although the role is not fully understood yet, it is apparent that in the absence of H1.X, the efficiency of LX-mediated ligation is defective. Studies in chicken cells have highlighted the need for the avian linker histone variant, H1.R, in the response to DSBs via the HR pathway (Hashimoto et al., 2007). Although the authors are unable to ascertain the functional significance of H1.R during HR, they hypothesise that there are defects in the accessibility or the efficiency of the HR protein machinery in the absence of H1.R protein.

The data in this thesis supports the aforementioned previous findings which together suggest a model for the involvement of linker histone variants during NHEJ (Figure 6.1). Under normal conditions, linker histone variants are positioned in between nucleosomes in an orderly fashion. It is unclear however, how the individual linker histone variants are distributed throughout the chromatin. Following DSB induction, the KU complex binds to the ends of the damaged DNA, followed by the subsequent recruitment of DNA-PK (Section 1.1.3.2.1). It is also plausible that after the induction of the DSB, the nucleosomes are removed from the DNA and the linker histone variants move in to bind the DNA in the vicinity of the break. DNA-PK then phosphorylates linker histones variants, causing them to be released from the DNA (Kysela et al., 2005). It is possible that the replication dependent

linker histone variants are phosphorylated on the conserved threonine residue (threonine 152 in H1.1) which is important for high affinity binding to DNA (Hendzel et al., 2004). This phosphorylation would reduce the affinity between the linker histone variants and the DNA (Dou et al., 2002, Lever et al., 2000). Evidence from this thesis supports this, as threonine 152 on linker histone variant H1.1 is phosphorylated by DNA-PK *in vitro*. However, as H1.X lacks these residues it is difficult to determine what effect the phosphorylation of H1.X has during NHEJ (Section 3.3.4). It has been demonstrated, however, that H1.X can interact with the LX complex *in vivo*, stimulating the end ligation by means of stabilising LX on the DNA ends, resulting in efficient ligation (Section 5.3.1 to Section 5.3.4; Figure 6.1A). More specifically, this interaction has been demonstrated in over-expressed cell lines and with native proteins. It is also not mediated by DNA, suggesting a physical interaction between H1.X and the LX complex occurs *in vivo*.

Under the circumstances where H1.X is depleted from cells, other linker histone variants are suspected to compensate (Y. Fan et al., 2003). However, due to the lack of linker histone variant H1.X, it is expected that H1.X mediated stimulation of LX does not occur, therefore the DNA ends are ligated less efficiently. This is confirmed by γH2A.X studies which show elevated levels of γH2A.X foci following IR in cells depleted for H1.X, but not for H1.2 (Section 4.3.3). It is also possible that there is a subset of DSBs that may specifically require the presence of H1.X to be repaired by NHEJ. Due to the failure to repair a significant proportion of DSBs when H1.X is depleted, the G2 to M checkpoint is activated for a longer period of time (Section 4.3.4). It is unclear, however, how cells depleted in H1.X escape the

G2 to M checkpoint resulting in the persistence of the DSB, leading to the formation of micronuclei (Section 4.3.5; Figure 6.1B).

The repair of DSBs is slightly different in cells compromised in NHEJ. For example, in the absence of DNA-PK, there is no suppression of B-NHEJ (Perrault et al., 2004). Therefore, H1.2 is able to activate PARP, and stimulate DNA ligase III specific end joining, resulting in DNA ligation by the slower B-NHEJ pathway (Audebert et al., 2004, H. Wang et al., 2005a) (Figure 6.1C).
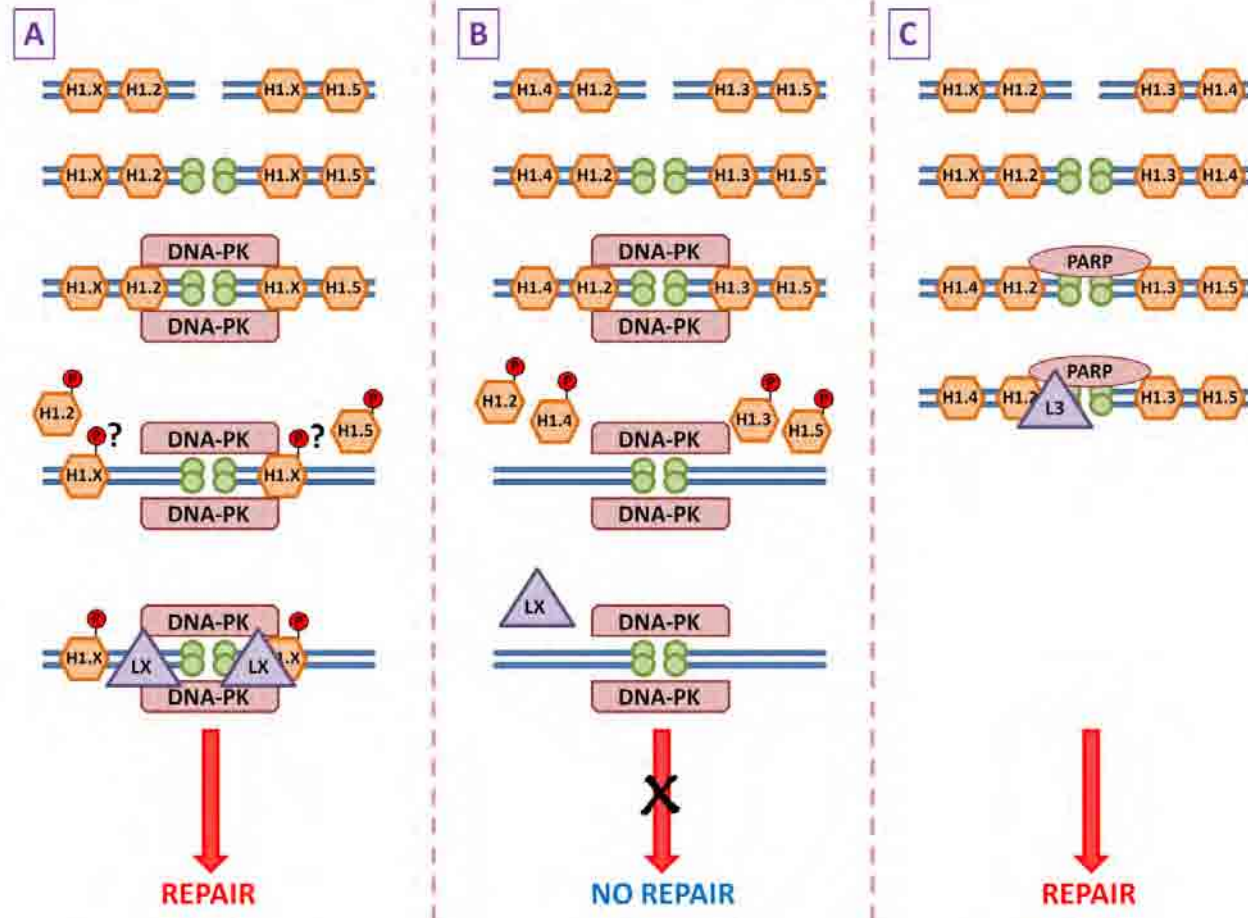
Figure 6.1 - Model for linker histone variants action during NHEJ
Three models proposed for the involvement of linker histone variants during NHEJ. **A**. After DSB induction and DNA-PK recruitment, linker histones are phosphorylated resulting in all but H1.X being released from the DNA. H1.X then aids in the recruitment and stimulation of the LX complex. **B**. In the absence of H1.X there is either reduced recruitment or stimulation of the LX complex resulting in no DNA repair. **C**. In NHEJ defective cells, linker histone variant H1.2 recruits PARP and DNA ligase III to the site of the repair, resulting in repair by the slower B-NHEJ pathway. Red circular 'P' denotes phosphorylation. L3 represents DNA ligase III. Green circles represent the KU complex.

6.2 H1.X and the DSB Specific Interaction with Nucleolin

Nucleolin has already been linked with the HR pathway due to its interaction with RAD51 which is believed to regulate HR (De et al., 2006). It has also been shown to interact with BRCA1 in the nucleoli, but following exposure to IR, BRCA1 disperses from the nucleoli (Tulchin et al., 2010). Interestingly, H1.X has an opposing function, whereby the interaction between H1.X and nucleolin is mediated following exposure to IR. This finding, coupled with the increase in nucleolar sites following exposure to IR, highlights the importance of this interaction, and opens up the possibilities of nucleolin having a role in the DNA damage response. It is plausible that H1.X is required specifically for the repair of damaged DNA within the nucleolar sites, and that this is mediated by nucleolin, although further investigation is required.

6.3 Future Experiments

This thesis has established the necessity for H1.X during NHEJ, along with the *in vitro* mechanistic analysis. However, how H1.X functions *in vivo* remains unknown. According to the model proposed in Section 6.1, there are still questions that need answering (Figure 6.1).

Primarily, it would be essential to ascertain whether H1.X is phosphorylated *in vivo* by either DNA-PK or ATM following IR, and then to map those phosphorylation sites. If phosphorylatable, it would be interesting to determine what effects phosphorylation has on H1.X's activity. Phosphorylation of a linker histone mix by DNA-PK, alleviated its inhibitory

effect (Kysela et al., 2005). This could be explained by the conserved threonine 152 and serine 183 residues found in the somatic linker histone variants, excluding H1.X (Hendzel et al., 2004). These sites are important for high affinity binding, and could be the target of phosphorylation to remove the linker histone variants from the DNA. H1.X does not contain these residues which could explain the differences between H1.X and the other linker histone variants.

It would also be interesting to determine how H1.X is able to stimulate ligation *in vivo*. H1.X could function similar to the KU complex to bridge the DNA ends, facilitating end-joining. H1.X could also be involved in the recruitment of LX to the site of the DSB, potentially following the PTM of H1.X after DSB induction. Also, the data presented in this thesis suggests that H1.X interacts with the LX complex, bringing about stimulation of ligation. It would be interesting to map the interacting regions on both H1.X and the LX complex.

The role of nucleolin within the DNA damage response, if any, would need to be established. This could be achieved by reducing protein levels by siRNA and assessing the cellular response to IR, and subsequently dissecting the interaction between nucleolin and H1.X.

Finally, it would be interesting to study the interplay between different linker histone variants at DNA ends. It has already been shown that H1.X stimulates LX-mediated ligation and H1.2 and H1.3 inhibit LX-mediated ligation (Section 5.3.1 and personal communication, Dr. Boris Kysela). Discovering which of the other linker histone variants stimulate and which inhibit LX-mediated ligation would be an important first step. Further characterisation of

their role *in vivo* by siRNA depletion would subsequently help to define the roles linker

histone variants have during NHEJ.

THE END

CHAPTER SEVEN: APPENDICES

Appendix A.

<u>Identity Scores Between Linker Histone Variants</u>

Linker Histone Variant	Protein Length	Linker Histone Variant	Protein Length	Identity Score
H1.0	194	H1.1	215	34
H1.0	194	H1.2	213	36
H1.0	194	H1.3	221	36
H1.0	194	H1.4	219	40
H1.0	194	H1.5	226	39
H1.0	194	H1.X	213	27
H1.0	194	H1.Foo	345	21
H1.0	194	H1.t	206	27
H1.0	194	H1.t2	255	17
H1.0	194	HILS1	231	9
H1.1	215	H1.2	213	64
H1.1	215	H1.3	221	67
H1.1	215	H1.4	219	72
H1.1	215	H1.5	226	65
H1.1	215	H1.X	213	29
H1.1	215	H1.Foo	345	23
H1.1	215	H1.t	206	43
H1.1	215	H1.t2	255	25
H1.1	215	HILS1	231	18
H1.2	213	H1.3	221	83
H1.2	213	H1.4	219	87
H1.2	213	H1.5	226	76
H1.2	213	H1.X	213	27
H1.2	213	H1.Foo	345	28
H1.2	213	H1.t	206	47
H1.2	213	H1.t2	255	22
H1.2	213	HILS1	231	17
H1.3	221	H1.4	219	86
H1.3	221	H1.5	226	74
H1.3	221	H1.X	213	29
H1.3	221	H1.Foo	345	27
H1.3	221	H1.t	206	44
H1.3	221	H1.t2	255	21
H1.3	221	HILS1	231	19
H1.4	219	H1.5	226	85
H1.4	219	H1.X	213	28
H1.4	219	H1.Foo	345	25
H1.4	219	H1.t	206	48
H1.4	219	H1.t2	255	21
H1.4	219	HILS1	231	15

H1.5	226	H1.X	213	30
H1.5	226	H1.Foo	345	20
H1.5	226	H1.t	206	45
H1.5	226	H1.t2	255	20
H1.5	226	HILS1	231	18
H1.X	213	H1.Foo	345	29
H1.X	213	H1.t	206	24
H1.X	213	H1.t2	255	20
H1.X	213	HILS1	231	10
H1.Foo	345	H1.t	206	22
H1.Foo	345	H1.t2	255	20
H1.Foo	345	HILS1	231	9
H1.t	206	H1.t2	255	18
H1.t	206	HILS1	231	17
H1.t2	255	HILS1	231	12

Appendix B.

Accession Numbers Used In This Thesis

Gene	Species	Accession Number
H1.0	*H. sapiens*	BI462123
H1.1	*H. sapiens*	BC069492
H1.2	*H. sapiens*	BC002649
H1.3	*H. sapiens*	BC104874
H1.4	*H. sapiens*	BC099632
H1.5	*H. sapiens*	BC101581
H1.X	*H. sapiens*	BC010435
H1.Foo	*H. sapiens*	BC047943
H1.t	*H. sapiens*	BC069517
H1.t2	*H. sapiens*	BC118635
HILS1	*H. sapiens*	BC033456
H1.X	*P. troglodytes*	XM_526304
H1.X	*B. taurus*	XM_589328
H1.X	*M. musculus*	BC048709
H1.X	*R. norvegicus*	XM_575600.3
H1.X	*G. gallus*	XM_425158.2
H1.X	*D. rerio*	BC047192
H1.0	*P. troglodytes*	XM_001147037.1
H1.0	*B. taurus*	BC122613
H1.0	*M. musculus*	BB661016
H1.0	*R. norvegicus*	BC061842
H1.0	*G. gallus*	X00169
H1.0	*D. rerio*	BC056596

Appendix C.

Flow Cytometry Images
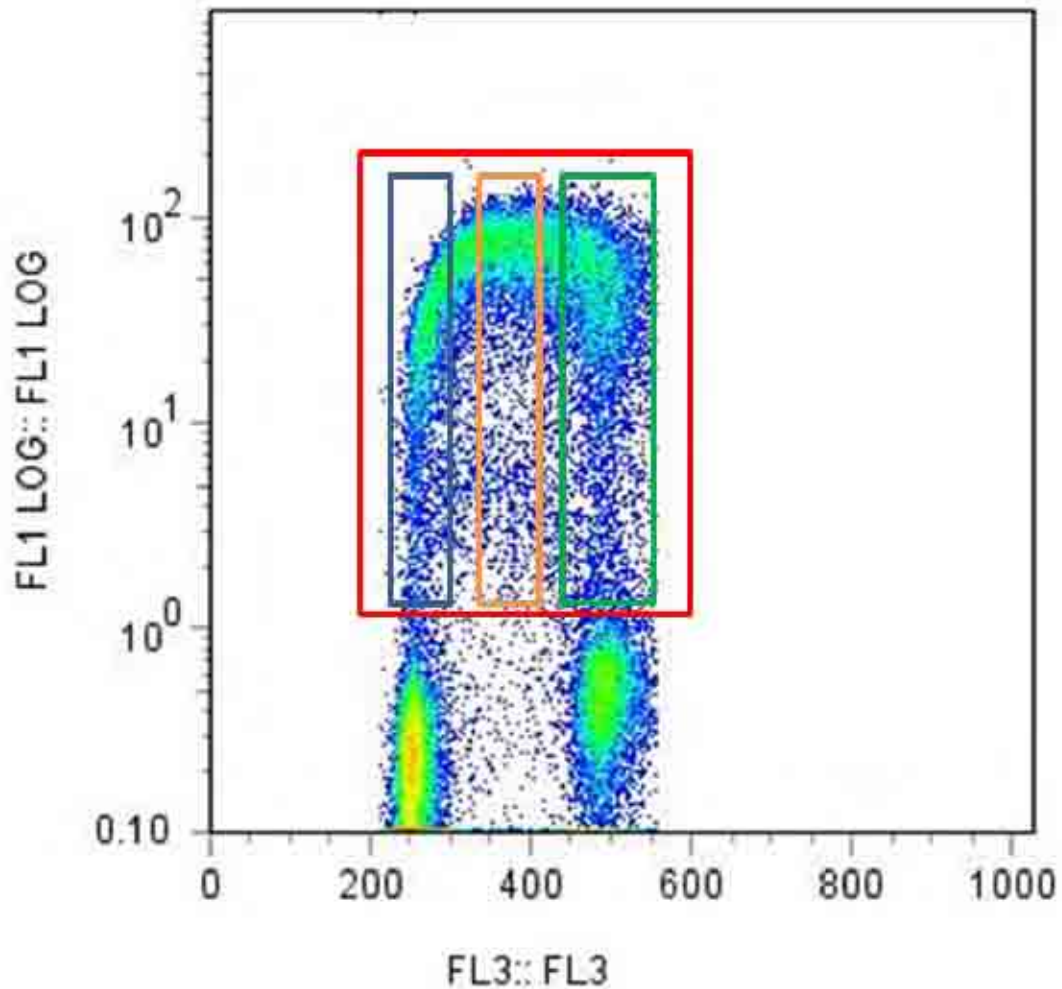
Figure 7.1 - Sample dot plot of flow cytometry data
Sample two parameter dot plot of cells stained with propidium iodide (DNA content, horizontal axis) and FITC labelled secondary antibody (BrdU, vertical axis). Four regions are highlighted on the dot plot. The red box, R1, contains the BrdU positive cell population. The blue box, R2, contains those cells which are BrdU positive and have a singular DNA content representative of cells in the G1 phase of the cell cycle. The orange box, R3, contains those cells which are BrdU positive and are currently synthesising DNA and is representative of those cells in the S phase of the cell cycle. The green box, R4, contains those cells which are BrdU positive and have twice the DNA content of cells in R2 which represents those cells in both G2 and M phases of the cell cycle.
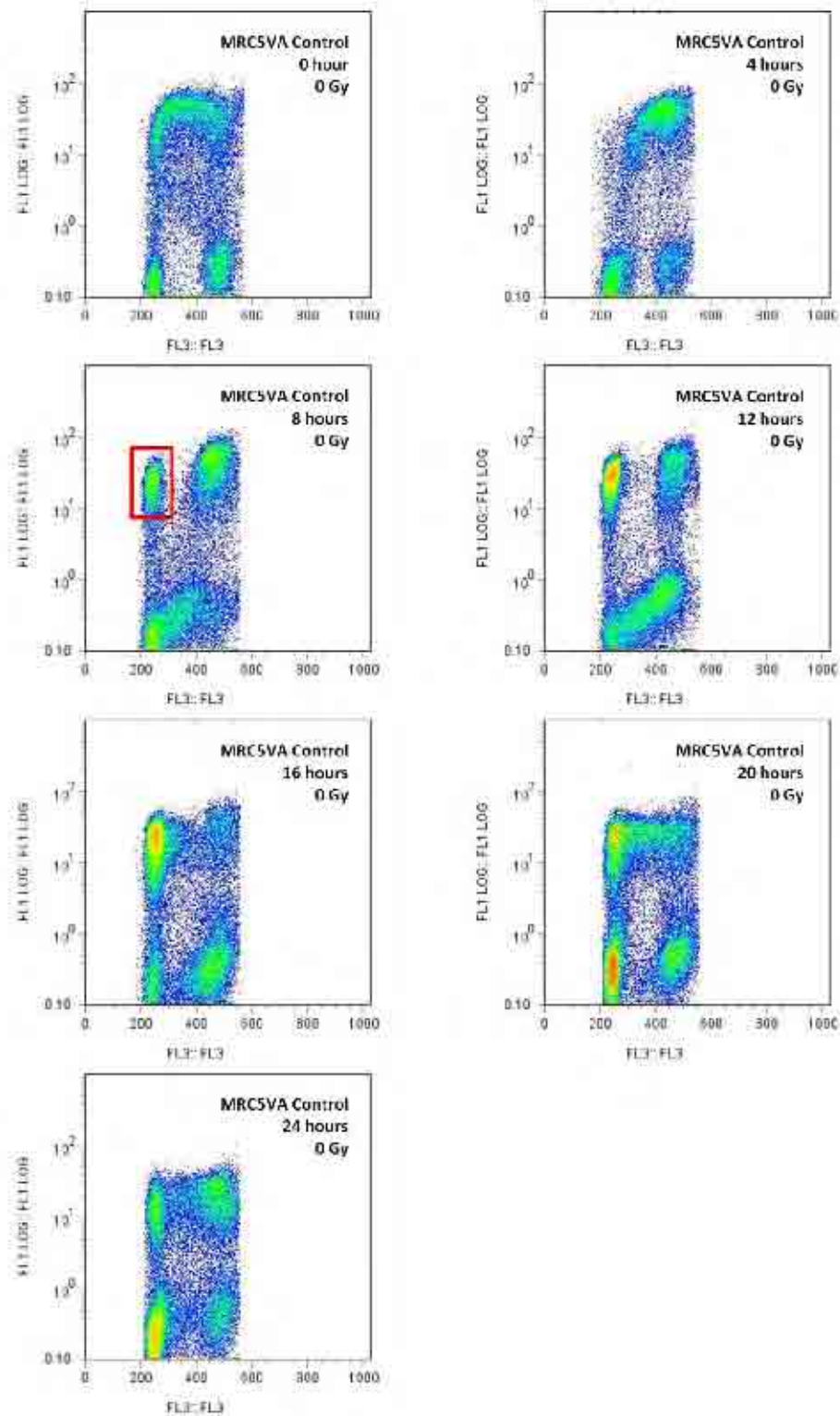
Figure 7.2 - Bivariate Cell Cycle Analysis of Un-Irradiated MRC5VA cells.
MRC5VA cells were incubated in the presence of BrdU for 20 mins. Samples were harvested every 4 hours and labelled with fluorescent anti-BrdU and propidium iodide and samples were analysed using FlowJo Flow Cytometry Analysis Software (Tree Star, Inc). The red box (8 hours) shows the re-emergence of the G1 population following mitosis.
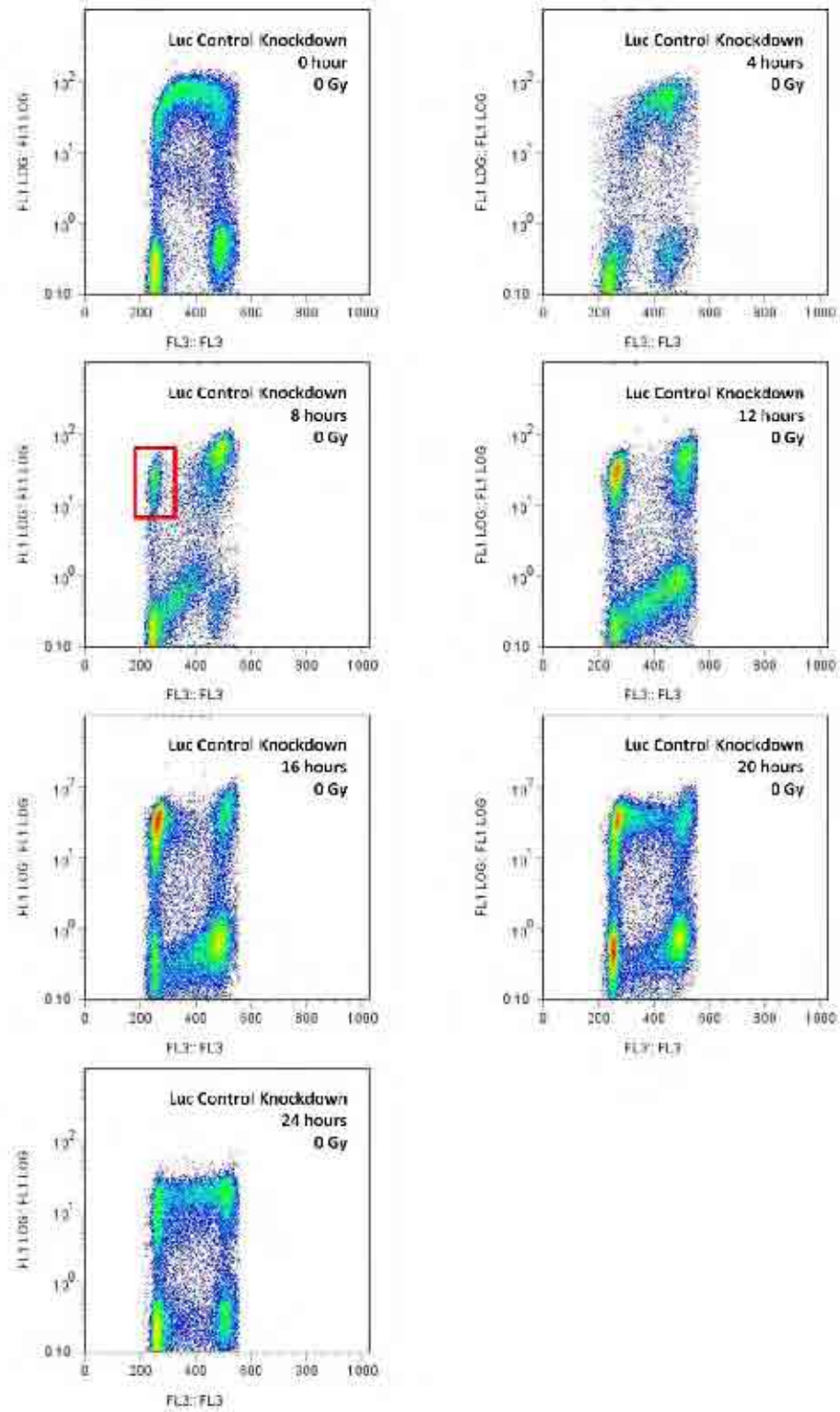
Figure 7.3 - Bivariate Cell Cycle Analysis of Un-Irradiated MRC5VA cells depleted of LUC.
MRC5VA cells depleted with control LUC siRNA were incubated in the presence of BrdU for 20 mins. Samples were harvested every 4 hours and labelled with fluorescent anti-BrdU and propidium iodide and samples were analysed using FlowJo Flow Cytometry Analysis Software (Tree Star, Inc). The red box (8 hours) shows the re-emergence of the G1 population following mitosis.
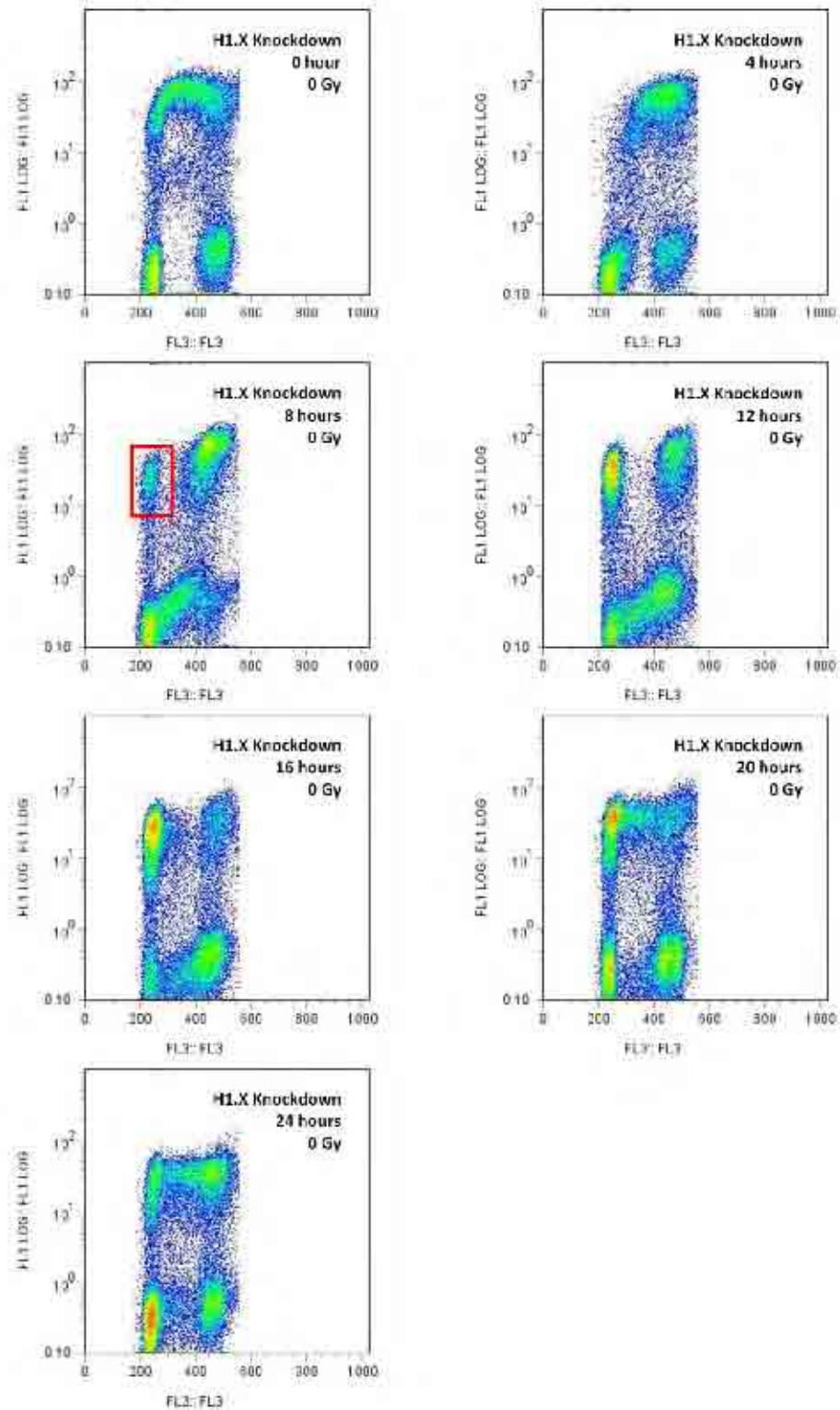
Figure 7.4 - Bivariate Cell Cycle Analysis of Un-Irradiated MRC5VA cells depleted of H1.X.
MRC5VA cells depleted of H1.X were incubated in the presence of BrdU for 20 mins. Samples were harvested every 4 hours and labelled with fluorescent anti-BrdU and propidium iodide and samples were analysed using FlowJo Flow Cytometry Analysis Software (Tree Star, Inc). The red box (8 hours) shows the re-emergence of the G1 population following mitosis which is consistent with that seen in the controls (Figure 7.2 & Figure 7.3).
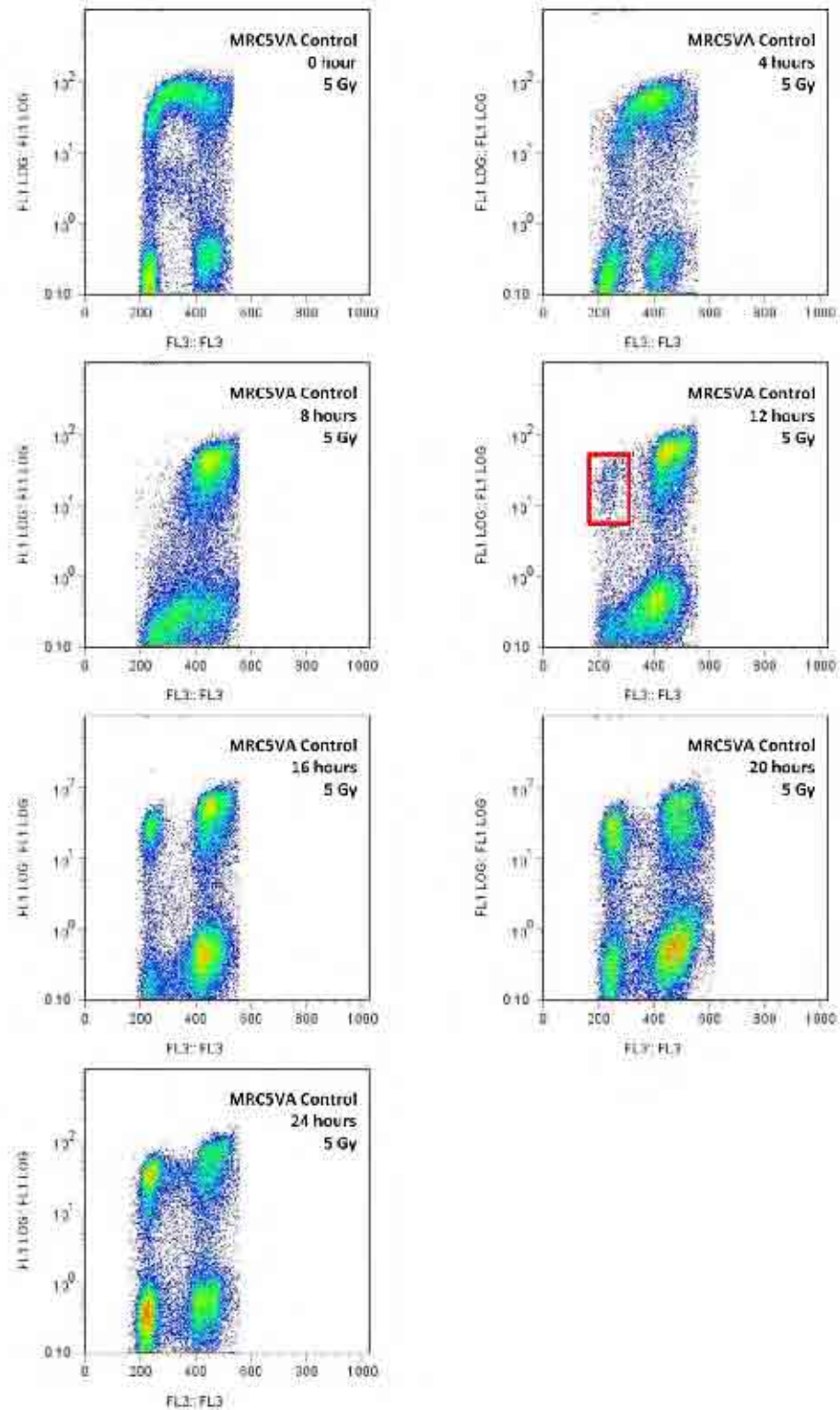
Figure 7.5 - Bivariate Cell Cycle Analysis of Irradiated MRC5VA cells.
Irradiated MRC5VA cells were incubated in the presence of BrdU for 20 mins. Samples were harvested every 4 hours and labelled with fluorescent anti-BrdU and propidium iodide and samples were analysed using FlowJo Flow Cytometry Analysis Software (Tree Star, Inc). The red box (12 hours) shows the re-emergence of the G1 population following mitosis which is delayed by 4 hours compared to the un-irradiated sample (Figure 7.2).
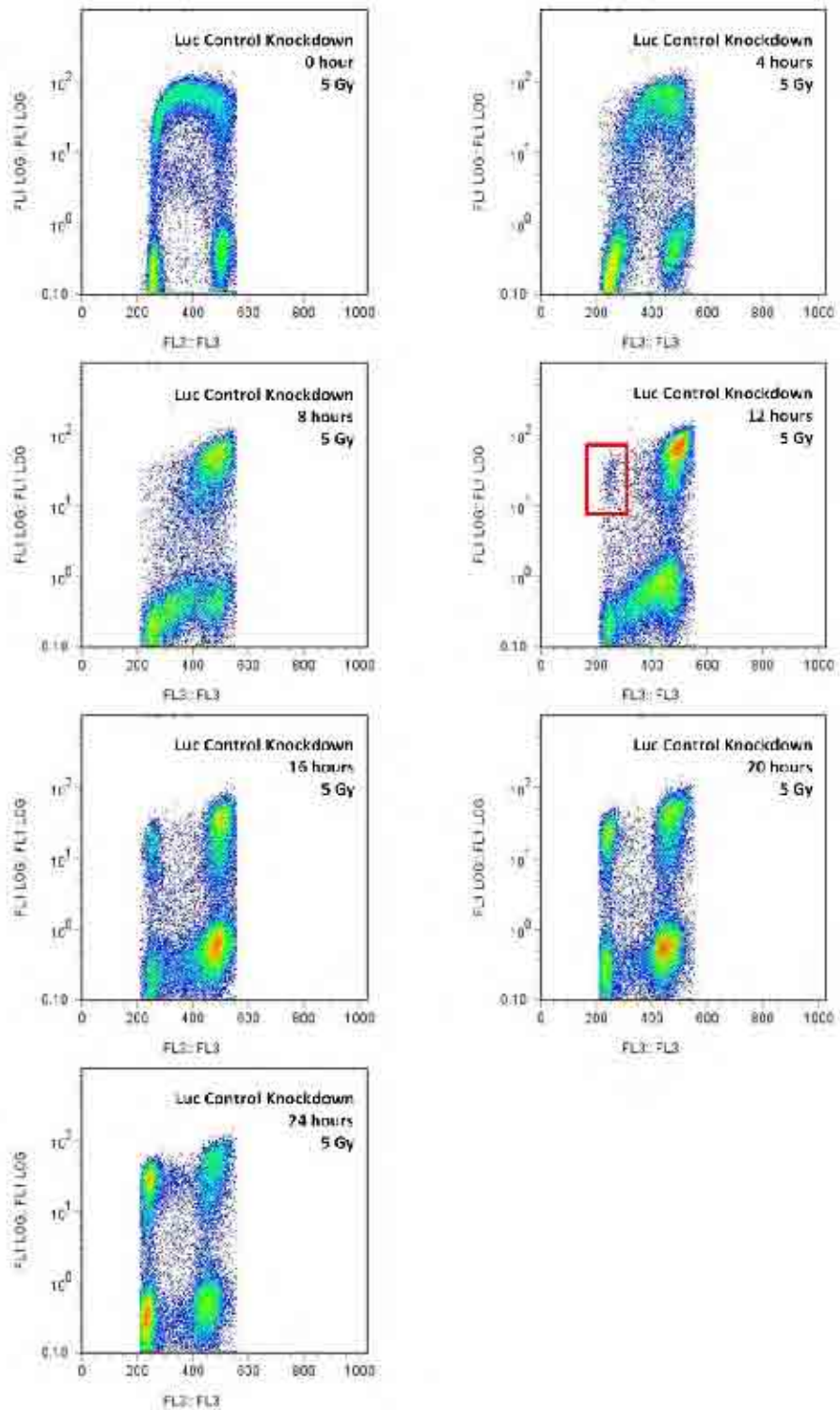
Figure 7.6 - Bivariate Cell Cycle Analysis of Irradiated MRC5VA cells depleted of LUC.
Irradiated MRC5VA cells depleted with control LUC siRNA were incubated in the presence of BrdU for 20 mins. Samples were harvested every 4 hours and labelled with fluorescent anti-BrdU and propidium iodide and samples were analysed using FlowJo Flow Cytometry Analysis Software (Tree Star, Inc). The red box (12 hours) shows the re-emergence of the G1 population following mitosis which is delayed by 4 hours compared to the un-irradiated sample (Figure 7.3).
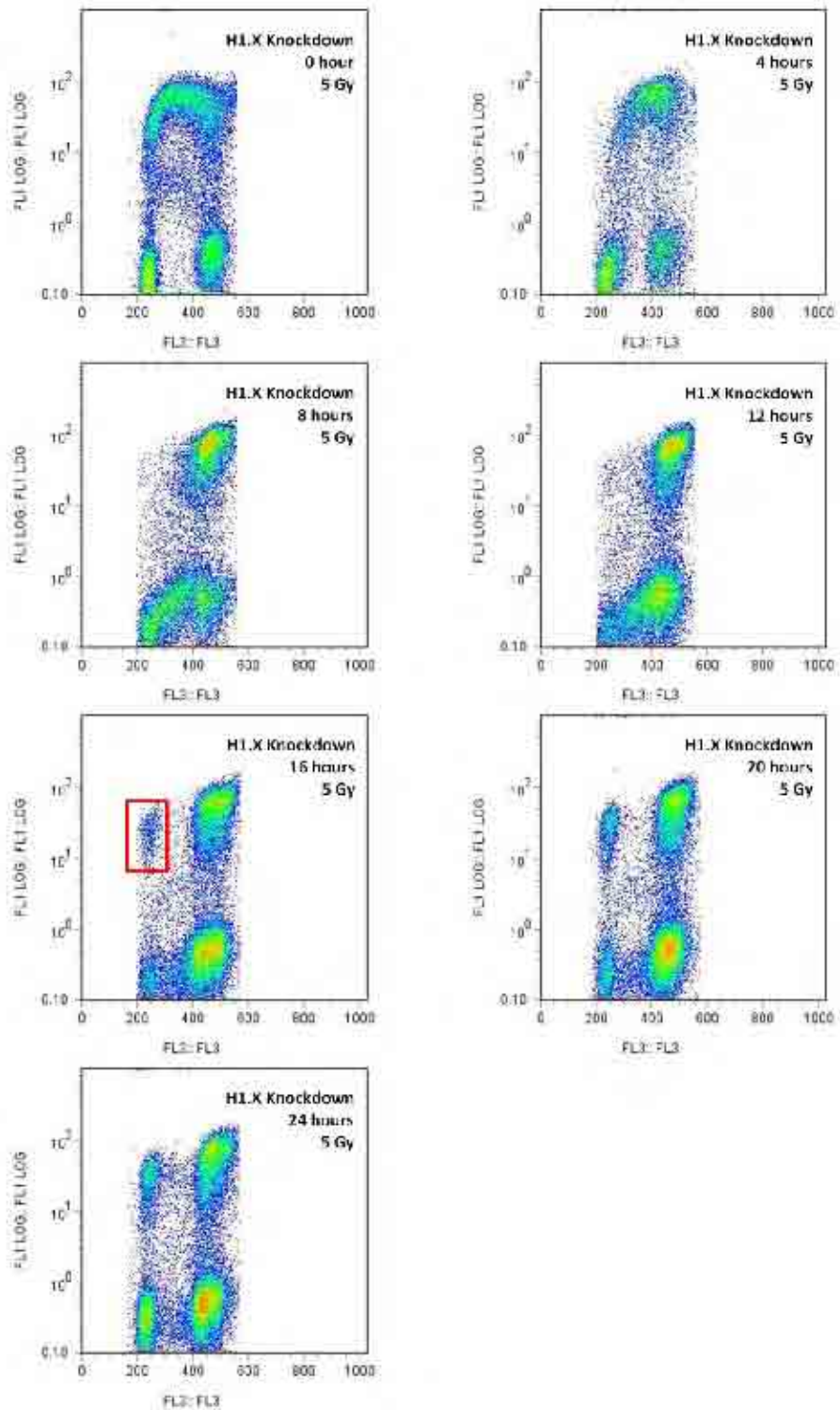
Figure 7.7 - Bivariate Cell Cycle Analysis of Irradiated MRC5VA cells depleted of H1.X.
Irradiated MRC5VA cells depleted of H1.X were incubated in the presence of BrdU for 20 mins. Samples were harvested every 4 hours and labelled with fluorescent anti-BrdU and propidium iodide and samples were analysed using FlowJo Flow Cytometry Analysis Software (Tree Star, Inc). The red box (16 hours) shows the re-emergence of the G1 population following mitosis which is delayed compared to the controls where this occurs at 12 hours (Figure 7.5 & Figure 7.6).

Appendix D.

Buffers Used In This Thesis

Reagent	Constituents
Supplemented DMEM	DMEM (containing 1000mg/L glucose) 10% (v/v) FBS 2mM L-glutamine 1mM sodium pyruvate 1% non-essential amino acids
G418 DMEM	As supplemented DMEM, with the addition of 600μg/mL G418
RIPA Buffer	50mM Tris-HCl pH7.5 1mM EDTA 150mM NaCl 0.1% SDS 0.5% deoxycholic acid 1% Igepal CA-360
SDS Running Buffer	25mM Tris 192mM glycine 0.1% SDS
SDS Loading Buffer	65mM Tris/HCl pH8 10% (v/v) glycerol 2.3% (w/v) SDS 0.01 bromophenol blue 1% dithiothreitol DTT
CAPS Buffer	10mM CAPS pH 11 10% methanol
Immuno-fluorescence Lysis Buffer	10mM PIPES pH 6.8 300mM sucrose 20mM NaCl 3mM $MgCl_2$ 0.5% Triton X-100
TBE	89 mM Tris-Base 89 mM boric acid 2mM EDTA
X10 DNA Loading Buffer	50% glycerol 0.05% bromophenol blue
EB Buffer	1.25M NaCl 50mM Tris/HCl, pH 8.5

	15% isopropanol (v/v)
His-tag Lysis Buffer	50mM Tris/HCl pH 7.5 750mM NaCl 0.02mM EDTA 0.02mM EGTA 1% Triton 0.06% ß-mercaptoethanol 1mM benzamidine 0.2mM PMSF Protease inhibitor cocktail (Roche)
His-tag High Salt Buffer	50mM Tris/HCl pH 7.5 500mM NaCl 0.02mM EDTA 0.02mM EGTA 0.03% Brij 35 20mM imidazole 0.06% ß-mercaptoethanol 1mM benzamidine 0.2mM PMSF
His-tag Low Salt Buffer	50mM Tris/HCl pH 7.5 150mM NaCl 0.02mM EDTA 0.02mM EGTA 0.03% Brij 35 20mM imidazole 0.06% ß-mercaptoethanol 1mM benzamidine 0.2mM PMSF
His-Tag Elution Buffer	50mM Tris/HCl pH 7.5 150mM NaCl 0.02mM EDTA 0.02mM EGTA 0.03% Brij 35 300mM imidazole 0.06% ß-mercaptoethanol 1mM benzamidine 0.2mM PMSF
TNB Buffer	10 mM Tris pH 8.0 50mM NaCl 1mM β-mercaptoethanol
Kinase Buffer	25mM HEPES pH 7.5 10mM $MgCl_2$ 1mM DTT

	0.1% Nonidet P-40 20% glycerol
X10 Ligation Buffer	66 mM Tris/HCl pH 7.5 5 mM MgCl$_2$ 1 mM DTT 1mM ATP 0.5mg/mL BSA
X10 EMSA Buffer	66 mM Tris/HCl pH 7.5 1 mM DTT 1mM ATP 0.5mg/mL BSA
IP Lysis Buffer	50mM Tris/HCl pH 7.5 1mM EGTA 1mM EDTA 50mM sodium fluoride 5mM sodium pyrophosphate 1mM sodium orthovanadate 0.27M sucrose 1% Triton X-100 0.1% β-mercaptoethanol Protease inhibitor cocktail
IP Wash Buffer	50mM Tris/HCl pH 7.5 1mM EGTA 1mM EDTA 50mM sodium fluoride 5mM sodium pyrophosphate 1mM sodium orthovanadate 0.27M sucrose 1% Triton X-100 0.1% β-mercaptoethanol Protease inhibitor cocktail

CHAPTER EIGHT: REFERENCES

Aboussekhra, A., Chanet, R., Adjiri, A., et al. (1992) Semidominant suppressors of Srs2 helicase mutations of Saccharomyces cerevisiae map in the RAD51 gene, whose sequence predicts a protein with similarities to procaryotic RecA proteins. **Mol Cell Biol**, 12: (7): 3224-3234.

Adam, M., Robert, F., Larochelle, M., et al. (2001) H2A.Z is required for global chromatin integrity and for recruitment of RNA polymerase II under specific conditions. **Mol Cell Biol**, 21: (18): 6270-6279.

Ahnesorg, P., Smith, P. and Jackson, S.P. (2006) XLF interacts with the XRCC4-DNA ligase IV complex to promote DNA nonhomologous end-joining. **Cell**, 124: (2): 301-313.

Albig, W., Meergans, T. and Doenecke, D. (1997) Characterization of the H1.5 gene completes the set of human H1 subtype genes. **Gene**, 184: (2): 141-148.

Allan, J., Mitchell, T., Harborne, N., et al. (1986) Roles of H1 domains in determining higher order chromatin structure and H1 location. **J Mol Biol**, 187: (4): 591-601.

Anderson, C.W. and Carter, T.H. (1996) The DNA-activated protein kinase -- DNA-PK. **Curr Top Microbiol Immunol**, 217: 91-111.

Ariumi, Y., Masutani, M., Copeland, T.D., et al. (1999) Suppression of the poly(ADP-ribose) polymerase activity by DNA-dependent protein kinase in vitro. **Oncogene**, 18: (32): 4616-4625.

Audebert, M., Salles, B. and Calsou, P. (2004) Involvement of poly(ADP-ribose) polymerase-1 and XRCC1/DNA ligase III in an alternative route for DNA double-strand breaks rejoining. **J Biol Chem**, 279: (53): 55117-55126.

Bakkenist, C.J. and Kastan, M.B. (2003) DNA damage activates ATM through intermolecular autophosphorylation and dimer dissociation. **Nature**, 421: (6922): 499-506.

Balajee, A.S. and Geard, C.R. (2004) Replication protein A and gamma-H2AX foci assembly is triggered by cellular response to DNA double-strand breaks. **Exp Cell Res**, 300: (2): 320-334.

Banin, S., Moyal, L., Shieh, S., et al. (1998) Enhanced phosphorylation of p53 by ATM in response to DNA damage. **Science**, 281: (5383): 1674-1677.

Bao, S., Tibbetts, R.S., Brumbaugh, K.M., et al. (2001) ATR/ATM-mediated phosphorylation of human Rad17 is required for genotoxic stress responses. **Nature**, 411: (6840): 969-974.

Bao, Y., Konesky, K., Park, Y.J., et al. (2004) Nucleosomes containing the histone variant H2A.Bbd organize only 118 base pairs of DNA. **EMBO J**, 23: (16): 3314-3324.

Barnes, D.E., Stamp, G., Rosewell, I., et al. (1998) Targeted disruption of the gene encoding DNA ligase IV leads to lethality in embryonic mice. **Curr Biol**, 8: (25): 1395-1398.

Basile, G., Aker, M. and Mortimer, R.K. (1992) Nucleotide sequence and transcriptional regulation of the yeast recombinational repair gene RAD51. **Mol Cell Biol**, 12: (7): 3235-3246.

Bassing, C.H., Swat, W. and Alt, F.W. (2002) The mechanism and regulation of chromosomal V(D)J recombination. **Cell**, 109 Suppl: (55): S45-55.

Baumann, P. and Cech, T.R. (2000) Protection of telomeres by the Ku protein in fission yeast. **Mol Biol Cell**, 11: (10): 3265-3275.

Benson, F.E., Baumann, P. and West, S.C. (1998) Synergistic actions of Rad51 and Rad52 in recombination and DNA repair. **Nature**, 391: (6665): 401-404.

Bharath, M.M., Khadake, J.R. and Rao, M.R. (1998) **Expression of rat histone H1d in Escherichia coli and its purification** [online]. http://www.ncbi.nlm.nih.gov/entrez/query.fcgi?cmd=Retrieve&db=PubMed&dopt=Citation &list_uids=9473455 Feb [Accessed 1 12]

Binz, S.K., Sheehan, A.M. and Wold, M.S. (2004) Replication protein A phosphorylation and the cellular response to DNA damage. **DNA Repair (Amst)**, 3: (8-9): 1015-1024.

Borer, R.A., Lehner, C.F., Eppenberger, H.M., et al. (1989) Major nucleolar proteins shuttle between nucleus and cytoplasm. **Cell**, 56: (3): 379-390.

Bork, P., Hofmann, K., Bucher, P., et al. (1997) A superfamily of conserved domains in DNA damage-responsive cell cycle checkpoint proteins. **FASEB J**, 11: (1): 68-76.

Botuyan, M.V., Lee, J., Ward, I.M., et al. (2006) Structural basis for the methylation state-specific recognition of histone H4-K20 by 53BP1 and Crb2 in DNA repair. **Cell**, 127: (7): 1361-1373.

Boulton, S.J. (2010) DNA repair: Decision at the break point. **Nature**, 465: (7296): 301-302.

Bradford, M.M. (1976) A rapid and sensitive method for the quantitation of microgram quantities of protein utilizing the principle of protein-dye binding. **Anal Biochem**, 72: 248-254.

Brown, D.T., Izard, T. and Misteli, T. (2006) Mapping the interaction surface of linker histone H1(0) with the nucleosome of native chromatin in vivo. **Nat Struct Mol Biol**, 13: (3): 250-255.

Buck, D., Malivert, L., de Chasseval, R., et al. (2006) Cernunnos, a novel nonhomologous end-joining factor, is mutated in human immunodeficiency with microcephaly. **Cell**, 124: (2): 287-299.

Bunting, S.F., Callen, E., Wong, N., et al. (2010) 53BP1 inhibits homologous recombination in Brca1-deficient cells by blocking resection of DNA breaks. **Cell**, 141: (2): 243-254.

Burma, S., Chen, B.P., Murphy, M., et al. (2001) ATM phosphorylates histone H2AX in response to DNA double-strand breaks. **J Biol Chem**, 276: (45): 42462-42467.

Cairns, B.R. (2009) The logic of chromatin architecture and remodelling at promoters. **Nature**, 461: (7261): 193-198.

Calsou, P., Delteil, C., Frit, P., et al. (2003) Coordinated assembly of Ku and p460 subunits of the DNA-dependent protein kinase on DNA ends is necessary for XRCC4-ligase IV recruitment. **J Mol Biol**, 326: (1): 93-103.

Canman, C.E., Lim, D.S., Cimprich, K.A., et al. (1998) Activation of the ATM kinase by ionizing radiation and phosphorylation of p53. **Science**, 281: (5383): 1677-1679.

Cao, Q.P., Pitt, S., Leszyk, J., et al. (1994) DNA-dependent ATPase from HeLa cells is related to human Ku autoantigen. **Biochemistry**, 33: (28): 8548-8557.

Carney, J.P., Maser, R.S., Olivares, H., et al. (1998) The hMre11/hRad50 protein complex and Nijmegen breakage syndrome: linkage of double-strand break repair to the cellular DNA damage response. **Cell**, 93: (3): 477-486.

Celeste, A., Fernandez-Capetillo, O., Kruhlak, M.J., et al. (2003) Histone H2AX phosphorylation is dispensable for the initial recognition of DNA breaks. **Nat Cell Biol**, 5: (7): 675-679.

Celeste, A., Petersen, S., Romanienko, P.J., et al. (2002) Genomic instability in mice lacking histone H2AX. **Science**, 296: (5569): 922-927.

Cha, H., Lowe, J.M., Li, H., et al. (2010) Wip1 directly dephosphorylates gamma-H2AX and attenuates the DNA damage response. **Cancer Res**, 70: (10): 4112-4122.

Chadwick, B.P. and Willard, H.F. (2001) A novel chromatin protein, distantly related to histone H2A, is largely excluded from the inactive X chromosome. **J Cell Biol**, 152: (2): 375-384.

Chan, D.W., Chen, B.P., Prithivirajsingh, S., et al. (2002) Autophosphorylation of the DNA-dependent protein kinase catalytic subunit is required for rejoining of DNA double-strand breaks. **Genes Dev**, 16: (18): 2333-2338.

Chan, D.W., Ye, R., Veillette, C.J., et al. (1999) DNA-dependent protein kinase phosphorylation sites in Ku 70/80 heterodimer. **Biochemistry**, 38: (6): 1819-1828.

Chehab, N.H., Malikzay, A., Appel, M., et al. (2000) Chk2/hCds1 functions as a DNA damage checkpoint in G(1) by stabilizing p53. **Genes Dev**, 14: (3): 278-288.

Chen, B.P., Uematsu, N., Kobayashi, J., et al. (2007) Ataxia telangiectasia mutated (ATM) is essential for DNA-PKcs phosphorylations at the Thr-2609 cluster upon DNA double strand break. **J Biol Chem**, 282: (9): 6582-6587.

Chen, L., Morio, T., Minegishi, Y., et al. (2005a) Ataxia-telangiectasia-mutated dependent phosphorylation of Artemis in response to DNA damage. **Cancer Sci**, 96: (2): 134-141.

Chen, L., Trujillo, K., Sung, P., et al. (2000) Interactions of the DNA ligase IV-XRCC4 complex with DNA ends and the DNA-dependent protein kinase. **J Biol Chem**, 275: (34): 26196-26205.

Chen, L., Trujillo, K.M., Van Komen, S., et al. (2005b) Effect of amino acid substitutions in the rad50 ATP binding domain on DNA double strand break repair in yeast. **J Biol Chem**, 280: (4): 2620-2627.

Chen, P.C., Dudley, S., Hagen, W., et al. (2005c) Contributions by MutL homologues Mlh3 and Pms2 to DNA mismatch repair and tumor suppression in the mouse. **Cancer Res**, 65: (19): 8662-8670.

Chen, X., Arciero, C.A., Wang, C., et al. (2006) BRCC36 is essential for ionizing radiation-induced BRCA1 phosphorylation and nuclear foci formation. **Cancer Res**, 66: (10): 5039-5046.

Chen, Y.R., Lees-Miller, S.P., Tegtmeyer, P., et al. (1991) The human DNA-activated protein kinase phosphorylates simian virus 40 T antigen at amino- and carboxy-terminal sites. **J Virol**, 65: (10): 5131-5140.

Chernikova, S.B., Wells, R.L. and Elkind, M.M. (1999) Wortmannin sensitizes mammalian cells to radiation by inhibiting the DNA-dependent protein kinase-mediated rejoining of double-strand breaks. **Radiat Res**, 151: (2): 159-166.

Chipuk, J.E., Moldoveanu, T., Llambi, F., et al. (2010) The BCL-2 family reunion. **Mol Cell**, 37: (3): 299-310.

Chowdhury, D., Keogh, M.C., Ishii, H., et al. (2005) gamma-H2AX dephosphorylation by protein phosphatase 2A facilitates DNA double-strand break repair. **Mol Cell**, 20: (5): 801-809.

Clever, B., Interthal, H., Schmuckli-Maurer, J., et al. (1997) Recombinational repair in yeast: functional interactions between Rad51 and Rad54 proteins. **EMBO J**, 16: (9): 2535-2544.

Cortez, D., Wang, Y., Qin, J., et al. (1999) Requirement of ATM-dependent phosphorylation of brca1 in the DNA damage response to double-strand breaks. **Science**, 286: (5442): 1162-1166.

Critchlow, S.E., Bowater, R.P. and Jackson, S.P. (1997) Mammalian DNA double-strand break repair protein XRCC4 interacts with DNA ligase IV. **Curr Biol**, 7: (8): 588-598.

Dai, Y., Kysela, B., Hanakahi, L.A., et al. (2003) Nonhomologous end joining and V(D)J recombination require an additional factor. **Proc Natl Acad Sci U S A**, 100: (5): 2462-2467.

Dalal, S.N., Schweitzer, C.M., Gan, J., et al. (1999) Cytoplasmic localization of human cdc25C during interphase requires an intact 14-3-3 binding site. **Mol Cell Biol**, 19: (6): 4465-4479.

Daujat, S., Zeissler, U., Waldmann, T., et al. (2005) HP1 binds specifically to Lys26-methylated histone H1.4, whereas simultaneous Ser27 phosphorylation blocks HP1 binding. **J Biol Chem**, 280: (45): 38090-38095.

Davey, C.A., Sargent, D.F., Luger, K., et al. (2002) Solvent mediated interactions in the structure of the nucleosome core particle at 1.9 a resolution. **J Mol Biol**, 319: (5): 1097-1113.

De, A., Donahue, S.L., Tabah, A., et al. (2006) A novel interaction [corrected] of nucleolin with Rad51. **Biochem Biophys Res Commun**, 344: (1): 206-213.

de Jager, M., van Noort, J., van Gent, D.C., et al. (2001) Human Rad50/Mre11 is a flexible complex that can tether DNA ends. **Mol Cell**, 8: (5): 1129-1135.

de Jager, M., Wyman, C., van Gent, D.C., et al. (2002) DNA end-binding specificity of human Rad50/Mre11 is influenced by ATP. **Nucleic Acids Res**, 30: (20): 4425-4431.

de Vries, E., van Driel, W., Bergsma, W.G., et al. (1989) HeLa nuclear protein recognizing DNA termini and translocating on DNA forming a regular DNA-multimeric protein complex. **J Mol Biol**, 208: (1): 65-78.

DeLeo, A.B., Jay, G., Appella, E., et al. (1979) Detection of a transformation-related antigen in chemically induced sarcomas and other transformed cells of the mouse. **Proc Natl Acad Sci U S A**, 76: (5): 2420-2424.

Desai-Mehta, A., Cerosaletti, K.M. and Concannon, P. (2001) Distinct functional domains of nibrin mediate Mre11 binding, focus formation, and nuclear localization. **Mol Cell Biol**, 21: (6): 2184-2191.

Deterding, L.J., Bunger, M.K., Banks, G.C., et al. (2008) Global changes in and characterization of specific sites of phosphorylation in mouse and human histone H1 Isoforms upon CDK inhibitor treatment using mass spectrometry. **J Proteome Res**, 7: (6): 2368-2379.

di Masi, A., Viganotti, M., Polticelli, F., et al. (2008) The R215W mutation in NBS1 impairs gamma-H2AX binding and affects DNA repair: molecular bases for the severe phenotype of 657del5/R215W Nijmegen breakage syndrome patients. **Biochem Biophys Res Commun**, 369: (3): 835-840.

Difilippantonio, S., Gapud, E., Wong, N., et al. (2008) 53BP1 facilitates long-range DNA end-joining during V(D)J recombination. **Nature**, 456: (7221): 529-533.

DiTullio, R.A., Jr., Mochan, T.A., Venere, M., et al. (2002) 53BP1 functions in an ATM-dependent checkpoint pathway that is constitutively activated in human cancer. **Nat Cell Biol**, 4: (12): 998-1002.

Dou, Y., Bowen, J., Liu, Y., et al. (2002) Phosphorylation and an ATP-dependent process increase the dynamic exchange of H1 in chromatin. **J Cell Biol**, 158: (7): 1161-1170.

Douglas, P., Gupta, S., Morrice, N., et al. (2005) DNA-PK-dependent phosphorylation of Ku70/80 is not required for non-homologous end joining. **DNA Repair (Amst)**, 4: (9): 1006-1018.

Douglas, P., Zhong, J., Ye, R., et al. (2010) Protein phosphatase 6 interacts with the DNA-dependent protein kinase catalytic subunit and dephosphorylates gamma-H2AX. **Mol Cell Biol**, 30: (6): 1368-1381.

Downs, J.A., Allard, S., Jobin-Robitaille, O., et al. (2004) Binding of chromatin-modifying activities to phosphorylated histone H2A at DNA damage sites. **Mol Cell**, 16: (6): 979-990.

Downs, J.A. and Jackson, S.P. (2004) A means to a DNA end: the many roles of Ku. **Nat Rev Mol Cell Biol**, 5: (5): 367-378.

Downs, J.A., Kosmidou, E., Morgan, A., et al. (2003) Suppression of homologous recombination by the Saccharomyces cerevisiae linker histone. **Mol Cell**, 11: (6): 1685-1692.

Doyen, C.M., Montel, F., Gautier, T., et al. (2006) Dissection of the unusual structural and functional properties of the variant H2A.Bbd nucleosome. **EMBO J**, 25: (18): 4234-4244.

Drabent, B., Bode, C. and Doenecke, D. (1993) Structure and expression of the mouse testicular H1 histone gene (H1t). **Biochim Biophys Acta**, 1216: (2): 311-313.

Draker, R. and Cheung, P. (2009) Transcriptional and epigenetic functions of histone variant H2A.Z. **Biochem Cell Biol**, 87: (1): 19-25.

Duggan, M.M. and Thomas, J.O. (2000) Two DNA-binding sites on the globular domain of histone H5 are required for binding to both bulk and 5 S reconstituted nucleosomes. **J Mol Biol**, 304: (1): 21-33.

Dupre, A., Boyer-Chatenet, L. and Gautier, J. (2006) Two-step activation of ATM by DNA and the Mre11-Rad50-Nbs1 complex. **Nat Struct Mol Biol**, 13: (5): 451-457.

Durocher, D., Henckel, J., Fersht, A.R., et al. (1999) The FHA domain is a modular phosphopeptide recognition motif. **Mol Cell**, 4: (3): 387-394.

Dvir, A., Peterson, S.R., Knuth, M.W., et al. (1992) Ku autoantigen is the regulatory component of a template-associated protein kinase that phosphorylates RNA polymerase II. **Proc Natl Acad Sci U S A**, 89: (24): 11920-11924.

Dynan, W.S. and Yoo, S. (1998) Interaction of Ku protein and DNA-dependent protein kinase catalytic subunit with nucleic acids. **Nucleic Acids Res**, 26: (7): 1551-1559.

el-Deiry, W.S., Tokino, T., Velculescu, V.E., et al. (1993) WAF1, a potential mediator of p53 tumor suppression. **Cell**, 75: (4): 817-825.

Faast, R., Thonglairoam, V., Schulz, T.C., et al. (2001) Histone variant H2A.Z is required for early mammalian development. **Curr Biol**, 11: (15): 1183-1187.

Falck, J., Coates, J. and Jackson, S.P. (2005) Conserved modes of recruitment of ATM, ATR and DNA-PKcs to sites of DNA damage. **Nature**, 434: (7033): 605-611.

Falck, J., Mailand, N., Syljuasen, R.G., et al. (2001) The ATM-Chk2-Cdc25A checkpoint pathway guards against radioresistant DNA synthesis. **Nature**, 410: (6830): 842-847.

Fan, J.Y., Rangasamy, D., Luger, K., et al. (2004) H2A.Z alters the nucleosome surface to promote HP1alpha-mediated chromatin fiber folding. **Mol Cell**, 16: (4): 655-661.

Fan, T.J., Han, L.H., Cong, R.S., et al. (2005) Caspase family proteases and apoptosis. **Acta Biochim Biophys Sin (Shanghai)**, 37: (11): 719-727.

Fan, Y., Nikitina, T., Morin-Kensicki, E.M., et al. (2003) H1 linker histones are essential for mouse development and affect nucleosome spacing in vivo. **Mol Cell Biol**, 23: (13): 4559-4572.

Fan, Y., Sirotkin, A., Russell, R.G., et al. (2001) Individual somatic H1 subtypes are dispensable for mouse development even in mice lacking the H1(0) replacement subtype. **Mol Cell Biol**, 21: (23): 7933-7943.

Fenech, M. (2007) Cytokinesis-block micronucleus cytome assay. **Nat Protoc**, 2: (5): 1084-1104.

Fenech, M. and Morley, A.A. (1985) Measurement of micronuclei in lymphocytes. **Mutat Res**, 147: (1-2): 29-36.

Feng, L., Huang, J. and Chen, J. (2009) MERIT40 facilitates BRCA1 localization and DNA damage repair. **Genes Dev**, 23: (6): 719-728.

Finch, J.T. and Klug, A. (1976) Solenoidal model for superstructure in chromatin. **Proc Natl Acad Sci U S A**, 73: (6): 1897-1901.

Fousteri, M. and Mullenders, L.H. (2008) Transcription-coupled nucleotide excision repair in mammalian cells: molecular mechanisms and biological effects. **Cell Res**, 18: (1): 73-84.

Franke, K., Drabent, B. and Doenecke, D. (1998) Testicular expression of the mouse histone H1.1 gene. **Histochem Cell Biol**, 109: (4): 383-390.

Fu, G., Ghadam, P., Sirotkin, A., et al. (2003) Mouse oocytes and early embryos express multiple histone H1 subtypes. **Biol Reprod**, 68: (5): 1569-1576.

Furuse, M., Nagase, Y., Tsubouchi, H., et al. (1998) Distinct roles of two separable in vitro activities of yeast Mre11 in mitotic and meiotic recombination. **EMBO J**, 17: (21): 6412-6425.

Furuya, M., Tanaka, M., Teranishi, T., et al. (2007) H1foo is indispensable for meiotic maturation of the mouse oocyte. **J Reprod Dev**, 53: (4): 895-902.

Game, J.C. and Mortimer, R.K. (1974) A genetic study of x-ray sensitive mutants in yeast. **Mutat Res**, 24: (3): 281-292.

Garcia, B.A., Busby, S.A., Barber, C.M., et al. (2004) Characterization of phosphorylation sites on histone H1 isoforms by tandem mass spectrometry. **J Proteome Res**, 3: (6): 1219-1227.

Gautier, T., Abbott, D.W., Molla, A., et al. (2004) Histone variant H2ABbd confers lower stability to the nucleosome. **EMBO Rep**, 5: (7): 715-720.

Gell, D. and Jackson, S.P. (1999) Mapping of protein-protein interactions within the DNA-dependent protein kinase complex. **Nucleic Acids Res**, 27: (17): 3494-3502.

Girard, P.M., Kysela, B., Harer, C.J., et al. (2004) Analysis of DNA ligase IV mutations found in LIG4 syndrome patients: the impact of two linked polymorphisms. **Hum Mol Genet**, 13: (20): 2369-2376.

Godde, J.S. and Ura, K. (2008) Cracking the enigmatic linker histone code. **J Biochem**, 143: (3): 287-293.

Goetz, J.D., Motycka, T.A., Han, M., et al. (2005) Reduced repair of DNA double-strand breaks by homologous recombination in a DNA ligase I-deficient human cell line. **DNA Repair (Amst)**, 4: (6): 649-654.

Goldberg, M., Stucki, M., Falck, J., et al. (2003) MDC1 is required for the intra-S-phase DNA damage checkpoint. **Nature**, 421: (6926): 952-956.

Goodarzi, A.A., Yu, Y., Riballo, E., et al. (2006) DNA-PK autophosphorylation facilitates Artemis endonuclease activity. **EMBO J**, 25: (16): 3880-3889.

Gottlieb, T.M. and Jackson, S.P. (1993) The DNA-dependent protein kinase: requirement for DNA ends and association with Ku antigen. **Cell**, 72: (1): 131-142.

Goytisolo, F.A., Gerchman, S.E., Yu, X., et al. (1996) Identification of two DNA-binding sites on the globular domain of histone H5. **EMBO J**, 15: (13): 3421-3429.

Grawunder, U., Wilm, M., Wu, X., et al. (1997) Activity of DNA ligase IV stimulated by complex formation with XRCC4 protein in mammalian cells. **Nature**, 388: (6641): 492-495.

Grawunder, U., Zimmer, D., Kulesza, P., et al. (1998) Requirement for an interaction of XRCC4 with DNA ligase IV for wild-type V(D)J recombination and DNA double-strand break repair in vivo. **J Biol Chem**, 273: (38): 24708-24714.

Green, G.R., Lee, H.J. and Poccia, D.L. (1993) Phosphorylation weakens DNA binding by peptides containing multiple "SPKK" sequences. **J Biol Chem**, 268: (15): 11247-11255.

Griffith, A.J., Blier, P.R., Mimori, T., et al. (1992) Ku polypeptides synthesized in vitro assemble into complexes which recognize ends of double-stranded DNA. **J Biol Chem**, 267: (1): 331-338.

Gu, J., Lu, H., Tippin, B., et al. (2007a) XRCC4:DNA ligase IV can ligate incompatible DNA ends and can ligate across gaps. **EMBO J**, 26: (4): 1010-1023.

Gu, J., Lu, H., Tsai, A.G., et al. (2007b) Single-stranded DNA ligation and XLF-stimulated incompatible DNA end ligation by the XRCC4-DNA ligase IV complex: influence of terminal DNA sequence. **Nucleic Acids Res**, 35: (17): 5755-5762.

Gu, Y., Rosenblatt, J. and Morgan, D.O. (1992) Cell cycle regulation of CDK2 activity by phosphorylation of Thr160 and Tyr15. **EMBO J**, 11: (11): 3995-4005.

Gu, Y., Turck, C.W. and Morgan, D.O. (1993) Inhibition of CDK2 activity in vivo by an associated 20K regulatory subunit. **Nature**, 366: (6456): 707-710.

Gurley, L.R., Valdez, J.G. and Buchanan, J.S. (1995) Characterization of the mitotic specific phosphorylation site of histone H1. Absence of a consensus sequence for the p34cdc2/cyclin B kinase. **J Biol Chem**, 270: (46): 27653-27660.

Hacques, M.F., Muller, S., De Murcia, G., et al. (1990) Use of an immobilized enzyme and specific antibodies to analyse the accessibility and role of histone tails in chromatin structure. **Biochem Biophys Res Commun**, 168: (2): 637-643.

Hakem, R., Hakem, A., Duncan, G.S., et al. (1998) Differential requirement for caspase 9 in apoptotic pathways in vivo. **Cell**, 94: (3): 339-352.

Hanakahi, L.A., Bu, Z. and Maizels, N. (2000) The C-terminal domain of nucleolin accelerates nucleic acid annealing. **Biochemistry**, 39: (50): 15493-15499.

Happel, N., Schulze, E. and Doenecke, D. (2005) Characterisation of human histone H1x. **Biol Chem**, 386: (6): 541-551.

Happel, N., Stoldt, S., Schmidt, B., et al. (2009) M phase-specific phosphorylation of histone H1.5 at threonine 10 by GSK-3. **J Mol Biol**, 386: (2): 339-350.

Harper, J.W., Adami, G.R., Wei, N., et al. (1993) The p21 Cdk-interacting protein Cip1 is a potent inhibitor of G1 cyclin-dependent kinases. **Cell**, 75: (4): 805-816.

Hartley, K.O., Gell, D., Smith, G.C., et al. (1995) DNA-dependent protein kinase catalytic subunit: a relative of phosphatidylinositol 3-kinase and the ataxia telangiectasia gene product. **Cell**, 82: (5): 849-856.

Hartman, P.G., Chapman, G.E., Moss, T., et al. (1977) Studies on the role and mode of operation of the very-lysine-rich histone H1 in eukaryote chromatin. The three structural regions of the histone H1 molecule. **Eur J Biochem**, 77: (1): 45-51.

Hashimoto, H., Sonoda, E., Takami, Y., et al. (2007) Histone H1 variant, H1R is involved in DNA damage response. **DNA Repair (Amst)**, 6: (11): 1584-1595.

Hefferin, M.L. and Tomkinson, A.E. (2005) Mechanism of DNA double-strand break repair by non-homologous end joining. **DNA Repair (Amst)**, 4: (6): 639-648.

Hellauer, K., Sirard, E. and Turcotte, B. (2001) Decreased expression of specific genes in yeast cells lacking histone H1. **J Biol Chem**, 276: (17): 13587-13592.

Hendzel, M.J., Lever, M.A., Crawford, E., et al. (2004) The C-terminal domain is the primary determinant of histone H1 binding to chromatin in vivo. **J Biol Chem**, 279: (19): 20028-20034.

Hofmann, K. and Bucher, P. (1995) The FHA domain: a putative nuclear signalling domain found in protein kinases and transcription factors. **Trends Biochem Sci**, 20: (9): 347-349.

Holliday, R. (1964) A mechanism for gene conversion in fungi. **Genetics Research**, 5: (02): 282-304.

Hopfner, K.P., Craig, L., Moncalian, G., et al. (2002) The Rad50 zinc-hook is a structure joining Mre11 complexes in DNA recombination and repair. **Nature**, 418: (6897): 562-566.

Hopfner, K.P., Karcher, A., Craig, L., et al. (2001) Structural biochemistry and interaction architecture of the DNA double-strand break repair Mre11 nuclease and Rad50-ATPase. **Cell**, 105: (4): 473-485.

Hovanessian, A.G., Puvion-Dutilleul, F., Nisole, S., et al. (2000) The cell-surface-expressed nucleolin is associated with the actin cytoskeleton. **Exp Cell Res**, 261: (2): 312-328.

Hsu, H.L., Yannone, S.M. and Chen, D.J. (2002) Defining interactions between DNA-PK and ligase IV/XRCC4. **DNA Repair (Amst)**, 1: (3): 225-235.

Huen, M.S., Grant, R., Manke, I., et al. (2007) RNF8 transduces the DNA-damage signal via histone ubiquitylation and checkpoint protein assembly. **Cell**, 131: (5): 901-914.

Inoue, T., Geyer, R.K., Howard, D., et al. (2001) MDM2 can promote the ubiquitination, nuclear export, and degradation of p53 in the absence of direct binding. **J Biol Chem**, 276: (48): 45255-45260.

Ip, S.C., Rass, U., Blanco, M.G., et al. (2008) Identification of Holliday junction resolvases from humans and yeast. **Nature**, 456: (7220): 357-361.

Irvin, B.J., Wood, L.D., Wang, L., et al. (2003) TEL, a putative tumor suppressor, induces apoptosis and represses transcription of Bcl-XL. **J Biol Chem**, 278: (47): 46378-46386.

Iwabuchi, K., Bartel, P.L., Li, B., et al. (1994) Two cellular proteins that bind to wild-type but not mutant p53. **Proc Natl Acad Sci U S A**, 91: (13): 6098-6102.

Jedrusik, M.A. and Schulze, E. (2001) A single histone H1 isoform (H1.1) is essential for chromatin silencing and germline development in Caenorhabditis elegans. **Development**, 128: (7): 1069-1080.

Johmann, C.A. and Gorovsky, M.A. (1976) Purification and characterization of the histones associated with the macronucleus of Tetrahymena. **Biochemistry**, 15: (6): 1249-1256.

Jungmichel, S. and Stucki, M. (2010) MDC1: The art of keeping things in focus. **Chromosoma**.

Kastan, M.B., Onyekwere, O., Sidransky, D., et al. (1991) Participation of p53 protein in the cellular response to DNA damage. **Cancer Res**, 51: (23 Pt 1): 6304-6311.

Kastan, M.B., Zhan, Q., el-Deiry, W.S., et al. (1992) A mammalian cell cycle checkpoint pathway utilizing p53 and GADD45 is defective in ataxia-telangiectasia. **Cell**, 71: (4): 587-597.

Keogh, M.C., Kim, J.A., Downey, M., et al. (2006) A phosphatase complex that dephosphorylates gammaH2AX regulates DNA damage checkpoint recovery. **Nature**, 439: (7075): 497-501.

Kim, H., Chen, J. and Yu, X. (2007a) Ubiquitin-binding protein RAP80 mediates BRCA1-dependent DNA damage response. **Science**, 316: (5828): 1202-1205.

Kim, H., Huang, J. and Chen, J. (2007b) CCDC98 is a BRCA1-BRCT domain-binding protein involved in the DNA damage response. **Nat Struct Mol Biol**, 14: (8): 710-715.

Kim, S.T., Lim, D.S., Canman, C.E., et al. (1999) Substrate specificities and identification of putative substrates of ATM kinase family members. **J Biol Chem**, 274: (53): 37538-37543.

Kim, S.T., Xu, B. and Kastan, M.B. (2002) Involvement of the cohesin protein, Smc1, in Atm-dependent and independent responses to DNA damage. **Genes Dev**, 16: (5): 560-570.

Kim, Y.C., Gerlitz, G., Furusawa, T., et al. (2009) Activation of ATM depends on chromatin interactions occurring before induction of DNA damage. **Nat Cell Biol**, 11: (1): 92-96.

Kluck, R.M., Bossy-Wetzel, E., Green, D.R., et al. (1997) The release of cytochrome c from mitochondria: a primary site for Bcl-2 regulation of apoptosis. **Science**, 275: (5303): 1132-1136.

Kobayashi, J., Tauchi, H., Sakamoto, S., et al. (2002) NBS1 localizes to gamma-H2AX foci through interaction with the FHA/BRCT domain. **Curr Biol**, 12: (21): 1846-1851.

Kolas, N.K., Chapman, J.R., Nakada, S., et al. (2007) Orchestration of the DNA-damage response by the RNF8 ubiquitin ligase. **Science**, 318: (5856): 1637-1640.

Konig, K. and Baisch, H. (1980) DNA synthesis and cell cycle progression of synchronized L-cells after irradiation in various phases of the cell cycle. **Radiat Environ Biophys**, 18: (4): 257-266.

Konishi, A., Shimizu, S., Hirota, J., et al. (2003) Involvement of histone H1.2 in apoptosis induced by DNA double-strand breaks. **Cell**, 114: (6): 673-688.

Kornberg, R.D. and Thomas, J.O. (1974) Chromatin structure; oligomers of the histones. **Science**, 184: (139): 865-868.

Kratzmeier, M., Albig, W., Meergans, T., et al. (1999) Changes in the protein pattern of H1 histones associated with apoptotic DNA fragmentation. **Biochem J**, 337 (Pt 2): 319-327.

Kuida, K., Haydar, T.F., Kuan, C.Y., et al. (1998) Reduced apoptosis and cytochrome c-mediated caspase activation in mice lacking caspase 9. **Cell**, 94: (3): 325-337.

Kurimasa, A., Kumano, S., Boubnov, N.V., et al. (1999) Requirement for the kinase activity of human DNA-dependent protein kinase catalytic subunit in DNA strand break rejoining. **Mol Cell Biol**, 19: (5): 3877-3884.

Kusch, T., Florens, L., Macdonald, W.H., et al. (2004) Acetylation by Tip60 is required for selective histone variant exchange at DNA lesions. **Science**, 306: (5704): 2084-2087.

Kysela, B., Chovanec, M. and Jeggo, P.A. (2005) Phosphorylation of linker histones by DNA-dependent protein kinase is required for DNA ligase IV-dependent ligation in the presence of histone H1. **Proc Natl Acad Sci U S A**, 102: (6): 1877-1882.

Kysela, B., Doherty, A.J., Chovanec, M., et al. (2003) Ku stimulation of DNA ligase IV-dependent ligation requires inward movement along the DNA molecule. **J Biol Chem**, 278: (25): 22466-22474.

Lai, J.S. and Herr, W. (1992) Ethidium bromide provides a simple tool for identifying genuine DNA-independent protein associations. **Proc Natl Acad Sci U S A**, 89: (15): 6958-6962.

Landsman, D. (1996) Histone H1 in Saccharomyces cerevisiae: a double mystery solved? **Trends Biochem Sci**, 21: (8): 287-288.

Lapeyre, B., Bourbon, H. and Amalric, F. (1987) Nucleolin, the major nucleolar protein of growing eukaryotic cells: an unusual protein structure revealed by the nucleotide sequence. **Proc Natl Acad Sci U S A**, 84: (6): 1472-1476.

Lee, J.H. and Paull, T.T. (2005) ATM activation by DNA double-strand breaks through the Mre11-Rad50-Nbs1 complex. **Science**, 308: (5721): 551-554.

Lee, M.S., Edwards, R.A., Thede, G.L., et al. (2005) Structure of the BRCT repeat domain of MDC1 and its specificity for the free COOH-terminal end of the gamma-H2AX histone tail. **J Biol Chem**, 280: (37): 32053-32056.

Lee, S.E., Pellicioli, A., Malkova, A., et al. (2001) The Saccharomyces recombination protein Tid1p is required for adaptation from G2/M arrest induced by a double-strand break. **Curr Biol**, 11: (13): 1053-1057.

Lees-Miller, S.P., Sakaguchi, K., Ullrich, S.J., et al. (1992) Human DNA-activated protein kinase phosphorylates serines 15 and 37 in the amino-terminal transactivation domain of human p53. **Mol Cell Biol**, 12: (11): 5041-5049.

Lever, M.A., Th'ng, J.P., Sun, X., et al. (2000) Rapid exchange of histone H1.1 on chromatin in living human cells. **Nature**, 408: (6814): 873-876.

Li, A., Yu, Y., Lee, S.C., et al. (2010) Phosphorylation of histone H2A.X by DNA-dependent Protein Kinase (DNA-PK) is not affected by core histone acetylation but it alters nucleosome stability and histone H1 binding. **J Biol Chem**.

Li, G.M. (2008) Mechanisms and functions of DNA mismatch repair. **Cell Res**, 18: (1): 85-98.

Li, Z., Otevrel, T., Gao, Y., et al. (1995) The XRCC4 gene encodes a novel protein involved in DNA double-strand break repair and V(D)J recombination. **Cell**, 83: (7): 1079-1089.

Lieber, M.R. (1999) The biochemistry and biological significance of nonhomologous DNA end joining: an essential repair process in multicellular eukaryotes. **Genes Cells**, 4: (2): 77-85.

Lim, D.S., Kim, S.T., Xu, B., et al. (2000) ATM phosphorylates p95/nbs1 in an S-phase checkpoint pathway. **Nature**, 404: (6778): 613-617.

Lin, Q., Inselman, A., Han, X., et al. (2004) Reductions in linker histone levels are tolerated in developing spermatocytes but cause changes in specific gene expression. **J Biol Chem**, 279: (22): 23525-23535.

Lindner, H.H. (2008) Analysis of histones, histone variants, and their post-translationally modified forms. **Electrophoresis**, 29: (12): 2516-2532.

Liu, Q., Guntuku, S., Cui, X.S., et al. (2000) Chk1 is an essential kinase that is regulated by Atr and required for the G(2)/M DNA damage checkpoint. **Genes Dev**, 14: (12): 1448-1459.

Liu, X., Li, B. and GorovskyMa (1996) Essential and nonessential histone H2A variants in Tetrahymena thermophila. **Mol Cell Biol**, 16: (8): 4305-4311.

Liu, Z., Wu, J. and Yu, X. (2007) CCDC98 targets BRCA1 to DNA damage sites. **Nat Struct Mol Biol**, 14: (8): 716-720.

Lodish, H., Berk, A., Kaiser, C., et al. (2007) **Molecular Cell Biology (Lodish, Molecular Cell Biology)**. W. H. Freeman.

Longhese, M.P., Plevani, P. and Lucchini, G. (1994) Replication factor A is required in vivo for DNA replication, repair, and recombination. **Mol Cell Biol**, 14: (12): 7884-7890.

Lou, Z., Minter-Dykhouse, K., Franco, S., et al. (2006) MDC1 maintains genomic stability by participating in the amplification of ATM-dependent DNA damage signals. **Mol Cell**, 21: (2): 187-200.

Luger, K., Mader, A.W., Richmond, R.K., et al. (1997) Crystal structure of the nucleosome core particle at 2.8 A resolution. **Nature**, 389: (6648): 251-260.

Luger, K. and Richmond, T.J. (1998) The histone tails of the nucleosome. **Curr Opin Genet Dev**, 8: (2): 140-146.

Ma, Y., Pannicke, U., Lu, H., et al. (2005) The DNA-dependent protein kinase catalytic subunit phosphorylation sites in human Artemis. **J Biol Chem**, 280: (40): 33839-33846.

Ma, Y., Pannicke, U., Schwarz, K., et al. (2002) Hairpin opening and overhang processing by an Artemis/DNA-dependent protein kinase complex in nonhomologous end joining and V(D)J recombination. **Cell**, 108: (6): 781-794.

Mailand, N., Bekker-Jensen, S., Faustrup, H., et al. (2007) RNF8 ubiquitylates histones at DNA double-strand breaks and promotes assembly of repair proteins. **Cell**, 131: (5): 887-900.

Mari, P.O., Florea, B.I., Persengiev, S.P., et al. (2006) Dynamic assembly of end-joining complexes requires interaction between Ku70/80 and XRCC4. **Proc Natl Acad Sci U S A**, 103: (49): 18597-18602.

Martianov, I., Brancorsini, S., Catena, R., et al. (2005) Polar nuclear localization of H1T2, a histone H1 variant, required for spermatid elongation and DNA condensation during spermiogenesis. **Proc Natl Acad Sci U S A**, 102: (8): 2808-2813.

Matsuoka, S., Huang, M. and Elledge, S.J. (1998) Linkage of ATM to cell cycle regulation by the Chk2 protein kinase. **Science**, 282: (5395): 1893-1897.

Matsuoka, S., Rotman, G., Ogawa, A., et al. (2000) Ataxia telangiectasia-mutated phosphorylates Chk2 in vivo and in vitro. **Proc Natl Acad Sci U S A**, 97: (19): 10389-10394.

Maya, R., Balass, M., Kim, S.T., et al. (2001) ATM-dependent phosphorylation of Mdm2 on serine 395: role in p53 activation by DNA damage. **Genes Dev**, 15: (9): 1067-1077.

Mayo, L.D., Turchi, J.J. and Berberich, S.J. (1997) Mdm-2 phosphorylation by DNA-dependent protein kinase prevents interaction with p53. **Cancer Res**, 57: (22): 5013-5016.

McBryant, S.J., Lu, X. and Hansen, J.C. (2010) Multifunctionality of the linker histones: an emerging role for protein-protein interactions. **Cell Res**, 20: (5): 519-528.

McNamee, L.M. and Brodsky, M.H. (2009) p53-independent apoptosis limits DNA damage-induced aneuploidy. **Genetics**, 182: (2): 423-435.

Meek, K., Douglas, P., Cui, X., et al. (2007) trans Autophosphorylation at DNA-dependent protein kinase's two major autophosphorylation site clusters facilitates end processing but not end joining. **Mol Cell Biol**, 27: (10): 3881-3890.

Meek, K., Gupta, S., Ramsden, D.A., et al. (2004) The DNA-dependent protein kinase: the director at the end. **Immunol Rev**, 200: 132-141.

Melander, F., Bekker-Jensen, S., Falck, J., et al. (2008) Phosphorylation of SDT repeats in the MDC1 N terminus triggers retention of NBS1 at the DNA damage-modified chromatin. **J Cell Biol**, 181: (2): 213-226.

Melino, G., Bernassola, F., Ranalli, M., et al. (2004) p73 Induces apoptosis via PUMA transactivation and Bax mitochondrial translocation. **J Biol Chem**, 279: (9): 8076-8083.

Mendez-Acuna, L., Di Tomaso, M.V., Palitti, F., et al. (2010) Histone post-translational modifications in DNA damage response. **Cytogenet Genome Res**, 128: (1-3): 28-36.

Miki, Y., Swensen, J., Shattuck-Eidens, D., et al. (1994) A strong candidate for the breast and ovarian cancer susceptibility gene BRCA1. **Science**, 266: (5182): 66-71.

Mimori, T. and Hardin, J.A. (1986) Mechanism of interaction between Ku protein and DNA. **J Biol Chem**, 261: (22): 10375-10379.

Misteli, T., Gunjan, A., Hock, R., et al. (2000) Dynamic binding of histone H1 to chromatin in living cells. **Nature**, 408: (6814): 877-881.

Miyashita, T., Krajewski, S., Krajewska, M., et al. (1994) Tumor suppressor p53 is a regulator of bcl-2 and bax gene expression in vitro and in vivo. **Oncogene**, 9: (6): 1799-1805.

Miyashita, T. and Reed, J.C. (1995) Tumor suppressor p53 is a direct transcriptional activator of the human bax gene. **Cell**, 80: (2): 293-299.

Modesti, M., Hesse, J.E. and Gellert, M. (1999) DNA binding of Xrcc4 protein is associated with V(D)J recombination but not with stimulation of DNA ligase IV activity. **EMBO J**, 18: (7): 2008-2018.

Moore, S.P., Erdile, L., Kelly, T., et al. (1991) The human homologous pairing protein HPP-1 is specifically stimulated by the cognate single-stranded binding protein hRP-A. **Proc Natl Acad Sci U S A**, 88: (20): 9067-9071.

Morrison, A.J., Highland, J., Krogan, N.J., et al. (2004) INO80 and gamma-H2AX interaction links ATP-dependent chromatin remodeling to DNA damage repair. **Cell**, 119: (6): 767-775.

Moshous, D., Callebaut, I., de Chasseval, R., et al. (2001) Artemis, a novel DNA double-strand break repair/V(D)J recombination protein, is mutated in human severe combined immune deficiency. **Cell**, 105: (2): 177-186.

Moshous, D., Li, L., Chasseval, R., et al. (2000) A new gene involved in DNA double-strand break repair and V(D)J recombination is located on human chromosome 10p. **Hum Mol Genet**, 9: (4): 583-588.

Moynahan, M.E., Chiu, J.W., Koller, B.H., et al. (1999) Brca1 controls homology-directed DNA repair. **Mol Cell**, 4: (4): 511-518.

Moynahan, M.E., Cui, T.Y. and Jasin, M. (2001) Homology-directed dna repair, mitomycin-c resistance, and chromosome stability is restored with correction of a Brca1 mutation. **Cancer Res**, 61: (12): 4842-4850.

Munshi, A., Hobbs, M. and Meyn, R.E. (2005) Clonogenic cell survival assay. **Methods Mol Med**, 110: 21-28.

Murga, M., Jaco, I., Fan, Y., et al. (2007) Global chromatin compaction limits the strength of the DNA damage response. **J Cell Biol**, 178: (7): 1101-1108.

Nakada, S., Chen, G.I., Gingras, A.C., et al. (2008) PP4 is a gamma H2AX phosphatase required for recovery from the DNA damage checkpoint. **EMBO Rep**, 9: (10): 1019-1026.

Nakano, K. and Vousden, K.H. (2001) PUMA, a novel proapoptotic gene, is induced by p53. **Mol Cell**, 7: (3): 683-694.

New, J.H., Sugiyama, T., Zaitseva, E., et al. (1998) Rad52 protein stimulates DNA strand exchange by Rad51 and replication protein A. **Nature**, 391: (6665): 407-410.

Nick McElhinny, S.A., Snowden, C.M., McCarville, J., et al. (2000) Ku recruits the XRCC4-ligase IV complex to DNA ends. **Mol Cell Biol**, 20: (9): 2996-3003.

Noll, M. and Kornberg, R.D. (1977) Action of micrococcal nuclease on chromatin and the location of histone H1. **J Mol Biol**, 109: (3): 393-404.

Ogg, S., Gabrielli, B. and Piwnica-Worms, H. (1994) Purification of a serine kinase that associates with and phosphorylates human Cdc25C on serine 216. **J Biol Chem**, 269: (48): 30461-30469.

Okuwaki, M., Kato, K., Shimahara, H., et al. (2005) Assembly and disassembly of nucleosome core particles containing histone variants by human nucleosome assembly protein I. **Mol Cell Biol**, 25: (23): 10639-10651.

Olins, A.L. and Olins, D.E. (1974) Spheroid chromatin units (v bodies). **Science**, 183: (4122): 330-332.

Olive, P.L., Banath, J.P. and Durand, R.E. (1990) Heterogeneity in radiation-induced DNA damage and repair in tumor and normal cells measured using the "comet" assay. **Radiat Res**, 122: (1): 86-94.

Olson, M.O., Dundr, M. and Szebeni, A. (2000) The nucleolus: an old factory with unexpected capabilities. **Trends Cell Biol**, 10: (5): 189-196.

Orrego, M., Ponte, I., Roque, A., et al. (2007) Differential affinity of mammalian histone H1 somatic subtypes for DNA and chromatin. **BMC Biol**, 5: 22.

Oudet, P., Gross-Bellard, M. and Chambon, P. (1975) Electron microscopic and biochemical evidence that chromatin structure is a repeating unit. **Cell**, 4: (4): 281-300.

Paillard, S. and Strauss, F. (1991) Analysis of the mechanism of interaction of simian Ku protein with DNA. **Nucleic Acids Res**, 19: (20): 5619-5624.

Pandita, T.K. (2003) A multifaceted role for ATM in genome maintenance. **Expert Rev Mol Med**, 5: (16): 1-21.

Panyim, S. and Chalkley, R. (1969) A new histone found only in mammalian tissues with little cell division. **Biochem Biophys Res Commun**, 37: (6): 1042-1049.

Pastwa, E. and Blasiak, J. (2003) Non-homologous DNA end joining. **Acta Biochim Pol**, 50: (4): 891-908.

Patterton, H.G., Landel, C.C., Landsman, D., et al. (1998) The biochemical and phenotypic characterization of Hho1p, the putative linker histone H1 of Saccharomyces cerevisiae. **J Biol Chem**, 273: (13): 7268-7276.

Paull, T.T. and Gellert, M. (1998) The 3' to 5' exonuclease activity of Mre 11 facilitates repair of DNA double-strand breaks. **Mol Cell**, 1: (7): 969-979.

Paull, T.T. and Gellert, M. (1999) Nbs1 potentiates ATP-driven DNA unwinding and endonuclease cleavage by the Mre11/Rad50 complex. **Genes Dev**, 13: (10): 1276-1288.

Paulovich, A.G. and Hartwell, L.H. (1995) A checkpoint regulates the rate of progression through S phase in S. cerevisiae in response to DNA damage. **Cell**, 82: (5): 841-847.

Peng, C.Y., Graves, P.R., Thoma, R.S., et al. (1997) Mitotic and G2 checkpoint control: regulation of 14-3-3 protein binding by phosphorylation of Cdc25C on serine-216. **Science**, 277: (5331): 1501-1505.

Perrault, R., Wang, H., Wang, M., et al. (2004) Backup pathways of NHEJ are suppressed by DNA-PK. **J Cell Biochem**, 92: (4): 781-794.

Petukhova, G., Stratton, S. and Sung, P. (1998) Catalysis of homologous DNA pairing by yeast Rad51 and Rad54 proteins. **Nature**, 393: (6680): 91-94.

Phair, R.D., Scaffidi, P., Elbi, C., et al. (2004) Global nature of dynamic protein-chromatin interactions in vivo: three-dimensional genome scanning and dynamic interaction networks of chromatin proteins. **Mol Cell Biol**, 24: (14): 6393-6402.

Polanowska, J., Martin, J.S., Garcia-Muse, T., et al. (2006) A conserved pathway to activate BRCA1-dependent ubiquitylation at DNA damage sites. **EMBO J**, 25: (10): 2178-2188.

Poltoratsky, V.P., Shi, X., York, J.D., et al. (1995) Human DNA-activated protein kinase (DNA-PK) is homologous to phosphatidylinositol kinases. **J Immunol**, 155: (10): 4529-4533.

Pradeepa, M.M. and Rao, M.R. (2007) Chromatin remodeling during mammalian spermatogenesis: role of testis specific histone variants and transition proteins. **Soc Reprod Fertil Suppl**, 63: 1-10.

Prolla, T.A., Baker, S.M., Harris, A.C., et al. (1998) Tumour susceptibility and spontaneous mutation in mice deficient in Mlh1, Pms1 and Pms2 DNA mismatch repair. **Nat Genet**, 18: (3): 276-279.

Ramakrishnan, V., Finch, J.T., Graziano, V., et al. (1993) Crystal structure of globular domain of histone H5 and its implications for nucleosome binding. **Nature**, 362: (6417): 219-223.

Ransom, M., Dennehey, B.K. and Tyler, J.K. (2010) Chaperoning histones during DNA replication and repair. **Cell**, 140: (2): 183-195.

Raynard, S., Bussen, W. and Sung, P. (2006) A double Holliday junction dissolvasome comprising BLM, topoisomerase IIIalpha, and BLAP75. **J Biol Chem**, 281: (20): 13861-13864.

Riballo, E., Doherty, A.J., Dai, Y., et al. (2001) Cellular and biochemical impact of a mutation in DNA ligase IV conferring clinical radiosensitivity. **J Biol Chem**, 276: (33): 31124-31132.

Robertson, A.B., Klungland, A., Rognes, T., et al. (2009) DNA repair in mammalian cells: Base excision repair: the long and short of it. **Cell Mol Life Sci**, 66: (6): 981-993.

Robinson, P.J. and Rhodes, D. (2006) Structure of the '30 nm' chromatin fibre: a key role for the linker histone. **Curr Opin Struct Biol**, 16: (3): 336-343.

Rogakou, E.P., Pilch, D.R., Orr, A.H., et al. (1998) DNA double-stranded breaks induce histone H2AX phosphorylation on serine 139. **J Biol Chem**, 273: (10): 5858-5868.

Rooney, S., Alt, F.W., Lombard, D., et al. (2003) Defective DNA repair and increased genomic instability in Artemis-deficient murine cells. **J Exp Med**, 197: (5): 553-565.

Roque, A., Ponte, I., Arrondo, J.L., et al. (2008) Phosphorylation of the carboxy-terminal domain of histone H1: effects on secondary structure and DNA condensation. **Nucleic Acids Res**, 36: (14): 4719-4726.

Rosidi, B., Wang, M., Wu, W., et al. (2008) Histone H1 functions as a stimulatory factor in backup pathways of NHEJ. **Nucleic Acids Res**, 36: (5): 1610-1623.

Rupnik, A., Lowndes, N.F. and Grenon, M. (2010) MRN and the race to the break. **Chromosoma**, 119: (2): 115-135.

Ruthenburg, A.J., Li, H., Patel, D.J., et al. (2007) Multivalent engagement of chromatin modifications by linked binding modules. **Nat Rev Mol Cell Biol**, 8: (12): 983-994.

Sanchez, Y., Wong, C., Thoma, R.S., et al. (1997) Conservation of the Chk1 checkpoint pathway in mammals: linkage of DNA damage to Cdk regulation through Cdc25. **Science**, 277: (5331): 1497-1501.

Sancho, M., Diani, E., Beato, M., et al. (2008) Depletion of human histone H1 variants uncovers specific roles in gene expression and cell growth. **PLoS Genet**, 4: (10): e1000227.

Sarg, B., Helliger, W., Talasz, H., et al. (2006) Histone H1 phosphorylation occurs site-specifically during interphase and mitosis: identification of a novel phosphorylation site on histone H1. **J Biol Chem**, 281: (10): 6573-6580.

Sartori, A.A., Lukas, C., Coates, J., et al. (2007) Human CtIP promotes DNA end resection. **Nature**, 450: (7169): 509-514.

Savitsky, K., Bar-Shira, A., Gilad, S., et al. (1995) A single ataxia telangiectasia gene with a product similar to PI-3 kinase. **Science**, 268: (5218): 1749-1753.

Sawada, M., Sun, W., Hayes, P., et al. (2003) Ku70 suppresses the apoptotic translocation of Bax to mitochondria. **Nat Cell Biol**, 5: (4): 320-329.

Schalch, T., Duda, S., Sargent, D.F., et al. (2005) X-ray structure of a tetranucleosome and its implications for the chromatin fibre. **Nature**, 436: (7047): 138-141.

Schultz, L.B., Chehab, N.H., Malikzay, A., et al. (2000) p53 binding protein 1 (53BP1) is an early participant in the cellular response to DNA double-strand breaks. **J Cell Biol**, 151: (7): 1381-1390.

Scully, R., Chen, J., Ochs, R.L., et al. (1997a) Dynamic changes of BRCA1 subnuclear location and phosphorylation state are initiated by DNA damage. **Cell**, 90: (3): 425-435.

Scully, R., Chen, J., Plug, A., et al. (1997b) Association of BRCA1 with Rad51 in mitotic and meiotic cells. **Cell**, 88: (2): 265-275.

Scully, R., Ganesan, S., Vlasakova, K., et al. (1999) Genetic analysis of BRCA1 function in a defined tumor cell line. **Mol Cell**, 4: (6): 1093-1099.

Semizarov, D., Frost, L., Sarthy, A., et al. (2003) Specificity of short interfering RNA determined through gene expression signatures. **Proc Natl Acad Sci U S A**, 100: (11): 6347-6352.

Shang, Y.L., Bodero, A.J. and Chen, P.L. (2003) NFBD1, a novel nuclear protein with signature motifs of FHA and BRCT, and an internal 41-amino acid repeat sequence, is an early participant in DNA damage response. **J Biol Chem**, 278: (8): 6323-6329.

Shao, G., Patterson-Fortin, J., Messick, T.E., et al. (2009) MERIT40 controls BRCA1-Rap80 complex integrity and recruitment to DNA double-strand breaks. **Genes Dev**, 23: (6): 740-754.

Sharples, G.J. and Leach, D.R. (1995) Structural and functional similarities between the SbcCD proteins of Escherichia coli and the RAD50 and MRE11 (RAD32) recombination and repair proteins of yeast. **Mol Microbiol**, 17: (6): 1215-1217.

Shen, X., Yu, L., Weir, J.W., et al. (1995) Linker histones are not essential and affect chromatin condensation in vivo. **Cell**, 82: (1): 47-56.

Shieh, S.Y., Ikeda, M., Taya, Y., et al. (1997) DNA damage-induced phosphorylation of p53 alleviates inhibition by MDM2. **Cell**, 91: (3): 325-334.

Shinohara, A., Ogawa, H. and Ogawa, T. (1992) Rad51 protein involved in repair and recombination in S. cerevisiae is a RecA-like protein. **Cell**, 69: (3): 457-470.

Shinohara, A. and Ogawa, T. (1998) Stimulation by Rad52 of yeast Rad51-mediated recombination. **Nature**, 391: (6665): 404-407.

Shivji, M.K., Davies, O.R., Savill, J.M., et al. (2006) A region of human BRCA2 containing multiple BRC repeats promotes RAD51-mediated strand exchange. **Nucleic Acids Res**, 34: (14): 4000-4011.

Shogren-Knaak, M., Ishii, H., Sun, J.M., et al. (2006) Histone H4-K16 acetylation controls chromatin structure and protein interactions. **Science**, 311: (5762): 844-847.

Shuck, S.C., Short, E.A. and Turchi, J.J. (2008) Eukaryotic nucleotide excision repair: from understanding mechanisms to influencing biology. **Cell Res**, 18: (1): 64-72.

Simpson, R.T. (1978) Structure of the chromatosome, a chromatin particle containing 160 base pairs of DNA and all the histones. **Biochemistry**, 17: (25): 5524-5531.

Singleton, B.K., Torres-Arzayus, M.I., Rottinghaus, S.T., et al. (1999) The C terminus of Ku80 activates the DNA-dependent protein kinase catalytic subunit. **Mol Cell Biol**, 19: (5): 3267-3277.

Sinha, D. and Shogren-Knaak, M.A. (2010) The role of direct interactions between the histone H4 tail and the H2A core in long-range nucleosome contacts. **J Biol Chem**.

Sirotkin, A.M., Edelmann, W., Cheng, G., et al. (1995) Mice develop normally without the H1(0) linker histone. **Proc Natl Acad Sci U S A**, 92: (14): 6434-6438.

Sivolob, A. and Prunell, A. (2003) Linker histone-dependent organization and dynamics of nucleosome entry/exit DNAs. **J Mol Biol**, 331: (5): 1025-1040.

Sobhian, B., Shao, G., Lilli, D.R., et al. (2007) RAP80 targets BRCA1 to specific ubiquitin structures at DNA damage sites. **Science**, 316: (5828): 1198-1202.

Spycher, C., Miller, E.S., Townsend, K., et al. (2008) Constitutive phosphorylation of MDC1 physically links the MRE11-RAD50-NBS1 complex to damaged chromatin. **J Cell Biol**, 181: (2): 227-240.

Stewart, G.S. (2009) Solving the RIDDLE of 53BP1 recruitment to sites of damage. **Cell Cycle**, 8: (10): 1532-1538.

Stewart, G.S., Maser, R.S., Stankovic, T., et al. (1999) The DNA double-strand break repair gene hMRE11 is mutated in individuals with an ataxia-telangiectasia-like disorder. **Cell**, 99: (6): 577-587.

Stewart, G.S., Panier, S., Townsend, K., et al. (2009) The RIDDLE syndrome protein mediates a ubiquitin-dependent signaling cascade at sites of DNA damage. **Cell**, 136: (3): 420-434.

Stewart, G.S., Wang, B., Bignell, C.R., et al. (2003) MDC1 is a mediator of the mammalian DNA damage checkpoint. **Nature**, 421: (6926): 961-966.

Stoldt, S., Wenzel, D., Schulze, E., et al. (2007) G1 phase-dependent nucleolar accumulation of human histone H1x. **Biol Cell**, 99: (10): 541-552.

Stucki, M., Clapperton, J.A., Mohammad, D., et al. (2005) MDC1 directly binds phosphorylated histone H2AX to regulate cellular responses to DNA double-strand breaks. **Cell**, 123: (7): 1213-1226.

Sun, Y., Jiang, X., Chen, S., et al. (2005) A role for the Tip60 histone acetyltransferase in the acetylation and activation of ATM. **Proc Natl Acad Sci U S A**, 102: (37): 13182-13187.

Sun, Y., Jiang, X., Xu, Y., et al. (2009) Histone H3 methylation links DNA damage detection to activation of the tumour suppressor Tip60. **Nat Cell Biol**, 11: (11): 1376-1382.

Suwa, A., Hirakata, M., Takeda, Y., et al. (1994) DNA-dependent protein kinase (Ku protein-p350 complex) assembles on double-stranded DNA. **Proc Natl Acad Sci U S A**, 91: (15): 6904-6908.

Suzuki, H., Kurita, M., Mizumoto, K., et al. (2003) p19ARF-induced p53-independent apoptosis largely occurs through BAX. **Biochem Biophys Res Commun**, 312: (4): 1273-1277.

Sweet, S.M., Creese, A.J. and Cooper, H.J. (2006) Strategy for the identification of sites of phosphorylation in proteins: neutral loss triggered electron capture dissociation. **Anal Chem**, 78: (21): 7563-7569.

Syed, S.H., Goutte-Gattat, D., Becker, N., et al. (2010) Single-base resolution mapping of H1-nucleosome interactions and 3D organization of the nucleosome. **Proc Natl Acad Sci U S A**, 107: (21): 9620-9625.

Taccioli, G.E., Gottlieb, T.M., Blunt, T., et al. (1994) Ku80: product of the XRCC5 gene and its role in DNA repair and V(D)J recombination. **Science**, 265: (5177): 1442-1445.

Takata, H., Matsunaga, S., Morimoto, A., et al. (2007) H1.X with different properties from other linker histones is required for mitotic progression. **FEBS Lett**, 581: (20): 3783-3788.

Talasz, H., Helliger, W., Puschendorf, B., et al. (1996) In vivo phosphorylation of histone H1 variants during the cell cycle. **Biochemistry**, 35: (6): 1761-1767.

Talasz, H., Sapojnikova, N., Helliger, W., et al. (1998) In vitro binding of H1 histone subtypes to nucleosomal organized mouse mammary tumor virus long terminal repeat promotor. **J Biol Chem**, 273: (48): 32236-32243.

Tanaka, M., Hennebold, J.D., Macfarlane, J., et al. (2001) A mammalian oocyte-specific linker histone gene H1oo: homology with the genes for the oocyte-specific cleavage stage histone (cs-H1) of sea urchin and the B4/H1M histone of the frog. **Development**, 128: (5): 655-664.

Taniguchi, T., Garcia-Higuera, I., Xu, B., et al. (2002) Convergence of the fanconi anemia and ataxia telangiectasia signaling pathways. **Cell**, 109: (4): 459-472.

Taylor, A.M., Harnden, D.G., Arlett, C.F., et al. (1975) Ataxia telangiectasia: a human mutation with abnormal radiation sensitivity. **Nature**, 258: (5534): 427-429.

Th'ng, J.P., Guo, X.W., Swank, R.A., et al. (1994) Inhibition of histone phosphorylation by staurosporine leads to chromosome decondensation. **J Biol Chem**, 269: (13): 9568-9573.

Th'ng, J.P., Sung, R., Ye, M., et al. (2005) H1 family histones in the nucleus. Control of binding and localization by the C-terminal domain. **J Biol Chem**, 280: (30): 27809-27814.

Thode, S., Schafer, A., Pfeiffer, P., et al. (1990) A novel pathway of DNA end-to-end joining. **Cell**, 60: (6): 921-928.

Travers, A. (1999) The location of the linker histone on the nucleosome. **Trends Biochem Sci**, 24: (1): 4-7.

Tremethick, D.J. (2007) Higher-order structures of chromatin: the elusive 30 nm fiber. **Cell**, 128: (4): 651-654.

Trujillo, K.M. and Sung, P. (2001) DNA structure-specific nuclease activities in the Saccharomyces cerevisiae Rad50*Mre11 complex. **J Biol Chem**, 276: (38): 35458-35464.

Trujillo, K.M., Yuan, S.S., Lee, E.Y., et al. (1998) Nuclease activities in a complex of human recombination and DNA repair factors Rad50, Mre11, and p95. **J Biol Chem**, 273: (34): 21447-21450.

Tulchin, N., Chambon, M., Juan, G., et al. (2010) BRCA1 protein and nucleolin colocalize in breast carcinoma tissue and cancer cell lines. **Am J Pathol**, 176: (3): 1203-1214.

Turchi, J.J., Henkels, K.M. and Zhou, Y. (2000) Cisplatin-DNA adducts inhibit translocation of the Ku subunits of DNA-PK. **Nucleic Acids Res**, 28: (23): 4634-4641.

Turner, B.M. (2007) Defining an epigenetic code. **Nat Cell Biol**, 9: (1): 2-6.

Uematsu, N., Weterings, E., Yano, K., et al. (2007) Autophosphorylation of DNA-PKCS regulates its dynamics at DNA double-strand breaks. **J Cell Biol**, 177: (2): 219-229.

Unger, T., Juven-Gershon, T., Moallem, E., et al. (1999) Critical role for Ser20 of human p53 in the negative regulation of p53 by Mdm2. **EMBO J**, 18: (7): 1805-1814.

Ushinsky, S.C., Bussey, H., Ahmed, A.A., et al. (1997) Histone H1 in Saccharomyces cerevisiae. **Yeast**, 13: (2): 151-161.

Uziel, T., Lerenthal, Y., Moyal, L., et al. (2003) Requirement of the MRN complex for ATM activation by DNA damage. **EMBO J**, 22: (20): 5612-5621.

Valko, M., Izakovic, M., Mazur, M., et al. (2004) Role of oxygen radicals in DNA damage and cancer incidence. **Mol Cell Biochem**, 266: (1-2): 37-56.

van Attikum, H., Fritsch, O., Hohn, B., et al. (2004) Recruitment of the INO80 complex by H2A phosphorylation links ATP-dependent chromatin remodeling with DNA double-strand break repair. **Cell**, 119: (6): 777-788.

van Attikum, H. and Gasser, S.M. (2005) ATP-dependent chromatin remodeling and DNA double-strand break repair. **Cell Cycle**, 4: (8): 1011-1014.

Vandersickel, V., Mancini, M., Slabbert, J., et al. (2010) The radiosensitizing effect of Ku70/80 knockdown in MCF10A cells irradiated with X-rays and p(66)+Be(40) neutrons. **Radiat Oncol**, 5: 30.

Varon, R., Vissinga, C., Platzer, M., et al. (1998) Nibrin, a novel DNA double-strand break repair protein, is mutated in Nijmegen breakage syndrome. **Cell**, 93: (3): 467-476.

Waldman, T., Kinzler, K.W. and Vogelstein, B. (1995) p21 is necessary for the p53-mediated G1 arrest in human cancer cells. **Cancer Res**, 55: (22): 5187-5190.

Walker, J.E., Saraste, M., Runswick, M.J., et al. (1982) Distantly related sequences in the alpha- and beta-subunits of ATP synthase, myosin, kinases and other ATP-requiring enzymes and a common nucleotide binding fold. **EMBO J**, 1: (8): 945-951.

Walker, J.R., Corpina, R.A. and Goldberg, J. (2001) Structure of the Ku heterodimer bound to DNA and its implications for double-strand break repair. **Nature**, 412: (6847): 607-614.

Walworth, N., Davey, S. and Beach, D. (1993) Fission yeast chk1 protein kinase links the rad checkpoint pathway to cdc2. **Nature**, 363: (6427): 368-371.

Wang, B. and Elledge, S.J. (2007) Ubc13/Rnf8 ubiquitin ligases control foci formation of the Rap80/Abraxas/Brca1/Brcc36 complex in response to DNA damage. **Proc Natl Acad Sci U S A**, 104: (52): 20759-20763.

Wang, B., Matsuoka, S., Ballif, B.A., et al. (2007) Abraxas and RAP80 form a BRCA1 protein complex required for the DNA damage response. **Science**, 316: (5828): 1194-1198.

Wang, B., Matsuoka, S., Carpenter, P.B., et al. (2002) 53BP1, a mediator of the DNA damage checkpoint. **Science**, 298: (5597): 1435-1438.

Wang, H., Rosidi, B., Perrault, R., et al. (2005a) DNA ligase III as a candidate component of backup pathways of nonhomologous end joining. **Cancer Res**, 65: (10): 4020-4030.

Wang, H., Zeng, Z.C., Bui, T.A., et al. (2001) Nonhomologous end-joining of ionizing radiation-induced DNA double-stranded breaks in human tumor cells deficient in BRCA1 or BRCA2. **Cancer Res**, 61: (1): 270-277.

Wang, J., Pluth, J.M., Cooper, P.K., et al. (2005b) Artemis deficiency confers a DNA double-strand break repair defect and Artemis phosphorylation status is altered by DNA damage and cell cycle progression. **DNA Repair (Amst)**, 4: (5): 556-570.

Ward, J.D., Muzzini, D.M., Petalcorin, M.I., et al. (2010) Overlapping mechanisms promote postsynaptic RAD-51 filament disassembly during meiotic double-strand break repair. **Mol Cell**, 37: (2): 259-272.

Warneboldt, J., Haller, F., Horstmann, O., et al. (2008) Histone H1x is highly expressed in human neuroendocrine cells and tumours. **BMC Cancer**, 8: 388.

West, M.H. and Bonner, W.M. (1980) Histone 2A, a heteromorphous family of eight protein species. **Biochemistry**, 19: (14): 3238-3245.

Whitaker, S.J. and McMillan, T.J. (1992) Pulsed-field gel electrophoresis in the measurement of DNA double-strand break repair in xrs-6 and CHO cell lines: DNA degradation under some conditions interferes with the assessment of double-strand break rejoining. **Radiat Res**, 130: (3): 389-392.

Williams, R.S., Moncalian, G., Williams, J.S., et al. (2008) Mre11 dimers coordinate DNA end bridging and nuclease processing in double-strand-break repair. **Cell**, 135: (1): 97-109.

Williams, S.P., Athey, B.D., Muglia, L.J., et al. (1986) Chromatin fibers are left-handed double helices with diameter and mass per unit length that depend on linker length. **Biophys J**, 49: (1): 233-248.

Wilson, T.E., Grawunder, U. and Lieber, M.R. (1997) Yeast DNA ligase IV mediates non-homologous DNA end joining. **Nature**, 388: (6641): 495-498.

Wisniewski, J.R., Zougman, A., Kruger, S., et al. (2007) Mass spectrometric mapping of linker histone H1 variants reveals multiple acetylations, methylations, and phosphorylation as well as differences between cell culture and tissue. **Mol Cell Proteomics**, 6: (1): 72-87.

Woodcock, C.L., Frado, L.L. and Rattner, J.B. (1984) The higher-order structure of chromatin: evidence for a helical ribbon arrangement. **J Cell Biol**, 99: (1 Pt 1): 42-52.

Wu, L., Bachrati, C.Z., Ou, J., et al. (2006) BLAP75/RMI1 promotes the BLM-dependent dissolution of homologous recombination intermediates. **Proc Natl Acad Sci U S A**, 103: (11): 4068-4073.

Wu, L. and Hickson, I.D. (2003) The Bloom's syndrome helicase suppresses crossing over during homologous recombination. **Nature**, 426: (6968): 870-874.

Wu, X., Petrini, J.H., Heine, W.F., et al. (2000a) Independence of R/M/N focus formation and the presence of intact BRCA1. **Science**, 289: (5476): 11.

Wu, X., Ranganathan, V., Weisman, D.S., et al. (2000b) ATM phosphorylation of Nijmegen breakage syndrome protein is required in a DNA damage response. **Nature**, 405: (6785): 477-482.

Xu, B., Kim, S. and Kastan, M.B. (2001) Involvement of Brca1 in S-phase and G(2)-phase checkpoints after ionizing irradiation. **Mol Cell Biol**, 21: (10): 3445-3450.

Xu, B., O'Donnell, A.H., Kim, S.T., et al. (2002) Phosphorylation of serine 1387 in Brca1 is specifically required for the Atm-mediated S-phase checkpoint after ionizing irradiation. **Cancer Res**, 62: (16): 4588-4591.

Yajima, H., Lee, K.J. and Chen, B.P. (2006) ATR-dependent phosphorylation of DNA-dependent protein kinase catalytic subunit in response to UV-induced replication stress. **Mol Cell Biol**, 26: (20): 7520-7528.

Yamamoto, T. and Horikoshi, M. (1996) Cloning of the cDNA encoding a novel subtype of histone H1. **Gene**, 173: (2): 281-285.

Yamanaka, S., Katayama, E., Yoshioka, K., et al. (2002) Nucleosome linker proteins HMGB1 and histone H1 differentially enhance DNA ligation reactions. **Biochem Biophys Res Commun**, 292: (1): 268-273.

Yan, J., Yang, X.P., Kim, Y.S., et al. (2008) RAP80 responds to DNA damage induced by both ionizing radiation and UV irradiation and is phosphorylated at Ser 205. **Cancer Res**, 68: (11): 4269-4276.

Yan, W., Ma, L., Burns, K.H., et al. (2003) HILS1 is a spermatid-specific linker histone H1-like protein implicated in chromatin remodeling during mammalian spermiogenesis. **Proc Natl Acad Sci U S A**, 100: (18): 10546-10551.

Yang, C., Kim, M.S., Chakravarty, D., et al. (2009) Nucleolin Binds to the Proliferating Cell Nuclear Antigen and Inhibits Nucleotide Excision Repair. **Mol Cell Pharmacol**, 1: (3): 130-137.

Yang, H., Jeffrey, P.D., Miller, J., et al. (2002) BRCA2 function in DNA binding and recombination from a BRCA2-DSS1-ssDNA structure. **Science**, 297: (5588): 1837-1848.

Yang, H., Li, Q., Fan, J., et al. (2005) The BRCA2 homologue Brh2 nucleates RAD51 filament formation at a dsDNA-ssDNA junction. **Nature**, 433: (7026): 653-657.

Yang, J., Liu, X., Bhalla, K., et al. (1997) Prevention of apoptosis by Bcl-2: release of cytochrome c from mitochondria blocked. **Science**, 275: (5303): 1129-1132.

Yu, J., Wang, Z., Kinzler, K.W., et al. (2003a) PUMA mediates the apoptotic response to p53 in colorectal cancer cells. **Proc Natl Acad Sci U S A**, 100: (4): 1931-1936.

Yu, J., Zhang, L., Hwang, P.M., et al. (2001) PUMA induces the rapid apoptosis of colorectal cancer cells. **Mol Cell**, 7: (3): 673-682.

Yu, X. and Chen, J. (2004) DNA damage-induced cell cycle checkpoint control requires CtIP, a phosphorylation-dependent binding partner of BRCA1 C-terminal domains. **Mol Cell Biol**, 24: (21): 9478-9486.

Yu, X., Chini, C.C., He, M., et al. (2003b) The BRCT domain is a phospho-protein binding domain. **Science**, 302: (5645): 639-642.

Yu, Y., Mahaney, B.L., Yano, K., et al. (2008) DNA-PK and ATM phosphorylation sites in XLF/Cernunnos are not required for repair of DNA double strand breaks. **DNA Repair (Amst)**, 7: (10): 1680-1692.

Yu, Y., Wang, W., Ding, Q., et al. (2003c) DNA-PK phosphorylation sites in XRCC4 are not required for survival after radiation or for V(D)J recombination. **DNA Repair (Amst)**, 2: (11): 1239-1252.

Yun, M.H. and Hiom, K. (2009) CtIP-BRCA1 modulates the choice of DNA double-strand-break repair pathway throughout the cell cycle. **Nature**, 459: (7245): 460-463.

Zernik-Kobak, M., Vasunia, K., Connelly, M., et al. (1997) Sites of UV-induced phosphorylation of the p34 subunit of replication protein A from HeLa cells. **J Biol Chem**, 272: (38): 23896-23904.

Zhang, J., Ma, Z., Treszezamsky, A., et al. (2005) MDC1 interacts with Rad51 and facilitates homologous recombination. **Nat Struct Mol Biol**, 12: (10): 902-909.

Zhang, L., Jones, K. and Gong, F. (2009) The molecular basis of chromatin dynamics during nucleotide excision repair. **Biochem Cell Biol**, 87: (1): 265-272.

Zhang, W.W. and Yaneva, M. (1992) On the mechanisms of Ku protein binding to DNA. **Biochem Biophys Res Commun**, 186: (1): 574-579.

Zhang, X., Succi, J., Feng, Z., et al. (2004) Artemis is a phosphorylation target of ATM and ATR and is involved in the G2/M DNA damage checkpoint response. **Mol Cell Biol**, 24: (20): 9207-9220.

Zhang, Y., Rohde, L.H., Emami, K., et al. (2008) Suppressed expression of non-DSB repair genes inhibits gamma-radiation-induced cytogenetic repair and cell cycle arrest. **DNA Repair (Amst)**, 7: (11): 1835-1845.

Zhang, Y. and Xiong, Y. (2001) Control of p53 ubiquitination and nuclear export by MDM2 and ARF. **Cell Growth Differ**, 12: (4): 175-186.

Zhao, H. and Piwnica-Worms, H. (2001) ATR-mediated checkpoint pathways regulate phosphorylation and activation of human Chk1. **Mol Cell Biol**, 21: (13): 4129-4139.

Zhao, H., Traganos, F. and Darzynkiewicz, Z. (2008) Phosphorylation of p53 on Ser15 during cell cycle caused by Topo I and Topo II inhibitors in relation to ATM and Chk2 activation. **Cell Cycle**, 7: (19): 3048-3055.

Zhong, Q., Boyer, T.G., Chen, P.L., et al. (2002) Deficient nonhomologous end-joining activity in cell-free extracts from Brca1-null fibroblasts. **Cancer Res**, 62: (14): 3966-3970.

Zhong, Q., Chen, C.F., Li, S., et al. (1999) Association of BRCA1 with the hRad50-hMre11-p95 complex and the DNA damage response. **Science**, 285: (5428): 747-750.

Zhou, B.B., Chaturvedi, P., Spring, K., et al. (2000) Caffeine abolishes the mammalian G(2)/M DNA damage checkpoint by inhibiting ataxia-telangiectasia-mutated kinase activity. **J Biol Chem**, 275: (14): 10342-10348.

Zhou, B.B. and Elledge, S.J. (2000) The DNA damage response: putting checkpoints in perspective. **Nature**, 408: (6811): 433-439.

Zhou, J., Fan, J.Y., Rangasamy, D., et al. (2007) The nucleosome surface regulates chromatin compaction and couples it with transcriptional repression. **Nat Struct Mol Biol**, 14: (11): 1070-1076.

Zlatanova, J. and Doenecke, D. (1994) Histone H1 zero: a major player in cell differentiation? **FASEB J**, 8: (15): 1260-1268.